PHOSPHORYLATION-REGULATED INTERACTION OF PHOSPHO-SER/THR-PRO BINDING MOTIFS WITH PROTEINS INVOLVED IN ALZHEIMER'S DISEASE & ASTHMA

A Dissertation

Presented to the Faculty of the Graduate School

of Cornell University

In Partial Fulfillment of the Requirements for the Degree of

Doctor of Philosophy

by

Monique Jeannette Rogals

May 2016

PHOSPHORYLATION-REGULATED INTERACTION OF PHOSPHO-SER/THR-PRO BINDING MOTIFS WITH PROTEINS INVOLVED IN ALZHEIMER'S DISEASE & ASTHMA

Monique Jeannette Rogals, Ph. D.

Cornell University 2016

The intrinsic bimodal conformation of the prolyl peptide bond, characterized by the *cis* and *trans* isomers, can act as a two-state molecular switch to regulate protein function and folding. Peptidylprolyl isomerase (PPIase) enzymes exist that accelerate the otherwise slow interconversion between *cis* and *trans* isomer states. One particular PPIase, Pin1, specifically targets prolyl peptide bonds immediately preceded by phosphorylated serine (pS) or threonine (pT). Such pS/pT-P motifs are abundant in the cell, but they are transiently populated depending on the relative kinase and phosphatase activities at each particular site. Two such phosphorylation-regulated proteins, which have also been linked to disease-related processes, are the subjects of this work.

The cytosolic tail of the amyloid precursor protein (APP) contains a single pT-P site (phosphoT668-P669) that has been implicated in the trafficking and proteolytic processing of APP, and elevated phosphorylation of this site is observed in Alzheimer's disease brain tissues. Work presented here shows that T668 phosphorylation weakens the core binding interface between APP and the major stress-induced heat shock factor Hsp70 that targets protein substrates for degradation. This result suggests that phosphorylation of T668 could reduce targeting of APP for degradation and thereby elevate APP levels, potentially adding a novel route by which T668 phosphorylation might increase production of the APP-derived, neurotoxic

amyloid beta peptide.

The interleukin-1 receptor-associated kinase 1 (IRAK1) is a key player in receptor-mediated innate immunity signaling. The IRAK1 undefined domain (UD) has multiple pS-P motifs that are autophosphorlyated in response to receptor stimulation. The sequence proximity of two pairs of pS-P motifs in IRAK1-UD suggests that the WW and PPIase domains of Pin1, both of which can interact with pS/pT-P motifs, could simultaneously bind to two neighboring motifs (i.e., bivalently). Quantification of individual affinities between each Pin1 domain and each of four pS-P IRAK1-UD sites formed the basis for computational modeling of the complex multi-state system that represents the putative bivalent interaction. These results suggest that the prevalence of pS/pT-P motifs in close proximity of one another in biological substrates of Pin1 might provide an important competitive advantage among the multitude of Pin1 substrates in the cell.

BIOGRAPHICAL SKETCH

The author was born to a sci-fi loving, Science News subscribing father and a mathematically minded mother who nurtured her scientific interests to the best of their ability, first supplying her with a refractor telescope and eventually with the initial investment for a place to live during graduate school. Her younger brother and sister provided her with her first experience in collaborations and in equipment sharing, invaluable lessons for graduate school. Her interests throughout elementary and middle school bounced around, generally pausing at writing, reading, art, classics and science of one variety or another. During high school her interests refined into a strong curiosity about microbiology and chemical makeup of the biological world. While other interests morphed into hobbies and useful tools, pursuit of scientific discovery became the focus of her career path. She graduated magna cum laude from the Honors College of the University of Vermont, receiving a B.S in Biochemistry. She did research under the mentorship of Dr. Kenneth G Mann and Dr. Thomas Orfeo, where she learned that she has an abiding love of minute details. They encouraged her to apply to Cornell University, where she was accepted as a graduate student in field of BMCB. She was accepted into the lab of Linda K. Nicholson, which allowed her to both explore fields like thermodynamics, protein NMR, and multi-state protein interactions and to volunteer, introducing children to biochemistry and science and raising money for a variety of projects from supporting cancer research to rebuilding houses destroyed by hurricane Katrina. She also formed friendships with her peers which will endure after she has left Ithaca. Through them she met Nick Michaluk, a material engineer. He helped her find balance in her life and currently the two spend free time crafting jewelry, chain maille, leather armor, and batik dying Ukrainian style easter eggs.

To my family, for all their love and support

ACKNOWLEDGMENTS

First and foremost, I would like to thank my advisor Linda Nicholson for periodically kicking me out of whatever local minimum I've fallen into and reminding me to look at the big picture. Her dedication to science drives the lab and showed me what is necessary to become a principal investigator at a research university. She also manages to find time to care about the people around her, volunteering in the community, acting as a student advisor, and even acting as the faculty advisor of GEEKS for several years. I would also like to thank her for her work in editing this dissertation.

I would also like to thank my committee members Robert Oswald and Chris Fromme for their insight on my graduate work as well as their help outside of my lab work with advice on my career. I'd like to thank our collaborator Kun Ping Lu whose work on Pin1ultimately led to my projects. I'd also like to thank Cynthia Kinsland for teaching me techniques for making constructs, Shu-Bing Qian for the initial Hsp70 construct, the Mao lab, Crane lab and especially the Ke lab for use of and training on various pieces of equipment. I have been financially supported by NIH-CMB training grants as well as by NIH and NSF research grants.

I would especially like to thank Alex Greenwoood for teaching me to analyze NMR data, introducing me to Excel Solver, editing assorted documents, and troubleshooting the in-house MATLAB codes as quickly as I could break them (at least for the first couple years). Thanks to both Alex and Soumya De for training me in all of the standard Nicholson lab protocols, including use of the NMR. I would like to thank Carolyn Fisher for helping me in a myriad of ways (unrelated to protein NMR, but essential to being a happy, well-balanced individual) over the years. Special thanks to Ross Resnick, who not only contributed the molecular biology work that led to the project summed up in chapter two, but was always available for discussions on religion and politics. I am also fortunate to have shared the lab with Jeahoo Kwon and Andrea Acevedo. Both are talented biophysicists who contributed to spotting early modeling inaccuracies as well as to my understanding of Korean and Columbian cuisine and politics. I would also like to thank Andrea for sharing my enjoyment of Stargate, Voyager, and all the other

science fiction I had no one to talk to about before she joined the lab as well as for continuing the GEEKS student organization that Carolyn and I founded. Our lab has also hosted a few undergraduate student researchers who I would like to thank: Jefferey Spence, Tori Knapp and Akito Nicols. Their enthusiasm made lab a little more light-hearted. They have also periodically sharpened my teaching skills.

I was very fortunate to be supported by family and friends throughout my time at Cornell. My parents supported me throughout my life and made sure I had what I needed to excel academically. They have also visited me often over the years, either just to visit or to assist me, with my mother helping me with my taxes the first year and my dad making emergency visits to fix my car. My sister Michelle and brother Michael have supported me as well via phone calls, emails, and, in the case of my sister, visiting me for a couple weeks to play video games. Nick Michaluk has taken amazing care of me, particularly the last six months as I worked to finish my dissertation, feeding me, encouraging me, cleaning the house, making library runs, helping me find some time to relax, and always being in my corner. I'd also like to thank Jared, Tawny, Rachel, Stavros, Crystal, Andrew, Adam, Kelly, Amy, and Veronica. I couldn't ask for more supportive friends.

TABLE OF CONTENTS

LIST OF FIGURES

LIST OF TABLES

LIST OF ABBREVIATIONS

α-secretase: protease that cleaves APP (ADAM17 for regulated cleavage and ADAM10 for constitutive cleavage)
Aβ: amyloidβ peptide
AD: Alzheimer's disease
AICD: APP intracellular domain
APP: amyloid precursor protein
APP695: isoform of APP expressed predominantly in neurons
APPc: cytosolic tail of APP
β-secretase: aspartyl protease that cleaves APP (predominantly BACE1)
BL21: *E. coli* strain optimized for protein expression
carbon$_\alpha$: alpha carbon in between the backbone nitrogen and the backbone carbonyl
CHO: Chinese hamster ovary cells
CMA: chaperone-mediated autophagy
CTD: C-terminal domain
CypA: cyclophilinA, a PPIase
DD: death domain
ER: endoplasmic reticulum
ERAD: ER-associated degradation, system for regulated destruction of membrane proteins
FL: full length
FRET: Förster resonance energy transfer, method to measure protein binding
γ-secretase: protease for intramembrane cleavage of APP
G2 arrest: pause at the end of the 2nd growth phase before entry into mitosis
H_N: hydrogen attached to the backbone nitrogen in a peptide
HEK 293 cells: human embryonic kidney cell line
Hsc70: heat shock cognate 70 kDA, member of HSP70 family, major constitutive heat shock protein
HSP70: family of proteins of about 70kDa, heat shock proteins
Hsp70: member of the HSP70 family, major inducible heat shock protein
HSQCs: heteronuclear single quantum coherence spectroscopy
ITC: isothermal calorimetry
KD: kinase domain
K_d: dissociation constant
kDa: kiloDaltons
LB: Luria broth, media for growing bacterial cultures
MDCK cells: Madin-Darby canine epithelial cell line
mM: millimolar (10^{-3} M)
μM: micromolar (10^{-6} M)
^{15}N: labeled nitrogen with a ½ nuclei so as to be visible by NMR
NMR: nuclear magnetic resonance
P3: fragment resulting from non-amyloidogenic cleavage of APP by both α-secretase and γ-secretase

PP2A: phosphatase 2A, capable of dephosphorylating T668 of APP
PPIase: peptidyl-prolyl isomerase
phospho/p: prefix attached to something phoshorylated
RNA pol II: RNA polymerase II
RNaseA: bovine pancreatic ribonuclease
sAPPα: secreted APPα, after
sAPPβ: β-secretase cleavage results in a large ectodomain fragment, secreted APPβ
SBD: substrate binding domain
SH2: phospho-tyrosine binding domain
SH3: phospho-tyrosine binding domain
TEV: tobacco etch virus protease, used to cut tags off of proteins
TGN: trans-Golgi network
TLR/IL-1R: Toll-Like receptor/Interleukin-1 receptor or in conjunction with pathway, the signaling pathway starting with said receptor
UD: undefined domain
WB: western blots
WCL: whole cell lysate
X: one-letter code for any amino acid
Xxx: three-letter code for any amino acid

LIST OF SYMBOLS

Δδ : chemical shift perturbation
$\Delta\delta_{bound}$: chemical shift perturbation associated with the bound species
ρ/rho : degrees of freedom
σ/sigma :variance expected in collected NMR titration data
φ/phi : torsion angle between the nitrogen and the $carbon_{\alpha}$ in a peptide backbone
ψ/psi : torsion angle between the carbonyl carbon and the $carbon_{\alpha}$ in a peptide backbone
ω /omega : torsion angle of the peptide bond, either 0º (*cis*) or 180 º (*trans*)
χ^2/chi-square : statistical analysis

CHAPTER 1

BACKGROUND & OVERVIEW

Proline (Figure 1.1) is one of the 20 common amino acids. It has an aliphatic side chain, meaning it is non-polar and hydrophobic. It is the only amino acid where the sidechain is attached to the backbone in two places, at both the standard carbon$_\alpha$ and at the backbone nitrogen, forming a ring. As a consequence it is the only amino acid with a secondary imino group, meaning that it lacks capacity to act as a hydrogen-bond donor (Lehninger and Nelson 2008). This also means that it is invisible to many standard NMR experiments that utilize the backbone H_N nucleus, including the HSQCs used in this study (Mori, Abeygunawardana et al. 1995). The ring structure of the proline (P) sidechain results in a restricted phi torsion angle (phi= -60° ± 15°) (Creighton 1993). This in turn leads to a preference for certain secondary structures including type I, II, III, and VIa β-turns and type II poly-prolyl helices (Creighton 1993). Proline is preordered to occupy the second residue position of type I, II, III, VIa β-turns (Creighton 1993). Due to this conformational preference, proline is often found in tight turns

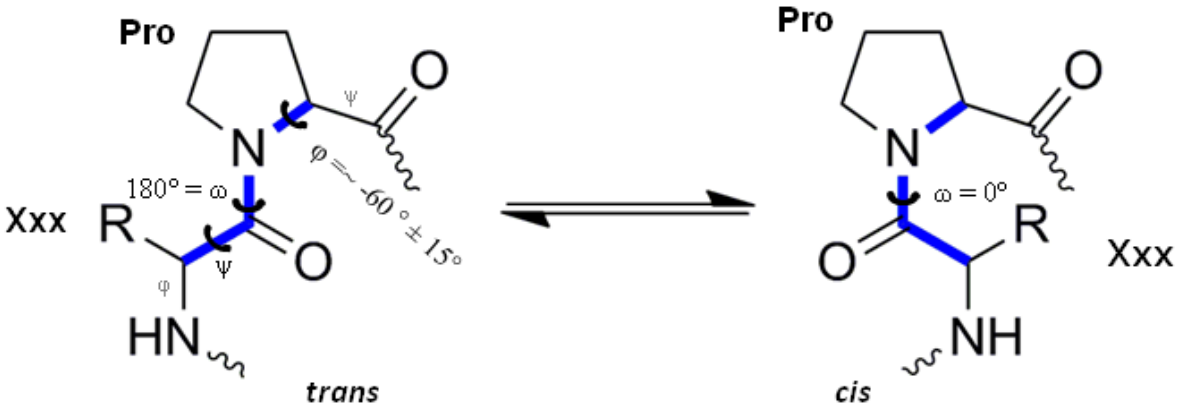

Figure 1.1 Xxx-Pro in either the *trans* or *cis* conformation. This diagram highlights the sidechain structure of proline as well as the torsion angles it can assume, where φ is restricted to -60°±15° and ω is 180 ° in the *trans* conformation and 0 ° in the *cis* conformation.

such as those between adjacent β-strands in an anti-parallel β-sheet.

Multiple consecutive prolines will often form a type II poly-prolyl helix with 3 residues per turn and 3.1 angstroms rise per turn, which has a considerably narrower radius and is more extended than an α-helix. The phi and psi torsion angles associated with a type II poly-prolyl helix are -75° and +145°, respectively, again ideal for proline (Adzhubei, Sternberg et al. 2013). The regular spacing of this helix means that it has a predictably folded length and as a helix adopts a fairly rigid structure which has led to the use of type II poly-prolyl helices as molecular rulers between molecular moieties (Daum, Lucke et al. 2007). If only one proline is in a stretch of amino acid residues that forms an α-helix, an uncommon occurrence in globular proteins and a common occurrence in transmembrane proteins, it not only lacks the ability to act as a hydrogen-bond donor, steric hindrance from the position of the sidechain leave it unable to assume the standard geometry of an α-helix leading to a kink or bend in the α-helix, which can play a critical role in transmembrane signaling (Sansom and Weinstein 2000).

Finally, proline is unique in that the Gibbs free energy for the *trans* (torsion angle omega (ω) = 180°) and *cis* (ω = 0°) forms of the X-P peptide bond can be very similar. With any other general amino acid, the peptide bond adopts the *trans* conformation 99% of the time due to the relative instability of the *cis* conformation (Lehninger and Nelson 2008). In fact, some X-P peptide bonds have a quite high propensity to exist in the *cis* form. For example, at equilibrium 40% of the population of tryptophan (W)-P assumed a *cis* conformation in 20 mM sodium phosphate buffer at 25°C and pH 6.0 (Reimer, Scherer et al. 1998). In a database of known protein structures, W-P *cis* was found in almost 13% of W-P motifs (Reimer, Scherer et al. 1998). The other aromatic residues also show enhanced propensity for forming *cis* X-P peptide bonds, although none so much as W. While both conformations exist at similar energetic

stability, the activation energy is 20 kcal/mol (Creighton 1993), quite significant. In fact, this barrier often takes minutes to overcome unassisted, putting this transition well outside the realm of molecular signaling (Papin, Hunter et al. 2005).

At first glance, the interconversion between *cis* and *trans* might seem irrelevant, as it occurs on a time scale that is very long relative to many biological processes. However there is a class of enzymes tooled to speed interconversion between X-P *cis* and *trans* states, reducing the activation barrier and bringing the transition between conformations into a biologically relevant time frame (Fischer, Bang et al. 1984). This class of enzymes is called peptidyl-prolyl isomerases, or PPIases. They include cyclophilins (Wang and Heitman 2005), parvulins (Mueller and Bayer 2008), FKPBs (Kang, Hong et al. 2008), and Pin1 (Lu and Zhou 2007). As one might imagine, the presence of this two-state, energetically stable peptide bond can lead to interesting biological consequences. Due to the structural uniqueness of proline, its presence in various proteins can lead to important structural consequences (Sansom and Weinstein 2000; Stukenberg and Kirschner 2001; Wedemeyer, Xu et al. 2002; Lehninger and Nelson 2008; Krishnamurthy, Ghazy et al. 2009; Nicholson and De 2011).

Importance of proline in biological systems

Sequences with prolines can play a critical role in the function of various proteins and therefore biological systems. One of the most well known proteins rich in proline is collagen. Proline and hydroxyl-proline make up 21% of the residues in collagen. Its repeat sequence is Gly-X-Y where X is often proline and Y is often hyroxy-proline. This creates an extended, type II poly-prolyl like structure where three strands can tightly pack and coil around each other (with an average phi, psi of -50°, +153°) to create a strong fiber that is essential to the function of

collagen (Lehninger and Nelson 2008). This is perhaps one of the reasons that proline is a non-essential amino acid. Large quantities are necessary to build and maintain collagen, which is so important for the maintenance of a multicellullar organism that if proline were an essential amino acid, it may prove difficult to scavenge sufficient amounts from food intake.

Prolines can also play important roles in the activity of proteins. For example, mutations of prolines in the proline-rich activation domain of CCAAT-binding transcription factor I (20% of the sequence) make it unable to function (Lehninger and Nelson 2008). The ability of X-P peptide bonds to assume both *cis* and *trans* conformations, coupled with the presence of PPIases, leads to structural consequences that affect biological activity in certain amino acid sequences. For instance, bovine pancreatic ribonuclease (RNaseA) has three critical X-P bonds where the *cis* conformation promotes folding, leading to the production of biologically active protein (Wedemeyer, Xu et al. 2002). PPIases increase the rate of folding *in vivo*. Cdc25c regulates the transition from G2 to mitosis and the presence of a PPIase, Pin1, causes changes in the conformation of a phosphoX-P peptide bond in cdc25c. The changed conformation disrupts the ability of phosphatase 2A (PP2A) to dephosphorylate cdc25c, leading in turn to G2 arrest, preventing entrance into mitosis (Stukenberg and Kirschner 2001).

Pin1 requires a specific target motif, phosphorylated serine or threonine followed by a proline, to catalyze isomerization of the peptide bond. Pin1 is unique among human PPIases in that it acts on a phosphorylated target (Ranganathan, Lu et al. 1997; Yaffe, Schutkowski et al. 1997). This implies that regulation of phosphorylation can control target availability. Not only can the *cis*-*trans* conformational equilibrium control access to targets of *trans*-specific phosphatases such as PP2A, it can likewise control access to *cis*-specific phosphatases as well. One instance of this type of interaction occurs in *S. cerevisiae* where Ssu72, a *cis*-specific

phosphatase, binds the unstructured, proline-rich C-terminal domain (CTD) of RNA pol II at a specific phosphoT/S-P motif. This interaction between SSu72 and RNA pol II is regulated by Ess1 (a yeast phosphorylation-directed PPIase), which controls the population of *cis* in that particular X-P motif on the CTD of RNA pol II, thereby affecting the ability of Ssu72 to bind RNA pol II (Krishnamurthy, Ghazy et al. 2009).

An instance where a PPIase, CypA, can induce a local *cis-trans* interconversion that affects the larger structure of the protein is Crk (Sarkar, Saleh et al. 2011) (Nicholson and De 2011). Crk is composed of three functional domains, an SH2 domain followed by an N-terminal SH3 domain and a C-terminal SH3 domain. In this case, the *trans* conformation of glycine (G)237-P238 results in an active form of the protein where the three domains are relatively mobile with respect to one another and where the SH2 and N-terminal SH3 domains are able to engage in signaling pathways. Conversion to a G237-P238*cis* peptide bond introduces a kink into the linker region between the N-terminal SH3 domain and the C-terminal SH3 domain, which brings the two SH3 domains into close contact, creating an autoinhibitory interface between the two functional domains. In this scenario, CypA is regulating a molecular switch (Nicholson and De 2011). These are only a few instances where one or multiple prolines in a peptide are critically important to the biological function of a protein (MacArthur and Thornton 1991; Kay, Williamson et al. 2000; Sansom and Weinstein 2000). There are many other interesting proline-containing sequences. The two described in detail below are involved in the progression of disease processes: Alzheimer's disease (AD) and the inflammatory pathway critical in Asthma.

A phosphoX-P motif in the cytosolic tail of the amyloid precursor protein and its role in Alzheimer's disease

The cytosolic tail of amyloid precursor protein (APPc) contains one proline, preceded by a threonine that can be phosphorylated by cdk5 (Iijima, Ando et al. 2000), GSKβ (Aplin, Gibb et al. 1996; Ma, Pastorino et al. 2012), p34cdc2 cyclin kinase(Suzuki, Cheung et al. 1994) and c-Jun N-terminal kinases (Kimberly, Zheng et al. 2005) and is therefore a target for the PPIase Pin1. Phosphorylation of the threonine leads to a disruption of the N-terminal α-helix capping box present prior to phosphorylation, leading to the appearance of a sizable 10% *cis* pT-P population (Ramelot and Nicholson 2001). The amyloidβ peptide (Aβ) is derived from APP via proteolytic processing and is a major causative agent in AD progression (Hardy and Higgins 1992; Hardy and Selkoe 2002; Zhang, Thompson et al. 2011). APP trafficking is largely governed by interactions between APPc and cellular factors that influence the maturation and localization of APP and act as adaptors for proteolytic processing (Pahlsson, Shakin-Eshleman et al. 1992; Pahlsson and Spitalnik 1996; Tomita, Kirino et al. 1998; Ando, Iijima et al. 2001; Andersen, Reiche et al. 2005; Andersen, Schmidt et al. 2006; Schmidt, Sporbert et al. 2007; Lee, Retamal et al. 2008; Saito, Sano et al. 2008; Burgos, Mardones et al. 2010). The trafficking-dependent proteolytic processing of APP is strongly implicated as a causative factor in AD progression (Hardy and Higgins 1992; Tomita, Kirino et al. 1998; Hardy and Selkoe 2002; Kamenetz, Tomita et al. 2003; Shankar, Li et al. 2008; Yankner and Lu 2009; Zhang, Thompson et al. 2011). To understand the importance of the cytosolic tail of APP, we need to consider the whole protein.

Amyloid precursor protein and regulated intramembrane cleavage

APP is expressed ubiquitously and there are three prevalent isoforms [16]. APP695 is the isoform found predominantly in the brain and is often the isoform used in AD motivated studies

(Tomita, Kirino et al. 1998; Chapman, White et al. 1999; Lee, Kao et al. 2003; Lesne, Koh et al. 2006). All APP discussed here, unless otherwise noted, refers to this isoform and numbering refers to APP695. APP is a type I transmembrane protein where the N-terminal ectodomain is translated into the ER lumen, and the C-terminal AICD into the cytosol. It is N-glycosylated at N467 (Pahlsson, Shakin-Eshleman et al. 1992) of the ectodomain and transported to the Golgi, where over the course of its transport from the cis Golgi to the trans Golgi network it is O-glycosylated in several locations and its N-glycosylation tag matures (Pahlsson and Spitalnik 1996). A western blot (WB) of either mouse or human brains shows three bands of APP, with the lowest molecular weight corresponding to the immature, N-glycosylated form, and higher bands corresponding to mature APP with different O-glycosylation patterns (Iijima, Ando et al. 2000). Mutation of the O-glycosylation site in HEK 293 cells transfected with APP, leads to changes in the distribution of APP where the strong majority appears to be immature APP retained in the ER (Tomita, Kirino et al. 1998). N-glycosylation is a standard sorting procedure for transport to the Golgi (Kingsley, Kozarsky et al. 1986; Remaley, Ugorski et al. 1991; Opdenakker, Rudd et al. 1993), but mutation of the N-glycosylated site has no effect on maturation and secretion of APP in CHO (Pahlsson and Spitalnik 1996) or HEK 293 (Tomita, Kirino et al. 1998) cells, suggesting that other processes might also mediate maturation/trafficking. APP is also subject to processing via two proteolytic pathways, the amyloidogenic and non-amyloidogenic processing pathways.

The level of proteolytic cleavage through each of the two APP processing pathways in healthy brains is kept static (Seubert, Vigo-Pelfrey et al. 1992; Shoji, Golde et al. 1992), but when the anabolic and catabolic systems become unbalanced and amyloidogenic processing increases relative to or in conjunction with non-amyloidogenic processing, pathologic Aβ production occurs (Puzzo, Privitera et al. 2008; Shankar and Walsh 2009; Morley, Farr et al.

2010) (Figure 1.2). In non-amyloidogenic processing, α-secretase (ADAM17 for regulated cleavage (Buxbaum, Liu et al. 1998) and ADAM10 for constitutive cleavage (Jorissen, Prox et al. 2010)) cleaves APP in the ectodomain after K687 and leads to the release of secreted APPα (sAPPα) (Esch, Keim et al. 1990) directly into the extracellular matrix, as α-secretase resides primarily in the plasma membrane (Sisodia 1992) with some additional activity in the ER and trans-Golgi network (TGN) (Chyung, Greenberg et al. 1997; Greenfield, Tsai et al. 1999; Shin, Saido et al. 2005). sAPPα has neuroprotective capabilities (Furukawa, Sopher et al. 1996; Mattson 1997; Ring, Weyer et al. 2007). Mechanistically, sAPPα binds to the ectodomain of APP, preventing APP dimerization, which would normally lead to starvation-induced cell death in neuroblastoma cells (Gralle, Botelho et al. 2009). Next, γ-secretase, a transmembrane complex minimally composed of presenilin (PS) I and/or PS II, APH1, presenilin enhancer (PEN)2 and nicastrin (Edbauer, Winkler et al. 2003), cleaves within the lipid bilayer at one of several sites (Haass and Steiner 2002), predominantly after V642, and leads to the release of the non-toxic fragment P3 into the extracellular matrix (Zhao, Tan et al. 2007). γ-secretase activity has been detected in the ER (Kovacs, Fausett et al. 1996), Golgi (Kovacs, Fausett et al. 1996), plasma membrane (Chyung, Raper et al. 2005), endosomes(Pasternak, Callahan et al. 2004), lysosomes (Pasternak, Bagshaw et al. 2003; Pasternak, Callahan et al. 2004), and the nuclear envelope (Annaert, Levesque et al. 1999).

The amyloidogenic pathway begins with β-secretase (predominantly the transmembrane aspartyl protease BACE1 (Sinha, Anderson et al. 1999; Vassar, Bennett et al. 1999; Yan, Bienkowski et al. 1999)) cleavage of APP after M596 (Seubert, Oltersdorf et al. 1993). Reports of the subcellular location of β-secretase activity vary, with some studies providing evidence that it is active within the ER and TGN (Greenfield, Tsai et al. 1999) and other studies showing that it

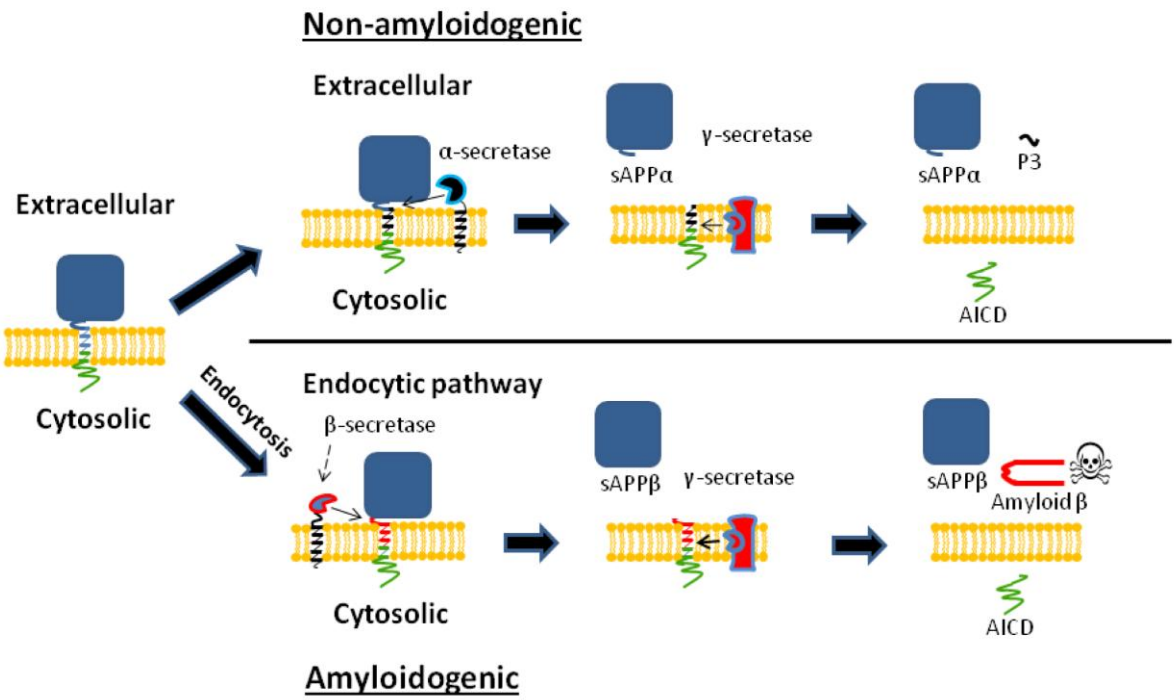

Figure 1.2 The two proteolytic processing routes for APP. The top pathway takes place mainly at the plasma membrane where APP is cleaved first by α-secretase and then by γ-secretase, generating secretedAPP α (sAPP α), P3 and amyloid intracellular domain (AICD). Amyloidogenic processing occurs mainly in the endocytic pathway where APP is cleaved by β-secretase and then by γ-secretase, releasing secretedAPPβ (sAPPβ), amyloidβ (Aβ) and the AICD.

is active within the endocytic pathway (Caporaso, Takei et al. 1994), while still other studies place a limited amount of activity at the plasma membrane (Vassar, Bennett et al. 1999; Huse, Pijak et al. 2000; Walter, Fluhrer et al. 2001; Huse, Liu et al. 2002). β-secretase cleavage results in a large ectodomain fragment, secreted APPβ (sAPPβ), which is eventually released into the extracellular matrix where it acts as a signal to promote cell death (Nikolaev, McLaughlin et al. 2009). The second cleavage event is again mediated by γ-secretase. The product eventually released into the extracellular matrix, Aβ, is a small, approximately 4 kDa peptide of 38,40,42,46 (Zhao, Mao et al. 2004; Zhao, Tan et al. 2007) or 49 residues (Sastre, Steiner et al. 2001; Weidemann, Eggert et al. 2002). The formation of soluble dodecameric oligomers of Aβ coincide with the first memory loss in transgenic AD mouse models (Lesne, Koh et al. 2006). Assemblies as small as dimers occur *in vivo* and may contribute to altered synaptic function (Podlisny, Ostaszewski et al. 1995; Walsh, Tseng et al. 2000; Walsh, Klyubin et al. 2002; Mucke and Selkoe 2012). By the end stages of AD, Aβ aggregates into the massive, insoluble plaques that are so characteristic of the disease (Selkoe 1998; Shankar and Walsh 2009).

Regardless of the processing pathway, the primarily cytosolic fragment of APP remaining after γ-secretase cleavage is the AICD (Figure 1.3). The AICD is around 12 residues longer than the APPc domain, with the extra residues coming from the portion of the AICD that was embedded in the membrane. The APPc is thought to play a role in the trafficking and/or processing of APP (Lane, Raines et al. 2010; Chaufty, Sullivan et al. 2012; Fjorback and Andersen 2012; Gustafsen, Glerup et al. 2013; Sullivan, Dillon et al. 2014). Many models focus on changes to the phosphorylation of APPc (Takahashi, Niidome et al. 2008; Barbagallo, Weldon et al. 2010). Phosphorylation is the most common reversible post-translational modification in the cell (Hunter 1998) and is integral to processes as diverse as metabolism,

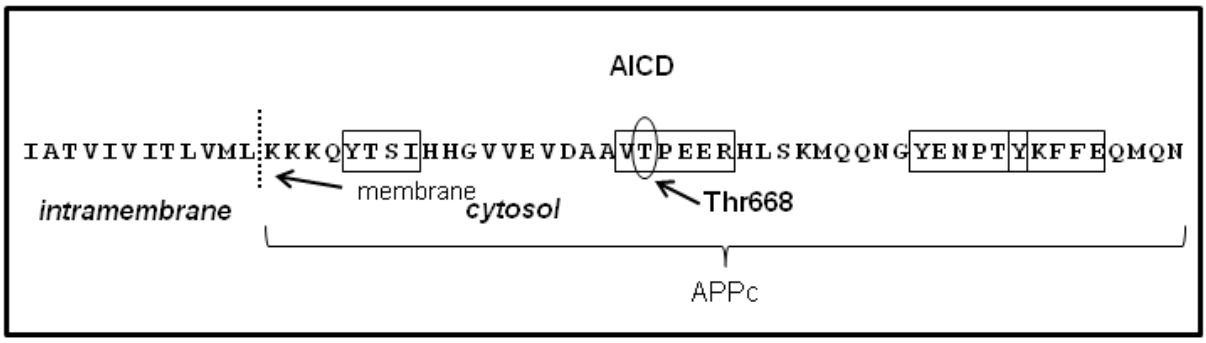

Figure 1.3 Sequence of the amyloid intracellular domain (AICD). The membrane (dotted line) marks the barrier for the cytosolic tail of APP (APPc). Threonine 668, used in phosphorylation dependence studies, is circled and the binding motifs, as defined in this study, are boxed.

protein-protein interaction, cytoskeletal arrangement, and gene transcription (Manning, Whyte et al. 2002; Ubersax and Ferrell 2007). Of the eight potential phosphorylation sites in APPc (Gandy, Czernik et al. 1988), seven have been observed phosphorylated in preserved slices of AD patient brains (Oishi, Nairn et al. 1997; Lee, Kao et al. 2003). Six of these seven sites are in any one of the four loosely defined binding motifs which can be seen in the sequence of the cytosolic tail of APP (APPc) as shown in Figure 1.3 (Chang and Suh 2010). The first motif, YTSI, is required for basolateral sorting in MDCK cells (Haass, Koo et al. 1995; Lai, Sisodia et al. 1995), while the second, VTPEER, interacts with 14-3-3γ (Sumioka, Nagaishi et al. 2005) and Pin1 (Lu, Hanes et al. 1996), the third, GYENTPY, is a standard endocytotic signal for membrane proteins (Lai, Sisodia et al. 1995), and the fourth, YKFFE binds to AP-4, which localizes APP to endosomes (Burgos, Mardones et al. 2010). The presence or absence of phosphorylation of differing sites has been shown to affect protein binding to APPc (Matsuda, Yasukawa et al. 2001; Tarr, Roncarati et al. 2002; Cavalli, Kujala et al. 2005).

Phosphorylation of the T668-P669 motif of APPc

Phosphorylation of T668 is of particular interest. Comparison of immunofluorescent staining of human hippocampal sections of AD patients and age-matched controls using an antibody against phosphorylated T668 (pT668) reveal a significant increase in pT668 in AD brains (Lee, Kao et al. 2003). The same study showed that pT668 APP (or some proteolytic product thereof) is predominantly localized to endosomes (in both AD brains and rat primary cortical neurons) along with BACE1, the major β-secretase (Lee, Kao et al. 2003; Brouwers, Sleegers et al. 2006). In rat cortical neurons, overexpression of T668A APP decreases secreted Aβ levels when compared with WT (Lee, Kao et al. 2003). Overexpression of human APP

abolishes synchronous calcium oscillations and mutating T668A, or inhibiting kinases that target T668, largely restores oscillations (Santos, Tasiaux et al. 2011). Inhibition of phosphorylation of T668 leads to a decrease in mature relative to immature APP (Colombo, Repici et al. 2007). During staurosporine-mediated apoptosis, the level of pT668, as measured using a phosphorylation-specific antibody, increases and may facilitate the generation of Aβ42 in an endocytic-dependent manner (Sodhi, Rampalli et al. 2004; Sodhi, Perez et al. 2008).

Interestingly, T668 phosphorylation also appears to confer resistance to caspace cleavage of the AICD (Gervais, Xu et al. 1999; Taru, Yoshikawa et al. 2004). Said cleavage contributes to neuronal apoptosis and AICD resistance of that cleavage, slows apoptosis, a fact which suggests a very complex role for pT668 in AD progression. It is worth noting that one study, conducted with mice homozygous for T668A APP, found T668A mice had no gross abnormalities when compared with APP null mice. APP null mice are viable, but show marked abnormalities (Zheng, Jiang et al. 1995). Importantly, this work suggests that APP is not fully redundant with APP-like1 or APP-like 2; however, it is insufficient evidence to prove that T668 completely lacks functional contribution to APP. Also consider that pT668 is increased in AD cells (Lee, Kao et al. 2003) and therefore much of the T668 in healthy brain tissue is probably not phosphorylated, so it is unreasonable to expect gross abnormalities in T668A mice when the experimental conditions (e.g. T668A) may come closer to mimicking the state of a healthy brain (non-phosphorylated T668) than an AD brain (phosphorylated T668). When looking for changes in the abnormal processing found in AD, it might be more revealing to use mice with APP containing mutations that are already prone to increased Aβ production or possibly a phosphomimetic mutant like T668E (Martin, Schrader-Fischer et al. 1995).

Protein interactions with APPc

Through a combination of proteomics studies (Colangelo, Schurr et al. 2002; Bai, Markham et al. 2008; Di Domenico, Sultana et al. 2011) and classic approaches a large interactome for APP has been documented (Perreau, Orchard et al. 2010). At the same time work has been done to understand changes in AD brains at the levels of expression (Colangelo, Schurr et al. 2002), transcription (Vogelsberg-Ragaglia, Schuck et al. 2001), translation and protein activity (Lian, Ladner et al. 2001; Di Domenico, Sultana et al. 2011). These resources allow us to target our studies to known protein binding partners of APP where dependence on the phosphorylation state of T668 is unknown and where T668 phosphorylation may affect the trafficking or processing of APP and ultimately the progression of AD.

There are several known proteins that interact with the APPc and play a role in APP metabolism and trafficking and AD progression. Several interactors, such as X11(Biederer, Cao et al. 2002; King, Perez et al. 2003), Fe65 (Zambrano, Buxbaum et al. 1997), and JNK interacting protein (JIP) (Matsuda, Yasukawa et al. 2001; Scheinfeld, Roncarati et al. 2002), contain a phoshoTyrosine binding domain (PTB) that can interact with the YENPTY motif on the APPc. These interactors are implicated primarily in trafficking (Guenette, Chen et al. 1999; King, Perez et al. 2003; Dumanis, Chamberlain et al. 2012; Fu and Holzbaur 2013). PAT1 is an interactor that binds to the N-terminal most motif on the APPc as well as microtubules and therefore helps mediate transport on the secretory pathway (Raychaudhuri and Mukhopadhyay 2007). SorLa (a.k.a LR11) is another interactor that appears to both reduce β-secretase mediated processing and play a role in APP trafficking (Vieira, Rebelo et al.; Spoelgen, von Arnim et al. 2006; Schmidt, Sporbert et al. 2007). It is down-regulated in AD brains (Grear, Ling et al. 2009) and some gene variants are associated with an increased risk for late-onset AD (Lee, Cheng et al.

2007; Rogaeva, Meng et al. 2007).

APP and Hsc70 (Heat shock cognate 70) are also known to interact (Kouchi, Sorimachi et al. 1999). Hsc70 expression is upregulated in Alzheimer's disease (Elliott, Laufer et al. 2009) and may promote APP degradation (i.e. destruction of the APP by reduction of the protein to component amino acids) as opposed to regulated proteolytic processing (i.e. processing resulting in production of specific fragments that have biological functions) (Wang, Cesca et al.; Lee, Kao et al. 2003; Massey, Zhang et al. 2006; Vingtdeux, Hamdane et al. 2007). Chip, an E3 ubiquitin ligase that interacts with Hsp70 (Heat shock protein 70) (Shin, Klucken et al. 2005), has been implicated in APP metabolism and is capable of ubiquitinating APP (Kumar, Ambasta et al. 2007). Ubiquitination could also occur later in the pathway with the cytosolic AICD or with a caspace-cleaved portion of the AICD (Zhang, Thompson et al. 2011). Hsp70 is a major stress-induced molecular chaperone (Mayer 2013). As T668 phosphorylation is both increased in AD patients and has an effect on APP metabolism, interactions that depend on the phosphorylation state of T668 will likely influence APP trafficking, degradation or regulated proteolytic processing. Understanding the interaction of the phosphoT-P motif of APPc with either Hsc70 or stress induced-Hsp70 could lead to valuable information on the trafficking of APP and, by extension, on the progression of AD. Chapter two of this dissertation focuses on the interaction of APPc and Hsp70 and the dependence of this interaction on T668 phosphorylation.

The undefined domain of IRAK1 contains multiple X-P motifs.

The second sequence of interest is the undefined domain (UD) of IRAK1. It is a 95 residue sequence containing 27 prolines, six of which are preceded by serines that could be phosphorylated at certain times *in vivo* (Tun-Kyi, Finn et al. 2011). They are viable target motifs

for Pin1 and, in fact, Pin1-catalyzed exchange between the *trans* and *cis* conformations has been shown at three sites: pS131-P132, pS144-P145, and pS173-P174 (Tun-Kyi, Finn et al. 2011). To understand the potential importance of the interaction of Pin1 with these motifs, the role of IRAK1 in innate immunity is now summarized.

IRAK1 in innate immunity/TLR signaling

IRAK1 is a kinase involved in immune system signaling (Figure 1.4), specifically operating in the Toll-Like receptor/Interleukin-1 receptor (TLR/IL-1R) signaling pathway. This system is an integral part of the innate immune system, which provides the first response to bacterial, viral, and fungal challenges (Moresco, LaVine et al. 2011). There are ten known human TLRs which recognize distinct sets of pathogen-associated molecules, dimerizing upon ligand recognition. The initial molecule recognition by TLRs leads to upregulation of various cytokines, chemokines and type 1 interferons (INF), which in turn activate interleukin-1 receptors (IL-1R). Each of these TLR and IL-1R receptors has a cytoplasmic TIR domain (TLR/IL-1R receptor domain) that, upon receptor activation, initiates formation of the same signaling complex that includes IRAK1 (Brown, Wang et al. 2011).

All IRAK family members share a general domain layout, with an N-terminal death domain (DD) followed by a proline-rich linker region called the undefined domain (UD), a kinase domain (KD), and a C-terminal domain (CTD). There are critical differences between family members as well. The kinase domain is non-functional in the case of IRAKM (Wesche, Gao et al. 1999) and the linker region varies quite extensively in sequence and length between family members (Flannery and Bowie 2010). IRAK4-DD binds to the DD of IRAK1 and other IRAK family members (Flannery and Bowie 2010). Upon TLR/IL-1R receptor stimulation and

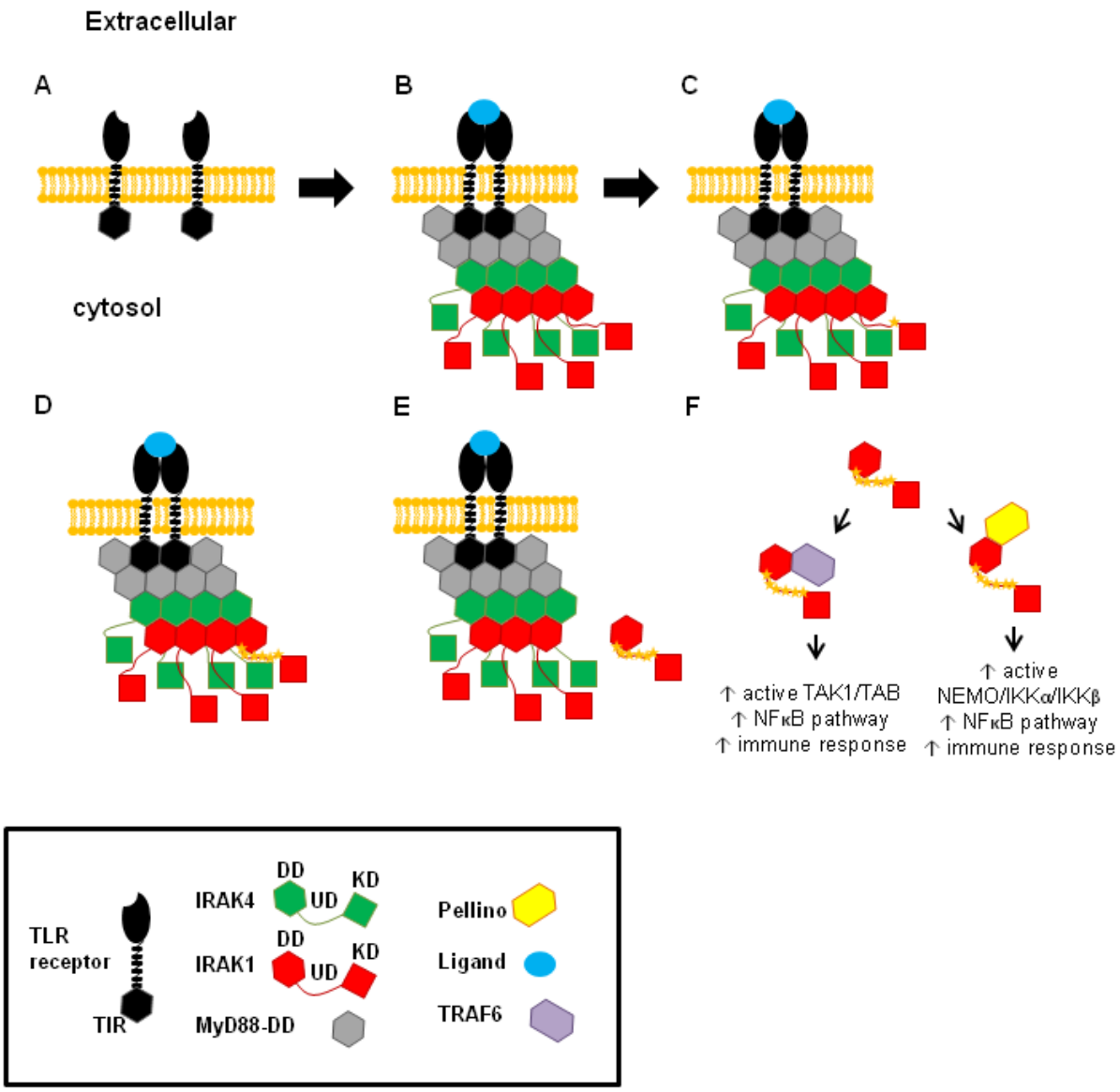

Figure 1.4 Portion of TLR signaling pathway with an emphasis on IRAK1. a). TLR receptors at the plasma membrane. b.) TLR receptors dimerize upon ligand binding and recruit a cytosolic scaffold complex thought to be comprised of six myD88 proteins (in this image only the death domains of MyD88 are represented), four IRAK4 proteins and other IRAK family members (in this case IRAK1). c.) the kinase domain of IRAK4 phosphorylates IRAK1 at T209. d). IRAK1UD then undergoes rapid autophosphorylation, leading to its dissociation from the scaffolding complex. f.)once freed, it can interact with Pellino and/or TRAF6, leading to activation of several pathways that ultimately upregulate immune response.

assembly of the cytosolic signaling complex, the KD of IRAK4 then phosphorylates IRAK1 at T209, after which the UD of IRAK1 undergoes rapid autophosphorylation (Kollewe, Mackensen et al. 2004).

This IRAK1 activation leads to dissociation from the receptor complex (Cao, Henzel et al. 1996; Gottipati, Rao et al. 2008) and allows interaction with TRAF6 and potentially Pellino (Lin, Huoh et al. 2008; Flannery and Bowie 2010; Haghayeghi, Sarac et al. 2010; Kim, Sung et al. 2011). TRAF6 binding is critical to subsequent signaling events via activation of the TAK1/TAB complex which leads to the activation of two additional signaling pathways, MAPK and NF-κB (Brown, Wang et al. 2011). IRAK1 deficient mice models have shown that lack of IRAK1 seriously attenuates and slows NFκB signaling and immune response, but does not wholly prevent it. Lack of IRAK1 also impairs MAPK signaling in some TLRs, although levels vary (reviewed in (Flannery and Bowie 2010)). Pellino is involved in ubiquitination of IRAK1 which leads to binding of NEMO and activation of NFκB signaling (Conze, Wu et al. 2008). Both TRAF6 and Pellino binding ultimately lead to increased cytokine production which further upregulates the innate immune response (TLR signaling is reviewed in (Brown, Wang et al. 2011)).

Another protein both capable of interacting with IRAK1 and critical in innate immune response is Pin1 (Figure 1.5). Mice lacking Pin1 showed an inability to mount a robust TLR-mediated innate immune response (Tun-Kyi, Finn et al. 2011). The similarity in those phenotypes did not go unnoticed and further experiments showed that activated, hyperphosphorylated IRAK1 could be pulled down with GST-Pin1. This interaction required that the IRAK1 kinase domain be functional, presumably in order to phosphorylate the UD of IRAK1, and deletion of the UD abrogates binding, suggesting that Pin1 binding occurs at one or

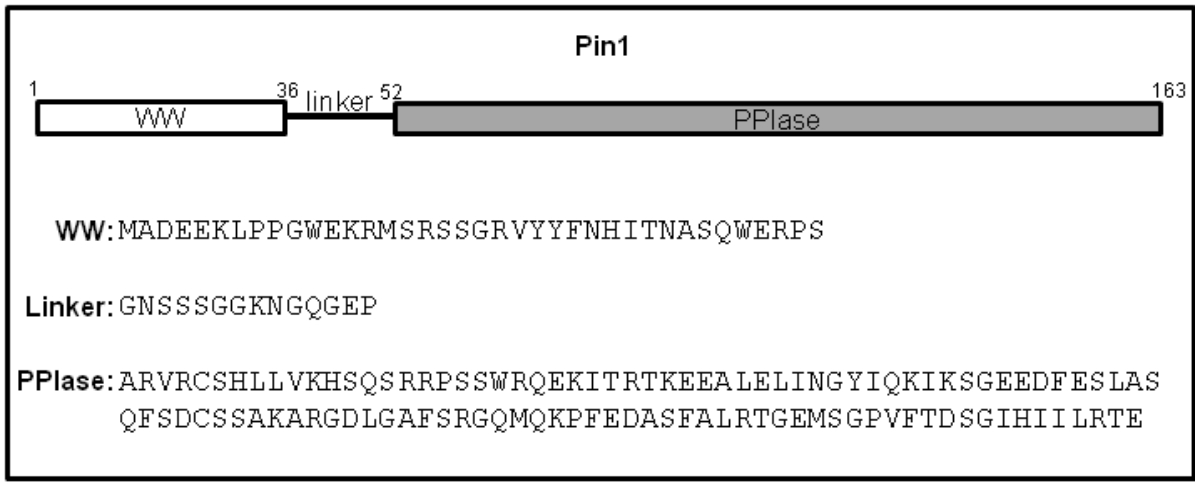

Figure 1.5 Diagram of domain architecture and sequence of Pin1. The rectangles represent areas of stable 3D structure and the lines is the intrinsically disordered linker region. The definition of domains in this case is taken from the Uniprot database accessed 04/11/2016.

more phosphoS-P sites on the UD. A series of mutations on phosphoS-P motifs identified three motifs critical for retaining the GST-Pin1 pulldown of IRAK1: S131-P132, S144-P145, and S173-P174. The binding affinity of these three sites for the isolated WW domain of Pin1 were 220 ± 15 μM, 120 ± 12 μM, and 260 ± 75 μM respectively, and the *cis/trans* isomerization of each motif could be catalyzed by Pin1 as well (Tun-Kyi, Finn et al. 2011). The results from the Lu and Nicholson labs are suggestive of a mechanism for IRAK1 activation, where IRAK1 becomes hyperphosphorylated and interacts with Pin1, which isomerizes it in key locations leading to its dissociation from IRAK4.

The importance of bivalent interactions with the IRAK1-UD S-P motifs

The aforementioned binding affinities are quite weak and leave some doubt as to whether any one site of the UD of IRAK1 could compete for Pin1 *in vivo* at low concentrations. In a cellular system the total IRAK1-UD site concentration is not reflective of the local concentrations that Pin1 might encounter. Firstly, there are three critical sites identified by Tun-Kyi et al. on a single UD, which does not account for other sites that, while not being major binding sites, could certainly interact with a molecule of Pin1, retaining it in the immediate vicinity of the UD. Secondly, TLRs appear to recruit a helical scaffold of proteins upon activation, based on structural studies, where ligand binding causes TLR dimerization followed by recruitment of six MyD88 death domains (DD), four IRAK4 DDs and then four IRAK2 DDs as seen in 3MOP.pdb (IRAK2 and IRAK1 are thought to bind to the signaling complex in the same manner) (Lin, Lo et al. 2010). Hence, the structure of this complex suggests that the activated receptor complex harbors multiple UDs of IRAK1 in close proximity. This is without even accounting for the possibility of receptor clustering, which has been demonstrated for TLR4

receptors (Kobayashi, Saitoh et al. 2006). During the process of autophosphorylation, IRAK1-UD exists at high local concentration.

In addition to the multiple Pin1 recognition motifs on IRAK1-UD, the binding equilibrium is further complicated by the fact that there are two domains on Pin1 that bind the same general motif. The question becomes, is it possible that avidity enhancement, where one domain binds at one site and increases the probability that it will bind at a second site (Mammen, Choi et al. 1998), actually occurs between Pin1 & IRAK1-UD and if so, what potential biological advantage would that provide in the context of innate immune response. The local concentration of IRAK1-UD drops after IRAK1 is hyperphosphorylated and it dissociates from the receptor complex (Flannery and Bowie 2010; Brown, Wang et al. 2011). As Pin1 interacts with IRAK1, preparing it for dissociation, it needs to be able to stay associated with IRAK1 despite the decreasing local concentration, and the ability to bind a UD bivalently would provide it with a tighter apparent binding affinity (Jencks 1981), potentially allowing the IRAK1-UD to outcompete other proteins for the available supply of Pin1 to facilitate a quick signaling response. Similar avidity enhancement has been used effectively in the development of dually phosphorylated Pin1 inhibitors (Daum, Lucke et al. 2007). Therefore, chapter three of this dissertation will focus on understanding which binding species contribute to the overall affinity in the complex scenario where the two binding domains of Pin1 interact with two binding motifs of IRAK1 and on what theoretical advantage that interaction would provide when compared with one binding motif.

Experimental Approach

Much of this work relies on the use of NMR spectroscopy, specifically on in vitro ^{15}N-^{1}H

HSQC titration experiments. These experiments yield spectra that distinguish between individual residues utilizing the chemical shift of their backbone N-Hs. By using ^{15}N-labeled recombinant protein and another peptide lacking all but the natural allotment of ^{15}N, binding can be monitored. The species lacking in ^{15}N is titrated against a constant concentration of ^{15}N-labeled protein and an ^{15}N-^{1}H HSQC is collected at each titration point. The series of HSQCs reflects the effect of adding the unlabeled protein to the system, where individual peaks representing specific residues, either shift as the chemical environment around those residues changes (if binding is in fast exchange) or display changes in intensity as a new set of peaks representing the bound state emerge (if binding is in slow exchange). This identifies residues that are affected by binding, such as those in the binding site. Also, because the peaks change as a reflection of the populations of bound and free residues, titrations reflect binding affinity of the unlabeled and labeled species even for complex systems. I additionally benefitted from the fact that NMR spectroscopy is well suited to measure moderate to weak binding affinities (K_d>10 µM) (Carbajo and Neira 2013). Because these NMR studies were conducted entirely *in vitro*, special care was taken to focus on systems where the interaction has already been demonstrated *in vivo* and where the interaction has been deemed biologically relevant. I also chose systems where the chemical shifts of at least one species were already known (Ramelot, Gentile et al. 2000; Bayer, Goettsch et al. 2003).

I explored the interaction between APPc and Hsp70 in terms of the binding affinity and location of the binding sites on APPc, and the influence of phosphorylation at T668 using NMR titrations. In order to keep within the molecular size constraint inherent in HSQCs, I utilized only the substrate binding domain (SBD) of Hsp70 (19 kDa as opposed to 70 kDa for full length (FL) Hsp70) as well as APPc-FL (~4 kDa) and even shorter peptides derived from the APPc. While

NMR experiments yielded important information regarding the relative affinity of Hsp70 SBD for phosphorylated T668 APPc-derived peptide versus non-phosphorylated peptide, the instability of Hsp70 SBD prevented accurate determination of binding affinities. Hence, NMR studies were supplemented with pulldowns and WBs. The pulldowns were conducted in whole cell lysates of H4 neuroglioma cells using biotinylated APPc-derived synthetic peptides and revealed that relative difference in affinity with phosphorylation was lost when the peptide was lengthened. The WBs were also used to bracket the affinity of the interaction of APPc and Hsp70-FL for the longer APPc-derived peptides.

I also investigated bivalent interactions as a mechanism for enhancing IRAK1 interaction with Pin1. I determined the binding affinities for the interaction of Pin1, both as individual domains and as intact domains in Pin1-FL, and a series of IRAK1-UD derived peptides. These peptides include the sites of interest, namely pS131-P132, pS144-P145, pS163-P164, and pS173-P174, both individually and with two dual phosphorylated peptides. This study was experimentally comprised entirely of ^{15}N-^{1}H HSQC titrations. Titration data obtained for individual Pin1 domains binding to singly phosphorylated peptides were fit using a simple two-state analysis. Titration data obtained for Pin1-FL binding to a singly phosphorylated peptide was analyzed using an analytically derived expression to take into account the four possible states in the system. Titration data obtained for interactions of Pin-FL and dually phosphorylated peptide, being exceedingly more complex, was analyzed using a model I built in Virtual Cell (Dubitzky, Wolkenhauer et al.), which utilizes a series ordinary differential equations to calculate the equilibrium populations for the multiple states in this model at each titration condition.

Both APPc and IRAK1-UD are critical players in disease relevant biological systems.

APPc is involved in trafficking, proteolytic processing and potentially degradation of APP, which is a key protein in Alzheimer's disease progression (Zhang, Thompson et al. 2011; van der Kant and Goldstein 2015). IRAK1-UD is critical to the regulation of TLR signaling and innate immune system activation (Flannery and Bowie 2010). Both sequences contain at least one proline residue that is thought to alter its interaction with another pivotal protein within each respective biological system. A thorough investigation of the details of these interactions could lead to a mechanistic understanding of how these critical interactions regulate aspects of each of the larger systems.

REFERENCES

Adzhubei, A. A., M. J. E. Sternberg, et al. (2013). "Polyproline-II helix in proteins: structure and function." Journal of molecular biology **425**(12): 2100-2132.

Andersen, O. M., J. Reiche, et al. (2005). "Neuronal sorting protein-related receptor sorLA/LR11 regulates processing of the amyloid precursor protein." Proc Natl Acad Sci U S A **102**(38): 13461-6.

Andersen, O. M., V. Schmidt, et al. (2006). "Molecular dissection of the interaction between amyloid precursor protein and its neuronal trafficking receptor SorLA/LR11." Biochemistry **45**(8): 2618-28.

Ando, K., K. I. Iijima, et al. (2001). "Phosphorylation-dependent regulation of the interaction of amyloid precursor protein with Fe65 affects the production of beta-amyloid." J Biol Chem **276**(43): 40353-61.

Annaert, W. G., L. Levesque, et al. (1999). "Presenilin 1 controls gamma-secretase processing of amyloid precursor protein in pre-golgi compartments of hippocampal neurons." J Cell Biol **147**(2): 277-94.

Aplin, A. E., G. M. Gibb, et al. (1996). "In vitro phosphorylation of the cytoplasmic domain of the amyloid precursor protein by glycogen synthase kinase-3beta." J Neurochem **67**(2): 699-707.

Bai, Y., K. Markham, et al. (2008). "The in vivo brain interactome of the amyloid precursor protein." Mol Cell Proteomics **7**(1): 15-34.

Barbagallo, A. P., R. Weldon, et al. (2010). "Tyr(682) in the intracellular domain of APP regulates amyloidogenic APP processing in vivo." PLoS One **5**(11): e15503.

Bayer, E., S. Goettsch, et al. (2003). "Structural analysis of the mitotic regulator hPin1 in solution: insights into domain architecture and substrate binding." J Biol Chem **278**(28): 26183-93.

Biederer, T., X. Cao, et al. (2002). "Regulation of APP-dependent transcription complexes by Mint/X11s: differential functions of Mint isoforms." J Neurosci **22**(17): 7340-51.

Brouwers, N., K. Sleegers, et al. (2006). "Genetic risk and transcriptional variability of amyloid

precursor protein in Alzheimer's disease." Brain **129**(Pt 11): 2984-91.

Brown, J., H. Wang, et al. (2011). "TLR-signaling networks: an integration of adaptor molecules, kinases, and cross-talk." J Dent Res **90**(4): 417-27.

Burgos, P. V., G. A. Mardones, et al. (2010). "Sorting of the Alzheimer's disease amyloid precursor protein mediated by the AP-4 complex." Dev Cell **18**(3): 425-36.

Buxbaum, J. D., K. N. Liu, et al. (1998). "Evidence that tumor necrosis factor alpha converting enzyme is involved in regulated alpha-secretase cleavage of the Alzheimer amyloid protein precursor." J Biol Chem **273**(43): 27765-7.

Cao, Z., W. J. Henzel, et al. (1996). "IRAK: a kinase associated with the interleukin-1 receptor." Science **271**(5252): 1128-31.

Caporaso, G. L., K. Takei, et al. (1994). "Morphologic and biochemical analysis of the intracellular trafficking of the Alzheimer beta/A4 amyloid precursor protein." J Neurosci **14**(5 Pt 2): 3122-38.

Carbajo, R. J. and J. L. Neira (2013). NMR for Chemists and Biologists, Springer Netherlands.

Cavalli, V., P. Kujala, et al. (2005). "Sunday Driver links axonal transport to damage signaling." J Cell Biol **168**(5): 775-87.

Chang, K. A. and Y. H. Suh (2010). "Possible roles of amyloid intracellular domain of amyloid precursor protein." BMB Rep **43**(10): 656-63.

Chapman, P. F., G. L. White, et al. (1999). "Impaired synaptic plasticity and learning in aged amyloid precursor protein transgenic mice." Nat Neurosci **2**(3): 271-6.

Chaufty, J., S. E. Sullivan, et al. (2012). "Intracellular amyloid precursor protein sorting and amyloid-beta secretion are regulated by Src-mediated phosphorylation of Mint2." J Neurosci **32**(28): 9613-25.

Chyung, A. S., B. D. Greenberg, et al. (1997). "Novel beta-secretase cleavage of beta-amyloid precursor protein in the endoplasmic reticulum/intermediate compartment of NT2N cells." J Cell Biol **138**(3): 671-80.

Chyung, J. H., D. M. Raper, et al. (2005). "Gamma-secretase exists on the plasma membrane as an intact complex that accepts substrates and effects intramembrane cleavage." J Biol Chem **280**(6): 4383-92.

Colangelo, V., J. Schurr, et al. (2002). "Gene expression profiling of 12633 genes in Alzheimer hippocampal CA1: transcription and neurotrophic factor down-regulation and up-regulation of apoptotic and pro-inflammatory signaling." J Neurosci Res **70**(3): 462-73.

Colombo, A., M. Repici, et al. (2007). "The TAT-JNK inhibitor peptide interferes with beta amyloid protein stability." Cell Death Differ **14**(10): 1845-8.

Conze, D. B., C. J. Wu, et al. (2008). "Lys63-linked polyubiquitination of IRAK-1 is required for interleukin-1 receptor- and toll-like receptor-mediated NF-kappaB activation." Mol Cell Biol **28**(10): 3538-47.

Creighton, T. E. (1993). Proteins: structures and molecular properties, Macmillan.

Daum, S., C. Lucke, et al. (2007). "On the benefit of bivalency in peptide ligand/pin1 interactions." J Mol Biol **374**(1): 147-61.

Di Domenico, F., R. Sultana, et al. (2011). "Quantitative proteomics analysis of phosphorylated proteins in the hippocampus of Alzheimer's disease subjects." J Proteomics **74**(7): 1091-103.

Dubitzky, W., O. Wolkenhauer, et al. Virtual Cell (VCell) Modeling and Analysis Platform. Encyclopedia of Systems Biology, Springer New York**:** 2342-2347.

Dumanis, S. B., K. A. Chamberlain, et al. (2012). "FE65 as a link between VLDLR and APP to regulate their trafficking and processing." Mol Neurodegener **7**: 9.

Edbauer, D., E. Winkler, et al. (2003). "Reconstitution of gamma-secretase activity." Nat Cell Biol **5**(5): 486-8.

Elliott, E., O. Laufer, et al. (2009). "BAG-1M is up-regulated in hippocampus of Alzheimer's disease patients and associates with tau and APP proteins." J Neurochem **109**(4): 1168-78.

Esch, F. S., P. S. Keim, et al. (1990). "Cleavage of amyloid beta peptide during constitutive processing of its precursor." Science **248**(4959): 1122-4.

Fischer, G., H. Bang, et al. (1984). "Conformational specificity of chymotrypsin toward proline-containing substrates." Biochim Biophys Acta **791**(1): 87-97.

Fjorback, A. W. and O. M. Andersen (2012). "SorLA is a molecular link for retromer-dependent sorting of the Amyloid precursor protein." Commun Integr Biol **5**(6): 616-9.

Flannery, S. and A. G. Bowie (2010). "The interleukin-1 receptor-associated kinases: critical regulators of innate immune signalling." Biochem Pharmacol **80**(12): 1981-91.

Fu, M. M. and E. L. Holzbaur (2013). "JIP1 regulates the directionality of APP axonal transport by coordinating kinesin and dynein motors." J Cell Biol **202**(3): 495-508.

Furukawa, K., B. L. Sopher, et al. (1996). "Increased activity-regulating and neuroprotective efficacy of alpha-secretase-derived secreted amyloid precursor protein conferred by a C-terminal heparin-binding domain." J Neurochem **67**(5): 1882-96.

Gandy, S., A. J. Czernik, et al. (1988). "Phosphorylation of Alzheimer disease amyloid precursor peptide by protein kinase C and Ca2+/calmodulin-dependent protein kinase II." Proc Natl Acad Sci U S A **85**(16): 6218-21.

Gervais, F. G., D. Xu, et al. (1999). "Involvement of caspases in proteolytic cleavage of Alzheimer's amyloid-beta precursor protein and amyloidogenic A beta peptide formation." Cell **97**(3): 395-406.

Gottipati, S., N. L. Rao, et al. (2008). "IRAK1: a critical signaling mediator of innate immunity." Cell Signal **20**(2): 269-76.

Gralle, M., M. G. Botelho, et al. (2009). "Neuroprotective secreted amyloid precursor protein acts by disrupting amyloid precursor protein dimers." J Biol Chem **284**(22): 15016-25.

Grear, K. E., I. F. Ling, et al. (2009). "Expression of SORL1 and a novel SORL1 splice variant in normal and Alzheimers disease brain." Mol Neurodegener **4**: 46.

Greenfield, J. P., J. Tsai, et al. (1999). "Endoplasmic reticulum and trans-Golgi network generate distinct populations of Alzheimer beta-amyloid peptides." Proc Natl Acad Sci U S A **96**(2): 742-7.

Guenette, S. Y., J. Chen, et al. (1999). "hFE65L influences amyloid precursor protein maturation

and secretion." J Neurochem **73**(3): 985-93.

Gustafsen, C., S. Glerup, et al. (2013). "Sortilin and SorLA display distinct roles in processing and trafficking of amyloid precursor protein." J Neurosci **33**(1): 64-71.

Haass, C., E. H. Koo, et al. (1995). "Polarized sorting of beta-amyloid precursor protein and its proteolytic products in MDCK cells is regulated by two independent signals." J Cell Biol **128**(4): 537-47.

Haass, C. and H. Steiner (2002). "Alzheimer disease gamma-secretase: a complex story of GxGD-type presenilin proteases." Trends Cell Biol **12**(12): 556-62.

Haghayeghi, A., A. Sarac, et al. (2010). "Pellino enhances innate immunity in Drosophila." Mech Dev **127**(5-6): 301-7.

Hardy, J. and D. J. Selkoe (2002). "The amyloid hypothesis of Alzheimer's disease: progress and problems on the road to therapeutics." Science **297**(5580): 353-6.

Hardy, J. A. and G. A. Higgins (1992). "Alzheimer's disease: the amyloid cascade hypothesis." Science **256**(5054): 184-5.

Hunter, T. (1998). "The Croonian Lecture 1997. The phosphorylation of proteins on tyrosine: its role in cell growth and disease." Philos Trans R Soc Lond B Biol Sci **353**(1368): 583-605.

Huse, J. T., K. Liu, et al. (2002). "Beta-secretase processing in the trans-Golgi network preferentially generates truncated amyloid species that accumulate in Alzheimer's disease brain." J Biol Chem **277**(18): 16278-84.

Huse, J. T., D. S. Pijak, et al. (2000). "Maturation and endosomal targeting of beta-site amyloid precursor protein-cleaving enzyme. The Alzheimer's disease beta-secretase." J Biol Chem **275**(43): 33729-37.

Iijima, K., K. Ando, et al. (2000). "Neuron-specific phosphorylation of Alzheimer's beta-amyloid precursor protein by cyclin-dependent kinase 5." J Neurochem **75**(3): 1085-91.

Jencks, W. P. (1981). "On the attribution and additivity of binding energies." Proc Natl Acad Sci U S A **78**(7): 4046-50.

Jorissen, E., J. Prox, et al. (2010). "The disintegrin/metalloproteinase ADAM10 is essential for the establishment of the brain cortex." J Neurosci **30**(14): 4833-44.

Kamenetz, F., T. Tomita, et al. (2003). "APP processing and synaptic function." Neuron **37**(6): 925-37.

Kang, C. B., Y. Hong, et al. (2008). "FKBP family proteins: immunophilins with versatile biological functions." Neurosignals **16**(4): 318-25.

Kay, B. K., M. P. Williamson, et al. (2000). "The importance of being proline: the interaction of proline-rich motifs in signaling proteins with their cognate domains." FASEB J **14**(2): 231-41.

Kim, J. H., K. S. Sung, et al. (2011). "Pellino-1, an adaptor protein of interleukin-1 receptor/toll-like receptor signaling, is sumoylated by Ubc9." Mol Cells **31**(1): 85-9.

Kimberly, W. T., J. B. Zheng, et al. (2005). "Physiological regulation of the beta-amyloid precursor protein signaling domain by c-Jun N-terminal kinase JNK3 during neuronal differentiation." J Neurosci **25**(23): 5533-43.

King, G. D., R. G. Perez, et al. (2003). "X11alpha modulates secretory and endocytic trafficking and metabolism of amyloid precursor protein: mutational analysis of the YENPTY sequence." Neuroscience **120**(1): 143-54.

Kingsley, D. M., K. F. Kozarsky, et al. (1986). "Reversible defects in O-linked glycosylation and LDL receptor expression in a UDP-Gal/UDP-GalNAc 4-epimerase deficient mutant." Cell **44**(5): 749-59.

Kobayashi, M., S. Saitoh, et al. (2006). "Regulatory roles for MD-2 and TLR4 in ligand-induced receptor clustering." J Immunol **176**(10): 6211-8.

Kollewe, C., A. C. Mackensen, et al. (2004). "Sequential autophosphorylation steps in the interleukin-1 receptor-associated kinase-1 regulate its availability as an adapter in interleukin-1 signaling." J Biol Chem **279**(7): 5227-36.

Kouchi, Z., H. Sorimachi, et al. (1999). "Proteasome inhibitors induce the association of Alzheimer's amyloid precursor protein with Hsc73." Biochem Biophys Res Commun **254**(3): 804-10.

Kovacs, D. M., H. J. Fausett, et al. (1996). "Alzheimer-associated presenilins 1 and 2: neuronal expression in brain and localization to intracellular membranes in mammalian cells." Nat Med **2**(2): 224-9.

Krishnamurthy, S., M. A. Ghazy, et al. (2009). "Functional interaction of the Ess1 prolyl isomerase with components of the RNA polymerase II initiation and termination machineries." Mol Cell Biol **29**(11): 2925-34.

Kumar, P., R. K. Ambasta, et al. (2007). "CHIP and HSPs interact with -APP in a proteasome-dependent manner and influence A metabolism." Human molecular genetics **16**(7): 848.

Lai, A., S. S. Sisodia, et al. (1995). "Characterization of sorting signals in the beta-amyloid precursor protein cytoplasmic domain." J Biol Chem **270**(8): 3565-73.

Lane, R. F., S. M. Raines, et al. (2010). "Diabetes-associated SorCS1 regulates Alzheimer's amyloid-beta metabolism: evidence for involvement of SorL1 and the retromer complex." J Neurosci **30**(39): 13110-5.

Lee, J., C. Retamal, et al. (2008). "Adaptor protein sorting nexin 17 regulates amyloid precursor protein trafficking and processing in the early endosomes." J Biol Chem **283**(17): 11501-8.

Lee, J. H., R. Cheng, et al. (2007). "The association between genetic variants in SORL1 and Alzheimer disease in an urban, multiethnic, community-based cohort." Arch Neurol **64**(4): 501-6.

Lee, M. S., S. C. Kao, et al. (2003). "APP processing is regulated by cytoplasmic phosphorylation." J Cell Biol **163**(1): 83-95.

Lehninger, N. and M. M. Nelson (2008). Cox, Principles of Biochemistry, WH Freeman & Co., New York.

Lesne, S., M. T. Koh, et al. (2006). "A specific amyloid-beta protein assembly in the brain impairs memory." Nature **440**(7082): 352-7.

Lian, Q., C. J. Ladner, et al. (2001). "Selective changes of calcineurin (protein phosphatase 2B) activity in Alzheimer's disease cerebral cortex." Exp Neurol **167**(1): 158-65.

Lin, C. C., Y. S. Huoh, et al. (2008). "Pellino proteins contain a cryptic FHA domain that

mediates interaction with phosphorylated IRAK1." Structure **16**(12): 1806-16.

Lin, S. C., Y. C. Lo, et al. (2010). "Helical assembly in the MyD88-IRAK4-IRAK2 complex in TLR/IL-1R signalling." Nature **465**(7300): 885-90.

Lu, K. P., S. D. Hanes, et al. (1996). "A human peptidyl-prolyl isomerase essential for regulation of mitosis." Nature **380**(6574): 544-7.

Lu, K. P. and X. Z. Zhou (2007). "The prolyl isomerase PIN1: a pivotal new twist in phosphorylation signalling and disease." Nat Rev Mol Cell Biol **8**(11): 904-16.

Ma, S. L., L. Pastorino, et al. (2012). "Prolyl isomerase Pin1 promotes amyloid precursor protein (APP) turnover by inhibiting glycogen synthase kinase-3beta (GSK3beta) activity: novel mechanism for Pin1 to protect against Alzheimer disease." J Biol Chem **287**(10): 6969-73.

MacArthur, M. W. and J. M. Thornton (1991). "Influence of proline residues on protein conformation." J Mol Biol **218**(2): 397-412.

Mammen, M., S.-K. Choi, et al. (1998). "Polyvalent interactions in biological systems: implications for design and use of multivalent ligands and inhibitors." Angewandte Chemie International Edition **37**(20): 2754-2794.

Manning, G., D. B. Whyte, et al. (2002). "The protein kinase complement of the human genome." Science **298**(5600): 1912-34.

Martin, B. L., G. Schrader-Fischer, et al. (1995). "Intracellular accumulation of beta-amyloid in cells expressing the Swedish mutant amyloid precursor protein." J Biol Chem **270**(45): 26727-30.

Massey, A. C., C. Zhang, et al. (2006). "Chaperone-mediated autophagy in aging and disease." Current topics in developmental biology **73**: 205-235.

Matsuda, S., T. Yasukawa, et al. (2001). "c-Jun N-terminal kinase (JNK)-interacting protein-1b/islet-brain-1 scaffolds Alzheimer's amyloid precursor protein with JNK." J Neurosci **21**(17): 6597-607.

Mattson, M. P. (1997). "Cellular actions of beta-amyloid precursor protein and its soluble and fibrillogenic derivatives." Physiol Rev **77**(4): 1081-132.

Mayer, M. P. (2013). "Hsp70 chaperone dynamics and molecular mechanism." Trends Biochem Sci **38**(10): 507-14.

Moresco, E. M., D. LaVine, et al. (2011). "Toll-like receptors." Curr Biol **21**(13): R488-93.

Mori, S., C. Abeygunawardana, et al. (1995). "Improved sensitivity of HSQC spectra of exchanging protons at short interscan delays using a new fast HSQC (FHSQC) detection scheme that avoids water saturation." J Magn Reson B **108**(1): 94-8.

Morley, J. E., S. A. Farr, et al. (2010). "A physiological role for amyloid-beta protein:enhancement of learning and memory." J Alzheimers Dis **19**(2): 441-9.

Mucke, L. and D. J. Selkoe (2012). "Neurotoxicity of amyloid beta-protein: synaptic and network dysfunction." Cold Spring Harb Perspect Med **2**(7): a006338.

Mueller, J. W. and P. Bayer (2008). "Small family with key contacts: par14 and par17 parvulin proteins, relatives of pin1, now emerge in biomedical research." Perspect Medicin Chem **2**: 11-20.

Nicholson, L. K. and S. De (2011). "Structural biology: The twist in Crk signaling revealed." Nat Chem Biol **7**(1): 5-6.

Nikolaev, A., T. McLaughlin, et al. (2009). "APP binds DR6 to trigger axon pruning and neuron death via distinct caspases." Nature **457**(7232): 981-9.

Oishi, M., A. C. Nairn, et al. (1997). "The cytoplasmic domain of Alzheimer's amyloid precursor protein is phosphorylated at Thr654, Ser655, and Thr668 in adult rat brain and cultured cells." Mol Med **3**(2): 111-23.

Opdenakker, G., P. M. Rudd, et al. (1993). "Concepts and principles of glycobiology." FASEB J **7**(14): 1330-7.

Pahlsson, P., S. H. Shakin-Eshleman, et al. (1992). "N-linked glycosylation of beta-amyloid precursor protein." Biochem Biophys Res Commun **189**(3): 1667-73.

Pahlsson, P. and S. L. Spitalnik (1996). "The role of glycosylation in synthesis and secretion of beta-amyloid precursor protein by Chinese hamster ovary cells." Arch Biochem Biophys **331**(2): 177-86.

Papin, J. A., T. Hunter, et al. (2005). "Reconstruction of cellular signalling networks and analysis of their properties." Nat Rev Mol Cell Biol **6**(2): 99-111.

Pasternak, S. H., R. D. Bagshaw, et al. (2003). "Presenilin-1, nicastrin, amyloid precursor protein, and gamma-secretase activity are co-localized in the lysosomal membrane." J Biol Chem **278**(29): 26687-94.

Pasternak, S. H., J. W. Callahan, et al. (2004). "The role of the endosomal/lysosomal system in amyloid-beta production and the pathophysiology of Alzheimer's disease: reexamining the spatial paradox from a lysosomal perspective." J Alzheimers Dis **6**(1): 53-65.

Perreau, V. M., S. Orchard, et al. (2010). "A domain level interaction network of amyloid precursor protein and Abeta of Alzheimer's disease." Proteomics **10**(12): 2377-95.

Podlisny, M. B., B. L. Ostaszewski, et al. (1995). "Aggregation of secreted amyloid beta-protein into sodium dodecyl sulfate-stable oligomers in cell culture." J Biol Chem **270**(16): 9564-70.

Puzzo, D., L. Privitera, et al. (2008). "Picomolar amyloid-beta positively modulates synaptic plasticity and memory in hippocampus." J Neurosci **28**(53): 14537-45.

Ramelot, T. A., L. N. Gentile, et al. (2000). "Transient structure of the amyloid precursor protein cytoplasmic tail indicates preordering of structure for binding to cytosolic factors." Biochemistry **39**(10): 2714-25.

Ramelot, T. A. and L. K. Nicholson (2001). "Phosphorylation-induced structural changes in the amyloid precursor protein cytoplasmic tail detected by NMR." J Mol Biol **307**(3): 871-84.

Ranganathan, R., K. P. Lu, et al. (1997). "Structural and functional analysis of the mitotic rotamase Pin1 suggests substrate recognition is phosphorylation dependent." Cell **89**(6): 875-86.

Raychaudhuri, M. and D. Mukhopadhyay (2007). "AICD and its adaptors - in search of new players." J Alzheimers Dis **11**(3): 343-58.

Reimer, U., G. Scherer, et al. (1998). "Side-chain effects on peptidyl-prolyl cis/trans isomerisation." J Mol Biol **279**(2): 449-60.

Remaley, A. T., M. Ugorski, et al. (1991). "Expression of human glycophorin A in wild type and

glycosylation-deficient Chinese hamster ovary cells. Role of N- and O-linked glycosylation in cell surface expression." J Biol Chem **266**(35): 24176-83.

Ring, S., S. W. Weyer, et al. (2007). "The secreted beta-amyloid precursor protein ectodomain APPs alpha is sufficient to rescue the anatomical, behavioral, and electrophysiological abnormalities of APP-deficient mice." J Neurosci **27**(29): 7817-26.

Rogaeva, E., Y. Meng, et al. (2007). "The neuronal sortilin-related receptor SORL1 is genetically associated with Alzheimer disease." Nat Genet **39**(2): 168-77.

Saito, Y., Y. Sano, et al. (2008). "X11 proteins regulate the translocation of amyloid beta-protein precursor (APP) into detergent-resistant membrane and suppress the amyloidogenic cleavage of APP by beta-site-cleaving enzyme in brain." J Biol Chem **283**(51): 35763-71.

Sansom, M. S. and H. Weinstein (2000). "Hinges, swivels and switches: the role of prolines in signalling via transmembrane alpha-helices." Trends Pharmacol Sci **21**(11): 445-51.

Santos, S. F., B. Tasiaux, et al. (2011). "Inhibition of neuronal calcium oscillations by cell surface APP phosphorylated on T668." Neurobiol Aging.

Sarkar, P., T. Saleh, et al. (2011). "Structural basis for regulation of the Crk signaling protein by a proline switch." Nat Chem Biol **7**(1): 51-7.

Sastre, M., H. Steiner, et al. (2001). "Presenilin-dependent gamma-secretase processing of beta-amyloid precursor protein at a site corresponding to the S3 cleavage of Notch." EMBO Rep **2**(9): 835-41.

Scheinfeld, M. H., R. Roncarati, et al. (2002). "Jun NH2-terminal kinase (JNK) interacting protein 1 (JIP1) binds the cytoplasmic domain of the Alzheimer's beta-amyloid precursor protein (APP)." J Biol Chem **277**(5): 3767-75.

Schmidt, V., A. Sporbert, et al. (2007). "SorLA/LR11 regulates processing of amyloid precursor protein via interaction with adaptors GGA and PACS-1." J Biol Chem **282**(45): 32956-64.

Selkoe, D. J. (1998). "The cell biology of beta-amyloid precursor protein and presenilin in Alzheimer's disease." Trends Cell Biol **8**(11): 447-53.

Seubert, P., T. Oltersdorf, et al. (1993). "Secretion of beta-amyloid precursor protein cleaved at

the amino terminus of the beta-amyloid peptide." Nature **361**(6409): 260-3.

Seubert, P., C. Vigo-Pelfrey, et al. (1992). "Isolation and quantification of soluble Alzheimer's beta-peptide from biological fluids." Nature **359**(6393): 325-7.

Shankar, G. M., S. Li, et al. (2008). "Amyloid-beta protein dimers isolated directly from Alzheimer's brains impair synaptic plasticity and memory." Nat Med **14**(8): 837-42.

Shankar, G. M. and D. M. Walsh (2009). "Alzheimer's disease: synaptic dysfunction and Abeta." Mol Neurodegener **4**: 48.

Shin, R. W., T. C. Saido, et al. (2005). "Novel alpha-secretase cleavage of Alzheimer's amyloid beta precursor protein in the endoplasmic reticulum of COS7 cells." Neurosci Lett **376**(1): 14-9.

Shin, Y., J. Klucken, et al. (2005). "The co-chaperone carboxyl terminus of Hsp70-interacting protein (CHIP) mediates alpha-synuclein degradation decisions between proteasomal and lysosomal pathways." J Biol Chem **280**(25): 23727-34.

Shoji, M., T. E. Golde, et al. (1992). "Production of the Alzheimer amyloid beta protein by normal proteolytic processing." Science **258**(5079): 126-9.

Sinha, S., J. P. Anderson, et al. (1999). "Purification and cloning of amyloid precursor protein beta-secretase from human brain." Nature **402**(6761): 537-40.

Sisodia, S. S. (1992). "Beta-amyloid precursor protein cleavage by a membrane-bound protease." Proc Natl Acad Sci U S A **89**(13): 6075-9.

Sodhi, C. P., R. G. Perez, et al. (2008). "Phosphorylation of beta-amyloid precursor protein (APP) cytoplasmic tail facilitates amyloidogenic processing during apoptosis." Brain Res **1198**: 204-12.

Sodhi, C. P., S. Rampalli, et al. (2004). "The endocytotic pathway is required for increased A beta 42 secretion during apoptosis." Brain Res Mol Brain Res **128**(2): 201-11.

Spoelgen, R., C. A. von Arnim, et al. (2006). "Interaction of the cytosolic domains of sorLA/LR11 with the amyloid precursor protein (APP) and beta-secretase beta-site APP-cleaving enzyme." J Neurosci **26**(2): 418-28.

Stukenberg, P. T. and M. W. Kirschner (2001). "Pin1 acts catalytically to promote a conformational change in Cdc25." Mol Cell **7**(5): 1071-83.

Sullivan, S. E., G. M. Dillon, et al. (2014). "Mint proteins are required for synaptic activity-dependent amyloid precursor protein (APP) trafficking and amyloid beta generation." J Biol Chem **289**(22): 15374-83.

Sumioka, A., S. Nagaishi, et al. (2005). "Role of 14-3-3gamma in FE65-dependent gene transactivation mediated by the amyloid beta-protein precursor cytoplasmic fragment." J Biol Chem **280**(51): 42364-74.

Suzuki, N., T. T. Cheung, et al. (1994). "An increased percentage of long amyloid beta protein secreted by familial amyloid beta protein precursor (beta APP717) mutants." Science **264**(5163): 1336-40.

Takahashi, K., T. Niidome, et al. (2008). "Phosphorylation of amyloid precursor protein (APP) at Tyr687 regulates APP processing by alpha- and gamma-secretase." Biochem Biophys Res Commun **377**(2): 544-9.

Tarr, P. E., R. Roncarati, et al. (2002). "Tyrosine phosphorylation of the beta-amyloid precursor protein cytoplasmic tail promotes interaction with Shc." J Biol Chem **277**(19): 16798-804.

Taru, H., K. Yoshikawa, et al. (2004). "Suppression of the caspase cleavage of beta-amyloid precursor protein by its cytoplasmic phosphorylation." FEBS Lett **567**(2-3): 248-52.

Tomita, S., Y. Kirino, et al. (1998). "Cleavage of Alzheimer's amyloid precursor protein (APP) by secretases occurs after O-glycosylation of APP in the protein secretory pathway. Identification of intracellular compartments in which APP cleavage occurs without using toxic agents that interfere with protein metabolism." J Biol Chem **273**(11): 6277-84.

Tun-Kyi, A., G. Finn, et al. (2011). "Essential role for the prolyl isomerase Pin1 in Toll-like receptor signaling and type I interferon-mediated immunity." Nat Immunol **12**(8): 733-41.

Ubersax, J. A. and J. E. Ferrell, Jr. (2007). "Mechanisms of specificity in protein phosphorylation." Nat Rev Mol Cell Biol **8**(7): 530-41.

van der Kant, R. and L. S. Goldstein (2015). "Cellular functions of the amyloid precursor protein from development to dementia." Dev Cell **32**(4): 502-15.

Vassar, R., B. D. Bennett, et al. (1999). "Beta-secretase cleavage of Alzheimer's amyloid precursor protein by the transmembrane aspartic protease BACE." Science **286**(5440): 735-41.

Vieira, S. I., S. Rebelo, et al. "Retrieval of the Alzheimer's amyloid precursor protein from the endosome to the TGN is S655 phosphorylation state-dependent and retromer-mediated." Mol Neurodegener **5**: 40.

Vingtdeux, V., M. Hamdane, et al. (2007). "Alkalizing drugs induce accumulation of amyloid precursor protein by-products in luminal vesicles of multivesicular bodies." Journal of Biological Chemistry **282**(25): 18197.

Vogelsberg-Ragaglia, V., T. Schuck, et al. (2001). "PP2A mRNA expression is quantitatively decreased in Alzheimer's disease hippocampus." Exp Neurol **168**(2): 402-12.

Walsh, D. M., I. Klyubin, et al. (2002). "Naturally secreted oligomers of amyloid beta protein potently inhibit hippocampal long-term potentiation in vivo." Nature **416**(6880): 535-9.

Walsh, D. M., B. P. Tseng, et al. (2000). "The oligomerization of amyloid beta-protein begins intracellularly in cells derived from human brain." Biochemistry **39**(35): 10831-9.

Walter, J., R. Fluhrer, et al. (2001). "Phosphorylation regulates intracellular trafficking of beta-secretase." J Biol Chem **276**(18): 14634-41.

Wang, P. and J. Heitman (2005). "The cyclophilins." Genome Biol **6**(7): 226.

Wang, S., F. Cesca, et al. "Synapsin I is an oligomannose-carrying glycoprotein, acts as an oligomannose-binding lectin, and promotes neurite outgrowth and neuronal survival when released via glia-derived exosomes." J Neurosci **31**(20): 7275-90.

Wedemeyer, W. J., X. Xu, et al. (2002). "Conformational propensities of protein folding intermediates: distribution of species in the 1S, 2S, and 3S ensembles of the [C40A,C95A] mutant of bovine pancreatic ribonuclease A." Biochemistry **41**(5): 1483-91.

Weidemann, A., S. Eggert, et al. (2002). "A novel epsilon-cleavage within the transmembrane domain of the Alzheimer amyloid precursor protein demonstrates homology with Notch processing." Biochemistry **41**(8): 2825-35.

Wesche, H., X. Gao, et al. (1999). "IRAK-M is a novel member of the Pelle/interleukin-1 receptor-associated kinase (IRAK) family." J Biol Chem **274**(27): 19403-10.

Yaffe, M. B., M. Schutkowski, et al. (1997). "Sequence-specific and phosphorylation-dependent proline isomerization: a potential mitotic regulatory mechanism." Science **278**(5345): 1957-60.

Yan, R., M. J. Bienkowski, et al. (1999). "Membrane-anchored aspartyl protease with Alzheimer's disease beta-secretase activity." Nature **402**(6761): 533-7.

Yankner, B. A. and T. Lu (2009). "Amyloid beta-protein toxicity and the pathogenesis of Alzheimer disease." J Biol Chem **284**(8): 4755-9.

Zambrano, N., J. D. Buxbaum, et al. (1997). "Interaction of the phosphotyrosine interaction/phosphotyrosine binding-related domains of Fe65 with wild-type and mutant Alzheimer's beta-amyloid precursor proteins." J Biol Chem **272**(10): 6399-405.

Zhang, Y. W., R. Thompson, et al. (2011). "APP processing in Alzheimer's disease." Mol Brain **4**: 3.

Zhao, G., G. Mao, et al. (2004). "Identification of a new presenilin-dependent zeta-cleavage site within the transmembrane domain of amyloid precursor protein." J Biol Chem **279**(49): 50647-50.

Zhao, G., J. Tan, et al. (2007). "The same gamma-secretase accounts for the multiple intramembrane cleavages of APP." J Neurochem **100**(5): 1234-46.

Zheng, H., M. Jiang, et al. (1995). "beta-Amyloid precursor protein-deficient mice show reactive gliosis and decreased locomotor activity." Cell **81**(4): 525-31.

CHAPTER 2

THE SENSITIVITY OF THE INTERACTION OF HSP70 SBD AND APP_C TO PHOSPHORYLATION OF THR668[1]

ABSTRACT

Alzheimer's disease (AD) is a neurodegenerative disease that affects one third of people age 85 and older. On a molecular level it is characterized in part by increased amyloidogenic processing of the transmembrane amyloid precursor protein (APP), resulting in the release of toxic product amyloid-beta (Aβ). In AD brains, APP has been shown to be phosphorylated at T668 (pT668) and pT668 has been associated with increased Aβ generation. Additionally, neurodegenerative diseases are strongly associated with inadequacies in the molecular chaperone system of the aging cell. Molecular chaperones play a role in the degradation of intramembrane proteins. If some APP were degraded rather than proteolytically processed, it may reduce formation of Aβ. It

[1]This chapter has been adapted from Rogals MJ, Resnick RJ, Nicholson LK (2016). The sensitivity of the interaction of Hsp70 SBD and APPc to phosphorylation of Thr668. Will be submitted to PLOS ONE.

has been shown that an increased APP stability increases the production of Aβ in cell models. APP co-immunoprecipitates with the Heat Shock Protein (HSP) family member Hsc70, which shares 89% identity with Hsp70 for the section of the substrate binding domain (SBD) used in this study. Hsc70 is a constitutive chaperone, but Hsp70 is a stress-induced HSP70 family member, which may be more analogous to condition of the AD brain. Pull-down experiments were conducted in H4 neuroglioma whole cell lysate using synthetic, biotinylated peptides derived from the cytosolic fragment of APP (APPc) either with or without pT668. Depending on the length of the APPc-derived peptide, the interaction was attenuated in the case of pT668. Using a series of HSQC spectra of ^{15}N-labeled cytosolic tail of APP (APPc), we identified the binding area for Hsp70 substrate binding domain (SBD) as a region on APPc from T654 to L674 (APP695 numbering). Titration series of HSQCs of ^{15}N-labeled Hsp70 with APPc-derived peptides (T668 or pT668) recapitulated the sensitivity to phosphorylation of the shorter peptide. This loss of sensitivity in the pulldown experiments with longer peptide could be due to the complex mixture of potential APPc binding partners present in whole cell lysate. Using pulldown titrations and semi-quantitative western blots with the longer APPc-derived peptide, an upper bound of the binding affinity for the interaction of APPc and Hsp70 has been determined. These and further studies on the interaction between the APPc and HSP70 family members may elucidate the possible connection between APPc interaction with molecular chaperones and APP degradation prior to proteolytic processing, which would in turn decrease a toxic product associated with AD progression.

INTRODUCTION

In the US, approximately one third of people age 85 and older have Alzheimer's disease (AD), a progressive, neurodegenerative disorder beginning with short-term memory loss and followed by increasing cognitive dysfunction (Association. 2016). AD costs an estimated 236 billion dollars a year and with a rapidly growing elderly population the expenditure is estimated to increase to 1.1 trillion dollars by 2050. The emotional costs for both the patient and caregivers cannot be measured. There are two molecular hallmarks of AD: neurofibrillary tangles and plaques. The plaques are made of Amyloidβ peptide (Aβ), which is a proteolyzed fragment of the amyloid precursor protein (APP) (Glenner and Wong 1984; Masters, Simms et al. 1985). APP is strongly indicated as a causative agent in AD as mutations in either APP itself (Chartier-Harlin, Crawford et al. 1991; Goate, Chartier-Harlin et al. 1991; Mullan, Crawford et al. 1992) or in one of the Presenilin (PS) (Scheuner, Eckman et al. 1996; Hardy and Crook 2001) proteins, which are involved in the processing of APP, are found in the majority of Familial AD patients. Down syndrome, resulting from an extra copy of chromosome 21, which contains the APP gene, almost inevitably results in early-onset AD (Mann 1988; Theuns, Brouwers et al. 2006), the exception being partial trisomy 21, where the portion of the chromosome containing APP is not present in triplicate (Prasher, Farrer et al. 1998).

APP is a type 1 transmembrane protein that undergoes proteolytic processing. There are two processing pathways leading to the generation of two sets of distinct, biologically active fragments. Which fate the APP undergoes is largely determined by where it is trafficked and the residence time in particular membranes (Zhi, Chia et al. 2011; van der Kant and Goldstein 2015). The non-amyloidogenic processing pathway starts with α-secretase cleavage of APP (Buxbaum, Liu et al. 1998; Jorissen, Prox et al. 2010). The ectodomain (secretedAPPα or sAPPα), which has

neuroprotective capabilities (Furukawa, Sopher et al. 1996; Mattson 1997; Bour, Little et al. 2004; Ring, Weyer et al. 2007; Young-Pearse, Chen et al. 2008), is released into the extracellular matrix (Esch, Keim et al. 1990). Next, γ-secretase, a transmembrane complex, cleaves within the lipid bilayer (Haass and Steiner 2002) leading to the release of fragment P3 into the extracellular matrix (Zhao, Tan et al. 2007). The remaining fragment, Amyloid intracellular domain (AICD), is embedded in the membrane and trails into the cytosol (Zhang, Thompson et al. 2011). The amyloidogenic pathway begins with β-secretase cleavage of APP (Sinha, Anderson et al. 1999; Vassar, Bennett et al. 1999; Yan, Bienkowski et al. 1999), producing secreted APPβ (sAPPβ) (Nikolaev, McLaughlin et al. 2009). The second cleavage event is again mediated by γ-secretase. The product released into the extracellular matrix, Aβ, contributes to altered synaptic function (Podlisny, Ostaszewski et al. 1995; Walsh, Tseng et al. 2000; Walsh, Klyubin et al. 2002; Lesne, Koh et al. 2006). Aβ is the major component of the insoluble plaques that accumulate in many AD brains (Selkoe 1998; Shankar and Walsh 2009). Both processing pathways occur in a healthy individual, but they are tightly regulated (Seubert, Vigo-Pelfrey et al. 1992; Shoji, Golde et al. 1992). If mis-regulation occurs, for instance changing the relative amounts of processing through each pathway, there could be pathologic buildup of Aβ (Puzzo, Privitera et al. 2008; Shankar and Walsh 2009; Morley, Farr et al. 2010).

Regardless of the processing pathway, the primarily cytosolic fragment of APP, the AICD, remains after γ-secretase cleavage. The cytosolic portion of the AICD or the full length APP or the partially processed C-terminal fragments will be referred to from this point of as APPc (Figure 2.1). The APPc plays a myriad of roles in the trafficking and/or processing of APP through its interaction with various proteins. Many studies on trafficking focus on changes to the phosphorylation state of the APPc (Takahashi, Niidome et al. 2008; Barbagallo, Weldon et al.

Figure 2.1 Sequence of APPc and peptides used in this study. A) The first sequence is the cytosolic tail of APP695 aka APPc (649-695). Under APPc are the APPc-derived peptides used in this study. Specifically the peptides used in the pulldown experiements ($APPc_{658-676}$ and $APPc_{657-687}$) and the NMR experiments ($APPc_{659-682}$).

2010) and the resultant effect on protein binding (Matsuda, Yasukawa et al. 2001; Tarr, Roncarati et al. 2002; Cavalli, Kujala et al. 2005), particularly the phosphorylation of seven sites that were observed in slices of AD patients' brains (Oishi, Nairn et al. 1997; Lee, Kao et al. 2003). One of these phosphorylation sites is a threonine directly preceding a proline. There is ample evidence suggesting that phosphorylation of APPc at T668 may impact AD progression (Lee, Kao et al. 2003; Sodhi, Rampalli et al. 2004; Colombo, Repici et al. 2007; Sodhi, Perez et al. 2008).

Phosphorylation of T668 has a measurable, structural impact on the AICD, and it is the only phosphorylation site known to induce such changes in the AICD (Ramelot, Gentile et al. 2000; Ramelot and Nicholson 2001). T668 phosphorylation leads to a destabilization of a transient helix capping box (Ramelot, Gentile et al. 2000). Loss of the hydrogen-bonding implicit in that capping box allows the T668-P669 peptide bond to sample not only the common *trans* (ω=180º) (Fanghanel 2003), but also the far more uncommon *cis* (ω=0º) (Fanghanel 2003) conformations (Ramelot, Gentile et al. 2000).

A combination of proteomic studies (Colangelo, Schurr et al. 2002; Bai, Markham et al. 2008; Di Domenico, Sultana et al. 2011) and more classical binding studies have produced an interactome for APP (Perreau, Orchard et al. 2010). Several cytosolic members of this interactome have been implicated in trafficking of APPc including X11 (King, Perez et al. 2003), Fe65 (Guenette, Chen et al. 1999), JIP (Scheinfeld, Roncarati et al. 2002; Fu and Holzbaur 2013), SorLa (Spoelgen, von Arnim et al. 2006; Schmidt, Sporbert et al. 2007; Vieira, Rebelo et al. 2010) and PAT1(Raychaudhuri and Mukhopadhyay 2007). Of these, only Fe65 is known to be affected by T668-P669 and it has been well-studied (Chang, Kim et al. 2006). There is, however, a family of proteins that could impact AD, bind to APPc at T668-P669 and be sensitive

to the phosphorylation state of T668 upon binding to APPc. They are molecular chaperones and more specifically members of the heat shock protein 70 kDa (HSP70) family.

Multiple HSP70 family members are upregulated during AD (Shin, Klucken et al. 2005; Elliott, Laufer et al. 2009) and have diverse, protective cellular functions. Some have a known interaction with APP. APP and Hsc70 (heat shock cognate 70) have been shown to co-IP in differentiating oligodendrocytes (Kouchi, Sorimachi et al. 1999). Through a series of C-terminal truncations of APP, the region sufficient to co-IP with Hsc70 has been narrowed down to K649-N680 on the APPc (APP695 isoform numbering, which will be used for the rest of this study). Deletions of the residues of APPc N-terminal to the minimal binding site were not conducted, leaving the actual position of the minimal binding site undetermined (Kouchi, Sorimachi et al. 1999). Hsc70 expression is also upregulated in Alzheimer's disease brains (Elliott, Laufer et al. 2009). While Hsc70 interacts with hydrophobic regions of unfolded protein, it also interacts with a loose signal motif containing both acidic and basic residues and conducts proteins containing said motif to the lysosome, resulting in chaperone-mediated autophagy (CMA) (Massey, Zhang et al. 2006). Hsc70 may use CMA to degrade a portion of the APPc or even full-length APP, though this would require APP dislocation from the membrane through a system like ERAD (ER-associated degradation) (Hirsch, Jarosch et al. 2004). Hsc70 is also a marker of exosomes (Wang, Cesca et al.), and APP has been both localized to the luminal vesicles (i.e. precursors of exosomes) in multi-vesicular bodies (Lee, Kao et al. 2003) and APP and its proteolytically processed constituents have been found in purified exosomes (Vingtdeux, Hamdane et al. 2007). Hsc70 is a constitutively expressed molecular chaperone nearly identical in substrate binding domain sequence to Hsp70, which is primarily induced upon stress (Elliott, Laufer et al. 2009).

Hsp70 is a major stress-induced heat shock protein in the cell (sharing 89% identity with

Hsc70 for the portion of the SBD used in the study as shown in Figure 2.2C) and it interacts with Chip, an E3 ubiquitin ligase (Shin, Klucken et al. 2005). Chip has been implicated in APP metabolism and is capable of ubiquitinating APP (Kumar, Ambasta et al. 2007). This could be a degradative signal for the APP, which does seem to respond to proteosomal inhibition (Colombo, Bastone et al. 2009). The ubiquitination could be of full-length APP which, following ERAD-like (Hirsch, Jarosch et al. 2004) mediated membrane dislocation, could be degraded via the proteosome. This could allow chaperone-bound APP to bypass regulated proteolytic processing in favor of degradation (i.e. decreased APP stability), which would decrease the amount of neurotoxic Aβ released into the extracellular matrix. Post-cleavage the AICD can be trafficked to the nucleus to regulate gene expression (Slomnicki and Lesniak 2008). In the nucleus, it has the potential to encounter another set of HSP70 family members, including Hsp70. Binding to HSP70 family members could alter its ability to regulate gene expression or target the AICD for destruction rather than allowing it to regulate gene expression. As molecular chaperones are present at increased concentrations in the brains of AD patients and they interact with APPc, and given that binding between APPc and Hsc70 occurs in a region that encompasses T668-P669 (Kouchi, Sorimachi et al. 1999), it is possible that the interaction of APPc and HSP70 family members is effected by T668-P669 phosphorylation and that interaction would likely influence APP trafficking, degradation or regulated proteolytic processing.

In this study we ascertain that multiple members of the HSP70 family, including Hsc70 and Hsp70, interact with varying degrees of affinity to biotinylated APPc-derived peptide, depending on the length of said peptide, via a pulldown using whole cell lysate. Also in this study we elucidate the binding site of Hsp70 on APPc. We then quantified the relative affinity for preferential binding of APPc to Hsp70 SBD that is unphosphorylated at T668. To further

Figure 2.2 HSP70 family members interact with APPc. A) a WB of a pulldown using $APPc_{658-676}$ either with a phosphorylated T668 or without phosphorylation in whole cell lysates from H4 neuroglioma cells. These are prominent members of the HSP70 family, these results were confirmed using mass spectrometry (not shown). This data was collected by Ross Resnick B) a WB of a pulldown using $APPc_{657-687}$ either with a phosphorylated T668 or without phosphorylation in whole cell lysates from H4 neuroglioma cells. This data was collected by Ross Resnick C) CLUSTAL Ω multiple sequence alignment of substrate binding domains (the portion corresponding to the construct used) of human Hsc70(hHsc70/HSPA8), human Bip(hBip/HSPA5), human Grp75(hGrp75/HSPA9), and *e.Coli* DNAK (DNAK e.Coli) to the substrate binding domain of human Hsp70(hHsp70/HSPA1A). The arrows represent β-strands and the rectangles represent α-helices from pdb 4PO2. The grey boxed letters correspond to residues that interact directly with substrate (Zhang, Marmorstein, 2014).

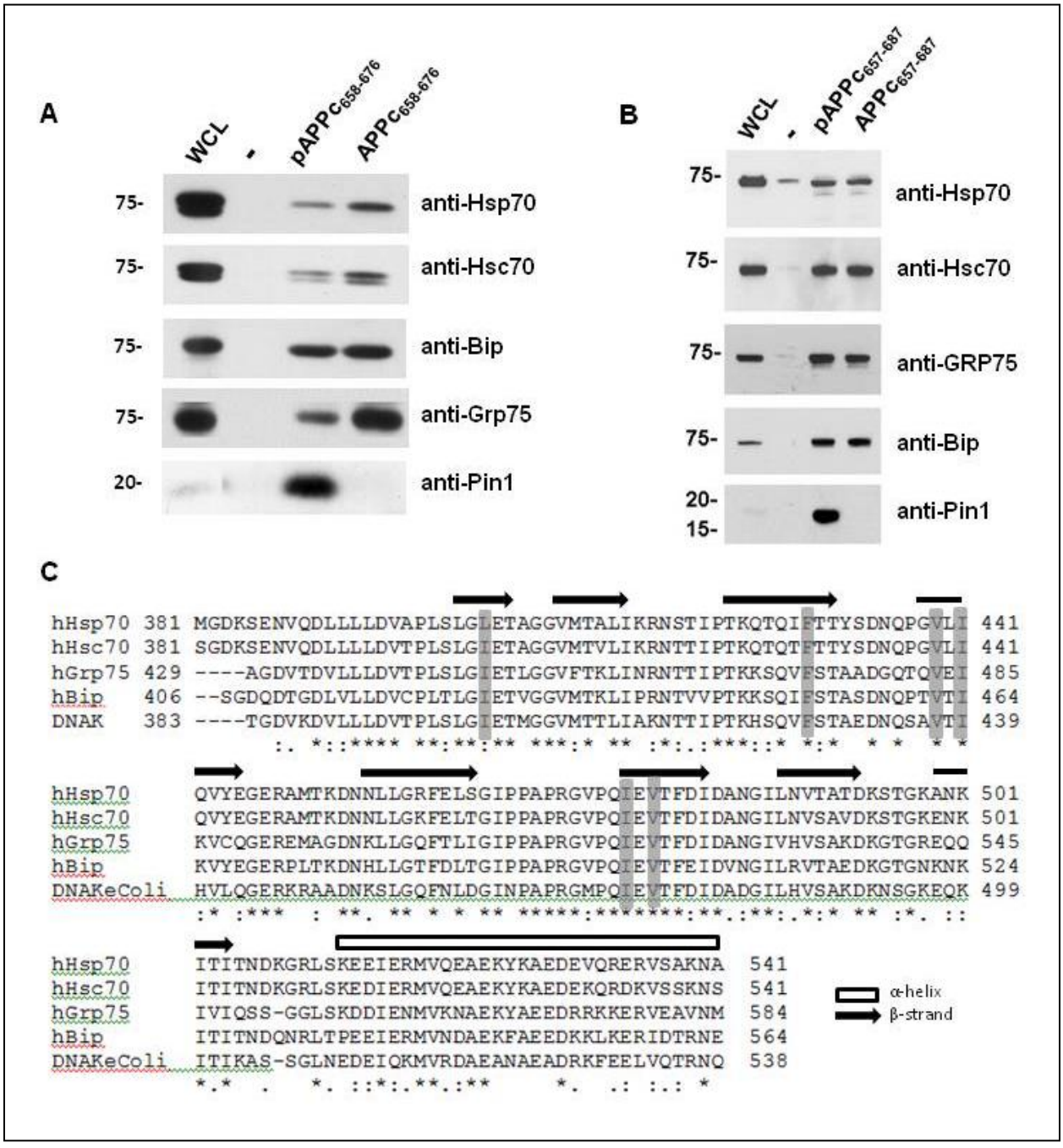
A
WCL
-
pAPPc658-676
APPc658-676
75-
anti-Hsp70
75-
anti-Hsc70
75-
anti-Bip
75-
anti-Grp75
20-
anti-Pin1
B
WCL
-
pAPPc657-687
APPc657-687
75-
anti-Hsp70
75-
anti-Hsc70
75-
anti-GRP75
75-
anti-Bip
20-
15-
anti-Pin1
C
hHsp70 381 MGDKSENVQDLLLLDVAPLSLGLETAGGVMTALIKRNSTIPTKQTQIFTTYSDNQPGVLI 441
hHsc70 381 SGDKSENVQDLLLLDVTPLSLGIETAGGVMTVLIKRNTTIPTKQTQTFTTYSDNQPGVLI 441
hGrp75 429 ----AGDVTDVLLLDVTPLSLGIETLGGVFTKLINRNTTIPTKKSQVFSTAADGQTQVEI 485
hBip 406 --SGDQDTGDLVLLDVCPLTLGIETVGGVMTKLIPRNTVVPTKKSQIFSTASDNQPTVTI 464
DNAK 383 ----TGDVKDVLLLDVTPLSLGIETMGGVMTTLIAKNTTIPTKHSQVFSTAEDNQSAVTI 439
hHsp70 QVYEGERAMTKDNNLLGRFELSGIPPAPRGVPQIEVTFDIDANGILNVTATDKSTGKANK 501
hHsc70 QVYEGERAMTKDNNLLGKFELTGIPPAPRGVPQIEVTFDIDANGILNVSAVDKSTGKENK 501
hGrp75 KVCQGEREMAGDNKLLGQFTLIGIPPAPRGVPQIEVTFDIDANGIVHVSAKDKGTGREQQ 545
hBip KVYEGERPLTKDNHLLGTFDLTGIPPAPRGVPQIEVTFEIDVNGILRVTAEDKGTGNKNK 524
DNAKeColi HVLQGERKRAADNKSLGQFNLDGINPAPRGMPQIEVTFDIDADGILHVSAKDKNSGKEQK 499
hHsp70 ITITNDKGRLSKEEIERMVQEAEKYKAEDEVQRERVSAKNA 541
hHsc70 ITITNDKGRLSKEDIERMVQEAEKYKAEDEKQRDKVSSKNS 541
hGrp75 IVIQSS-GGLSKDDIENMVKNAEKYAEEDRRKKERVEAVNM 584
hBip ITITNDQNRLTPEEIERMVNDAEKFAEEDKKLKERIDTRNE 564
DNAKeColi ITIKAS-SGLNEDEIQKMVRDAEANAEADRKFEELVQTRNQ 538
α-helix
β-strand

expand our understanding of the binding affinity we ran series of pulldowns to bracket the binding affinity between Hsp70 SBD and APPc. From the binding information elucidated through our study, we may be able to glean some understanding of the impact of phosphorylation of T668, as seen in AD, and its effect on APP processing and degradation.

RESULTS & DISCUSSION

In order to investigate the effect of APPc phosphorylation at T668 on the interaction of APPc with HSP70 family members, pulldowns were conducted in H4 neuroglioma whole cell lysates (WCL) using either of two synthetic, biotinylated peptide mimics of APPc residues 658-676 ($APPc_{658-676}$ Figure 2.2A&B). One peptide was phosphorylated at T668 ($pAPPc_{658-676}$) while the other peptide was unphosphorylated ($APPc_{658-676}$). HSP70 family members pulled down by each biotinylated peptide were probed via western blot (WB) using anti-Hsp70, -Hsc70, -BiP (Grp78), and -Grp75 (Figure 2.2B). Each of these family members interacted more strongly with the unphosphorylated, biotinylated peptide, indicating that phosphorylation of T668 consistently reduced the interaction with the four representative family members that were probed.

To further investigate the possible influence of flanking APPc sequences that contain known binding motifs for other proteins, the same pulldown experiments were performed using longer biotinylated peptides containing APPc residues 657-687 ($pAPPc_{657-687}$ and $APPc_{657-687}$) (Figure 2.1). In contrast to results from pulldowns with the shorter peptides, these longer versions displayed no preference between the T668-phosphorylated and unphosphorylated forms for binding to the same HSP70 family members (Figure 2.2B). The N-terminal extension of the sequence by one residue (to H657) allowed the essential region for G_o binding, H657–K676 (Nishimoto, Okamoto et al. 1993; Okamoto, Takeda et al. 1995), to be fully encompassed.

Notably, deletion of just one N-terminal histidine (H657) from a 20-residue APPc-derived peptide (H657-K676) eliminated the G_o-activating function of this APP peptide (Nishimoto, Okamoto et al. 1993), pointing to an essential role for H657 in this functional interaction. Similarly, the C-terminal extension by 11 residues to Y687 fully incorporates APP residues essential for binding to X11 (Zhang, Lee et al. 1997), but does not extend to the full Fe65-PID2 binding region (Li, Koshiba et al. 2008; Radzimanowski, Simon et al. 2008). Hence, lengthening of the biotinylated peptide sequence in both the N-terminal and C-terminal directions broadened the potential interactome of the peptides, increasing the potential for competitive and cooperative effects that might influence the binding of HSP70 family members.

The consistent APPc binding behaviors observed here across the four HSP70 family members probed reflect the high sequence conservation among their respective substrate binding domains (SBDs) (Figure 2.2C). Specifically, the residues that directly interact with substrate in the deep hydrophobic pocket (Morshauser, Hu et al. 1999) (shown in grey boxes in Figure 2.2C) are absolutely conserved across Hsp70, Hsc70, Bip, and Grp75. Based on their similar sequences and APPc binding behaviors, the binding of any member of this cohort should be informative of the binding to any other member. X-ray structures of the human Hsp70 SBD have been solved bound to a peptide substrate (4po2.pdb) (Zhang, Leu et al. 2014) and bound to the natural product novolactone (Hassan, Kirby et al. 2015). The Hsp70 SBD is of particular interest, since it is the major stress-induced form in the cytosol (Pierpaoli 2005), and its upregulation has been shown to reduce neurotoxicity in another neurodegenerative disease, Huntington's disease (Chafekar, Wisen et al. 2012; Wang, Miyata et al. 2013).

To further investigate the phospho-T668 dependence of APPc interaction with HSP70 family members observed with the shorter APPc sequence, recombinant human Hsp70 SBD

(residues 381 – 544) was prepared. To first verify the binding function of the recombinant Hsp70 SBD, a pulldown experiment was performed using $pAPPc_{657-687}$ and $APPc_{657-687}$ biotinylated peptides. Captured proteins were separated by SDS-PAGE and visualized by Coomassie stain (Figure 2.3A). A band at the Hsp70 SBD molecular weight (19 kDa) was present in both $pAPPc_{657-687}$ and $APPc_{657-687}$ lanes and not in the control lane, confirming that the recombinant Hsp70 SBD directly binds to both T668-phosphorylated and unphosphorylated forms of $APPc_{657-687}$.

Although the approximate region of APP sufficient for interaction with Hsc70 in COS-7 cells was determined by serial C-terminal truncations of APP (Kouchi, Sorimachi et al. 1999), the residues on the N-terminal end of APPc that are essential for interaction were not identified, and APPc residues required for interaction with human Hsp70 SBD has not been previously investigated. In order to identify the APPc residues that participate in the interaction with Hsp70 SBD, recombinant ^{15}N-APPc (unphosphorylated) was titrated with Hsp70 SBD (Figure 2.3B) and ^{15}N-^{1}H HSQCs were acquired at each titration point. The previously determined APPc resonance assignments (Ramelot, Gentile et al. 2000) allowed residue-specific changes to be monitored in the acquired spectra. The lack of peak walking and the appearance of small new peaks (the most prominent of which are labeled as bound peaks in Figure 2.3B) at high Hsp70 SBD concentrations demonstrate that this interaction occurs in the slow-exchange regime, but (contrary to a typical slow-exchange interaction) appears to be extremely weak. The changes in peak intensity and volume induced by addition of Hsp70 SBD were too minor for reliable quantification of APPc binding to Hsp70 SBD. However, clear changes in peak volume do occur, but not for all peaks (Figure 2.2C&D). Quantification of residue-specific differences in normalized peak volume (ΔV) between the apo spectrum and the spectrum with the highest

Figure 2.3 Interaction of ^{15}N-APPc and Hsp70 SBD. A) SDS-PAGE of 25 μM recombinant human Hsp70 SBD(363-538) was pulled down using 25 μM APPc$_{657-681}$ peptide *in vitro*. B) ^{15}N-HSQC of recombinant, ^{15}N-labeled APPc titrated Hsp70 SBD, where the apo spectrum is red and the spectrum with the most Hsp70 SBD is blue. The minimum contour levels set in this Sparky generated image are 7e04 and are set that low to emphasize the small, bound peaks that arise over the course of the titration. The largest bound peaks are labeled numerically for reference. C) Cross-sections of the center of G681, an example of a non-titratable peak. Cross-section images were generated using LineShapeKin extension in Sparky. D) Cross-section of the center of A665, an example of an APPc peak sensitive to binding Hsp70 SBD. E) Plot of the normalized volume change for each residue of APP from the sample of the titration containing the most Hsp70 SBD to the sample containing no Hsp70 SBD.

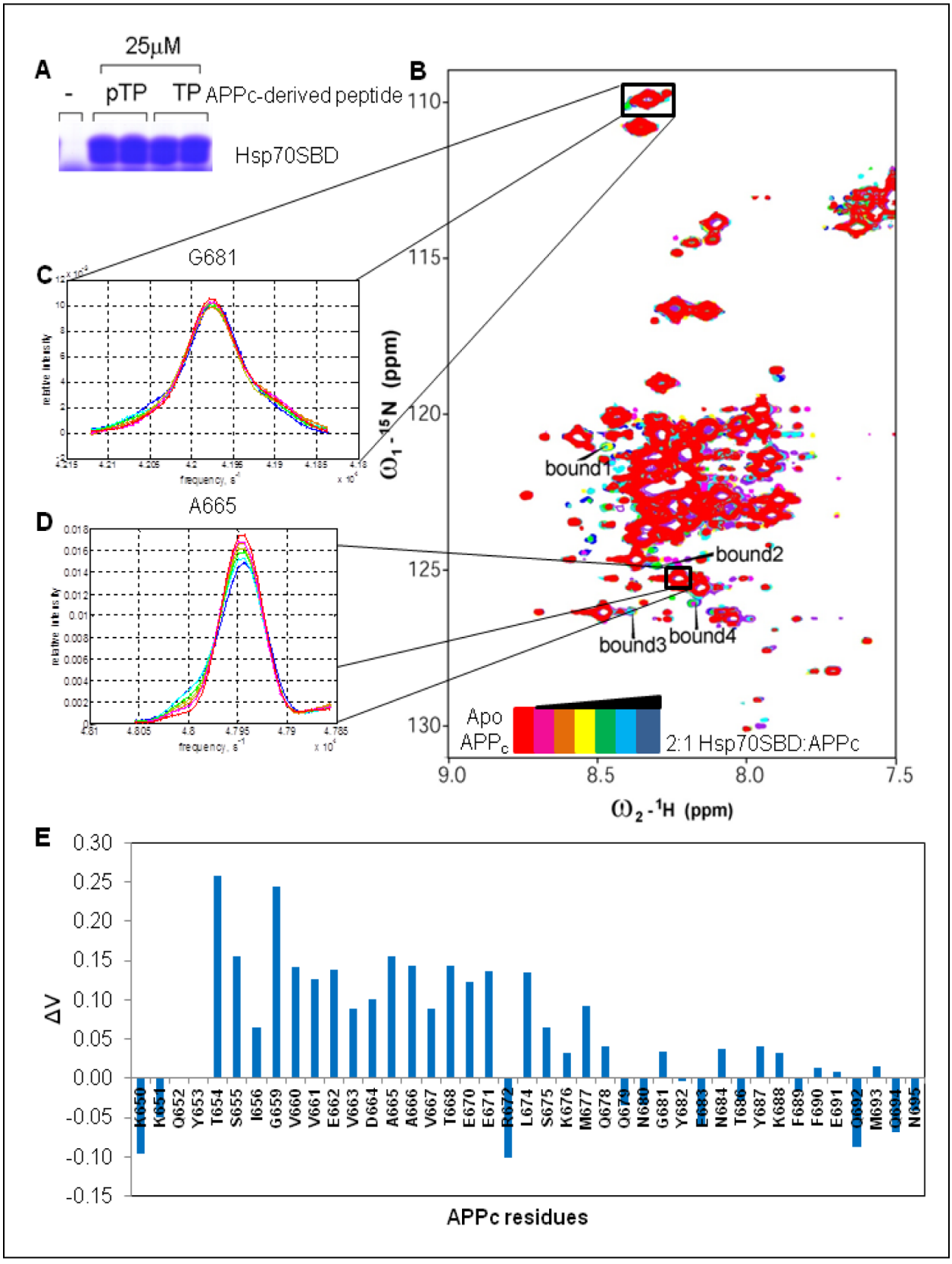
A
25μM
-
pTP
TP
APPc-derived peptide
Hsp70SBD
B
C
G681
D
A665
bound1
bound2
bound3
bound4
Apo
APPc
2:1 Hsp70SBD:APPc
ω1 - 15N (ppm)
ω2 - 1H (ppm)
E
ΔV
APPc residues

Hsp70 SBD concentration unambiguously shows a stretch of APPc residues affected by the presence of Hsp70 SBD. APPc residues T654 – L674 show ΔV values that either exceed a threshold of 0.1 or are between two other residues that exceed a threshold of 0.1. This stretch of residues coincides, approximately, with the region previously identified as sufficient for binding to Hsc70 through serial C-terminal truncations of APP in COS-7 cells (Kouchi, Sorimachi et al. 1999). The hydrophobic groove on the SBD of Hsp70 accommodates seven residues (Morshauser, Hu et al. 1999), suggesting that the part of APPc actually sitting in the hydrophobic groove is V660-V667.

The residues in unphosphorylated ^{15}N-APPc identified above as interacting with Hsp70 SBD indeed include T668. However, monitoring the APP:Hsp70 SBD binding reaction from the ^{15}N-APPc perspective did not allow phospho-T668 vs T668 comparison, since phosphor-T668 is not readily available in the recombinant form of APPc. Therefore, since synthetic phosphopeptides are commercially available, the phospho-T668 dependence of the APPc:Hsp70 SBD interaction was investigated from the ^{15}N-Hsp70 SBD perspective using peptides that contain APPc residues 659-682 ($APPc_{659-682}$), which contain the defined interaction region. The ^{15}N-Hsp70 SBD apo spectrum (Figure 2.4A) is indicative of mobile, solvent exposed polypeptide, displaying little chemical shift dispersion with peaks clustered within a narrow frequency range. This was unexpected, given the predominantly β-sheet structure of Hsc70 SBD (Morshauser, Hu et al. 1999; Zhang, Leu et al. 2014; Hassan, Kirby et al. 2015). Moreover, the observed peaks do not account for the full Hsp70 SBD sequence; for example, the sequence contains 12 glycine residues, yet only three strong peaks are observed in the typical glycine region of the spectrum, although two additional weaker peaks are apparent (Figure 2.4A). This indicates that much of the ^{15}N-Hsp70 SBD sequence is "invisible" by NMR under these

Figure 2.4 Interaction of ^{15}N-Hsp70 SBD and APPc-derived peptides via NMR. A) ^{15}N-^{1}H HSQC of apo Hsp70 SBD. B) ^{15}N-^{1}H HSQC of Hsp70 SBD in the presence of 11.9mM (unphosphorylated) $APPc_{659-682}$ peptide (blue) or 15.3mM $pAPPc_{659-682}$ peptide (red).

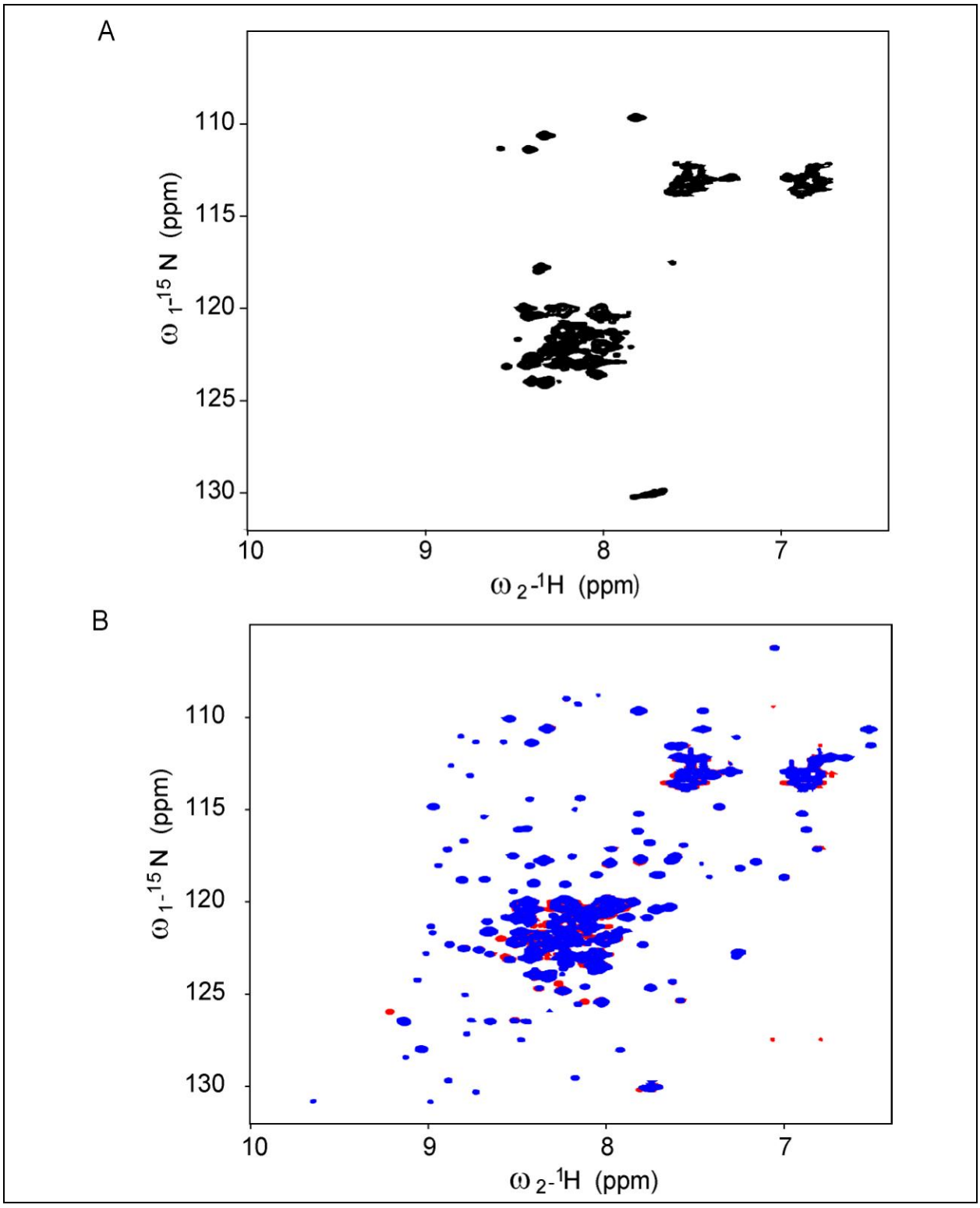
A
110
115
120
125
130
ω 1-15 N (ppm)
10
9
8
7
ω 2-1H (ppm)
B
110
115
120
125
130
ω 1-15 N (ppm)
10
9
8
7
ω 2-1H (ppm)

experimental conditions.

Interestingly, as ^{15}N-Hsp70 SBD was titrated with unlabeled and unphosphorylated APPc$_{659-682}$ peptide, a population of small dispersed peaks began to appear that are indicative of folded protein (Figure 2.4B). These peaks were strong enough to measure the change in peak intensity over the course of the titration. These peak intensity changes versus peptide concentration were fit to a binding curve for a two-state interaction (Figure 2.5). The apparent K_d for the interaction of APPc$_{659-682}$ and Hsp70 SBD is 655 ± 189 μM (Figure 2.5A&B). ^{15}N-Hsp70 SBD was also titrated with pAPPc$_{659-682}$ to rigorously test whether or not phosphorylation at T668 directly affects binding to Hsp70 SBD. The apparent K_d measured in this case was 2.08 ± 0.29 mM (Figure 2.5C&D). This confirms that binding to the unphosphorylated APPc$_{659-682}$ peptide is more than three-fold tighter than the peptide phosphorylated at T668, consistent with the differences in full-length Hsp70 pulled down by biotinylated peptides pAPPc$_{658-676}$ and APPc$_{658-676}$. Notably, an overlay of ^{15}N-Hsp70 SBD bound to pAPPc$_{658-676}$ or APPc$_{658-676}$ peptides shows clear differences in the bound chemical shift of at least five distinct residues (Figure 2.4B). This is consistent with the result of titrating recombinant ^{15}N-APPc with Hsp70 SBD, where T668 is in the region of the peptide that experiences a different local chemical environment upon binding. If T668 undergoes modification, such as phosphorylation, any residues on the Hsp70 SBD in the vicinity of APPc T668 would likely see a disparate chemical environment and thus have a different bound chemical shift.

While both binding events appear to be quite weak at first, it is necessary to consider how much Hsp70 SBD is actually binding-capable given the nature of the apo spectrum. Indeed, the slow-exchange observed in the ^{15}N-APPc and ^{15}N-Hsp70 SBD titrations suggests tight binding, which could in fact be the case if only a fraction of the total Hsp70 SBD molecules in the

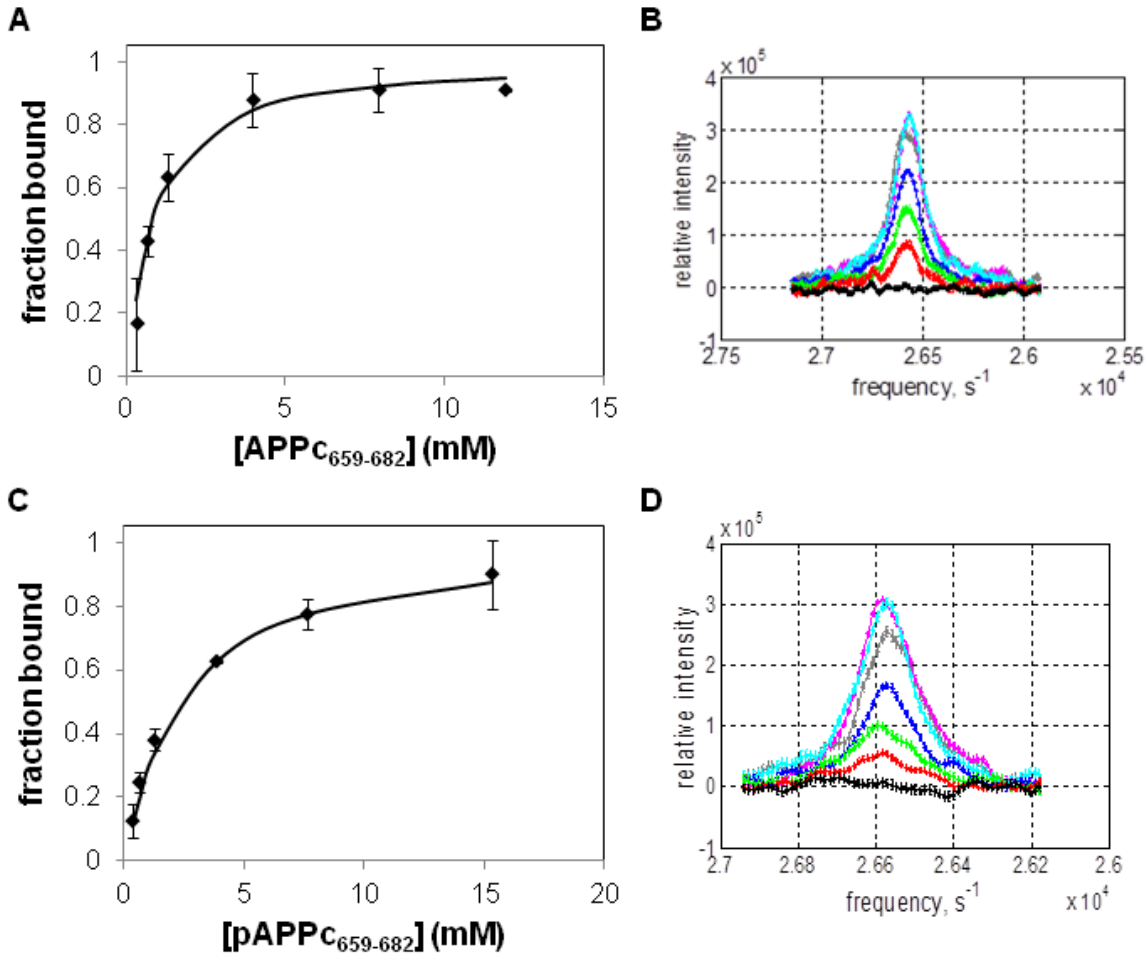

Figure 2.5 Quantification of binding affinity for ^{15}N-Hsp70 SBD and APPc-derived peptides via NMR. A) Plot of a fit of the fraction bound when 0.5 mM ^{15}N-Hsp70 SBD is titrated with unphosphorylated APPc$_{659-682}$ where the data points represent the mean fraction bound of 10 residues and the error bars are standard deviation from the mean. The line is the fit. B)Slice of example peak from the titration of ^{15}N-Hsp70 SBD with APPc$_{659-682}$, where black corresponds to the apo ^{15}N -Hsp70 SBD and the pink peak slice corresponds to the spectrum with the most APPc$_{659-682}$. C) Plot of a fit of the fraction bound when 0.5 mM ^{15}N-Hsp70 SBD is titrated with pAPPc$_{659-682}$ where the line represents the fit, the diamonds represent the mean fraction bound of 10 residues, the standard deviation from the mean is the error. D)Slice of example peak from the titration of ^{15}N-Hsp70 SBD with pAPPc$_{659-682}$, where black corresponds to the apo ^{15}N -Hsp70 SBD spectrum and the pink spectrum represents the sample with the most APPc$_{659-682}$.

ensemble are competent to bind. One explanation for the lack of peaks in the spectrum could be that an ensemble of states exist that exchange on a timescale invisible by NMR. Another possible explanation is oligomerization, where the size of the oligomer would slow its tumbling, making the larger species invisible by NMR. The peaks that are actually visible in the spectrum could correspond to mobile loops and tails, which would retain some freedom to rotate even as the protein oligomerizes allowing them to give rise to a sharper, stronger signal (Carbajo and Neira 2013).

In order to determine if the lack of peaks in the apo spectrum is dependent on concentration, and affects the binding-capable concentration, the effects of serial dilution of ^{15}N-Hsp70 SBD were monitored by acquiring an ^{15}N-HSQC spectrum at each dilution. While peaks in the apo spectrum attributed to mobile tails and loops scale linearly with concentration (Figure 2.6B), the peaks indicative of folded protein do not (Figure 2.6A). These small peaks arising from folded protein actually remain of similar intensity throughout the dilution series, which suggests that as the sample is diluted a larger fraction of the total protein may become binding-capable either by having the necessary space to fold or a stronger propensity to be monomeric. These results support a model in which the APPc:Hsp70 SBD binding equilibrium is coupled to an Hsp70 SBD equilibrium between binding-capable and binding-incapable states.

The next logical course of action was to determine the equilibrium constant (K_{eq}) between binding-capable and binding-incapable Hsp70 SBD states in order to back out a true binding affinity for the interaction of Hsp70SBD and $APPc_{659-682}$ or to remove the species that is not binding competent from the system. Attempts to use circular dichroism, analytical ultracentrifugation and isothermal calorimetry (ITC) to determine the K_{eq} were unsuccessful. I used circular dichroism to monitor secondary structure of Hsp70 SBD over a temperature range

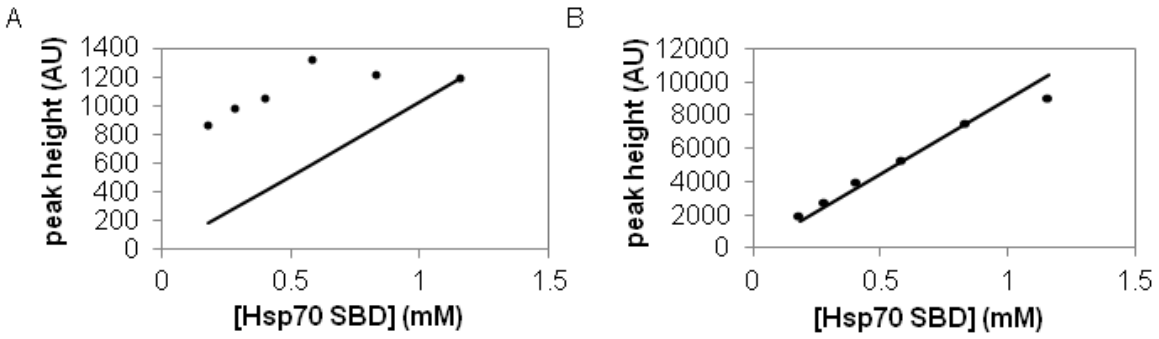

Figure 2.6 Serial dilution of ^{15}N -labeled Hsp70 SBD and subsequent signal loss as measured via NMR. A) Plot of the peak height (circles) of an Hsp70 SBD residue from a series of ^{15}N HSQCs using serial dilutions of Hsp70 SBD as well as the simulated theoretical peak height at a given Hsp70 SBD concentration using the height at the highest concentration and treating it as fully folded, monomeric protein and scaling down linearly with concentration. B) Plot of one of the peaks that gives off a strong signal in each spectrum collected, where it's been linearly fit to minimize error across data points.

of 4°C to 75°C and saw no fluctuations. Attempts to use APPc-derived peptide, thereby creating a "folded" population, required so much peptide that the Hsp70 SBD signal was completely hidden. Analytical ultracentrifugation fared little better as a way to obtain the K_{eq} of "folding". While the concentrations that I tested yielded data not indicative of a monomer, they all yielded similarly complex datasets. I was unable to find a set of conditions where the data became tractable. In an attempt to get the binding directly under conditions where Hsp70 SBD was less concentrated than in the NMR titrations, I used ITC. I was not able to measure a binding event under any of the conditions tried, which could be due to the presumably small (judging by the serial dilution of ^{15}N-labeled Hsp70 SBD) population of binding capable protein or it could be that the K_d is not in a range conducive to measurement by ITC. I was also unable to measure a reversible oligomerization event (a possibility given the ^{15}N-labeled Hsp70 SBD serial dilution).

In order to avoid even needing to determine the K_{eq}, 1D ^{1}H and 2D ^{15}N HSQC spectra of Hsp70 SBD were taken with Hsp70 SBD under a range of temperatures (15-37ºC), pHs (5-7.5), and variations on the ionic strength of the salt used in the sample. These attempts at finding conditions that contained "folded" peaks were met with minimal success. The increasing pH resulted in better signal to noise, but that gain was soon mitigated by the peak broadening associated with pHs that are that high (Figure 2.7). A close look at Morshauser et al. revealed that the solution NMR structure showed a structure where the leucine (L542) from the end of the construct used was bound in the deep hydrophobic groove of the SBD and that binding event had a sufficient binding affinity that they were unable to compete off the end of the construct (Morshauser, Hu et al. 1999). To avoid this, the construct used in this study was truncated to just before the L542. As this construct does not produce much stably folded, monomeric Hsp70SBD, it was altered to remove more of the end of the construct, truncating it to the point where the

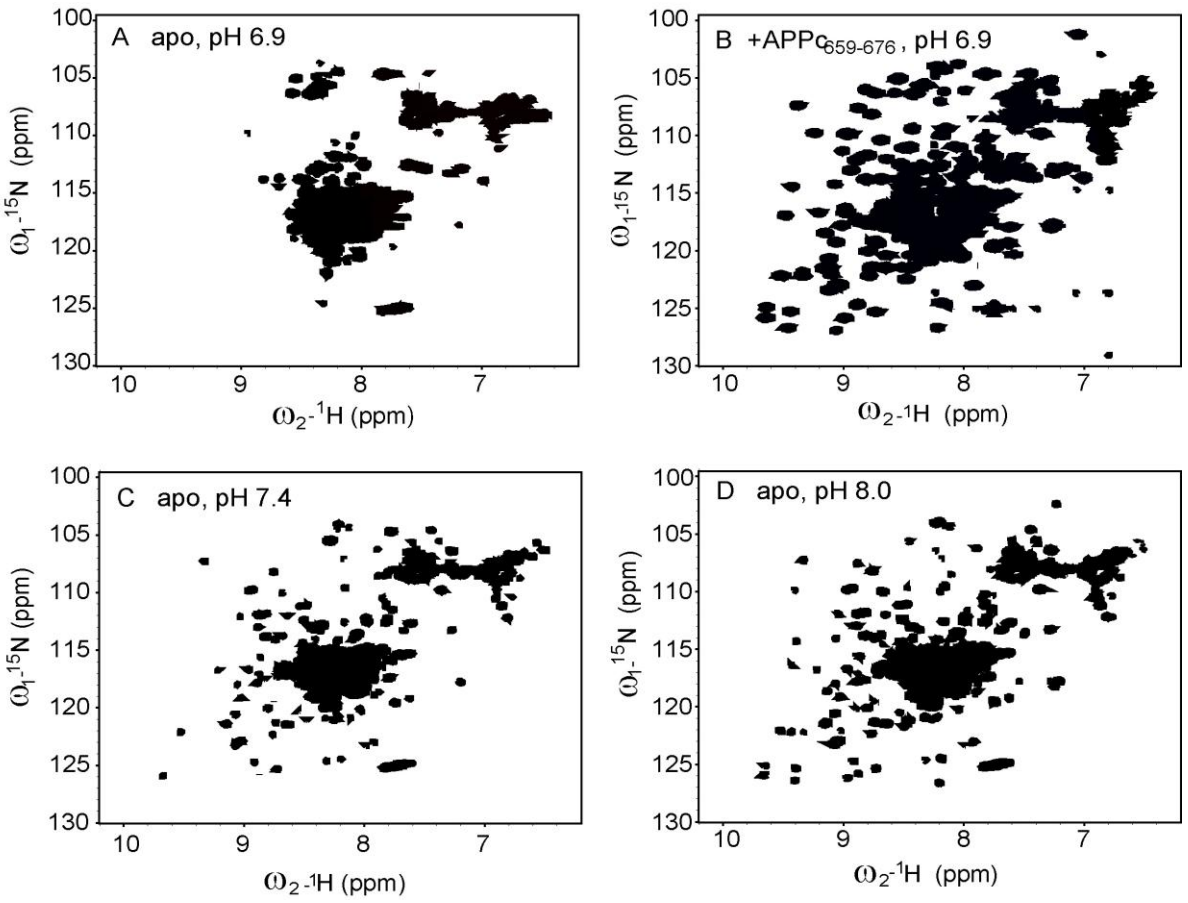

Figure 2.7 ^{15}N-^{1}H HSQC of Hsp70 SBD under varying conditions. The minimum contour level of each Sparky generated image is 6e04. A) ^{15}N-^{1}H HSQC of apo Hsp70 SBD at pH 6.9. B) ^{15}N-^{1}H HSQC of Hsp70 SBD in the presence of 11.9mM unphosphorylated APPc$_{659-676}$ peptide at pH 6.9., leading to a small population of distinct peaks which could correspond to a folded or monomeric population. C) ^{15}N-^{1}H HSQC of Hsp70 SBD at pH 7.4 D) ^{15}N-^{1}H HSQC of Hsp70 SBD at pH 8.0

β-sheet region of the domain ends instead of including a portion of the α-helical subdomain. Given that Morshauser used rat Hsc70 SBD, human Hsc70 SBD containing both the β-sheet binding section and the entire α-helical lid was also generated in the hopes that the presence of the full lid would protect L542 from interacting with the binding site of the SBD. Notably, these constructs were also purified either with or without a His-tag to check if they would be less prone to oligomerization in one state or the other. As none of these attempts were successful, another strategy was devised for obtaining information on the strength of the interaction.

Instead of trying to find the absolute K_d of $APPc_{657-687}$ binding to SBD, a larger question was addressed. How strongly does APPc interact with endogenous, full-length Hsp70 in the context of a complicated mixture of proteins, lipids, and small molecules? A titration series was carried out by lab member Ross Resnick (Figure 2.8A), where the concentration of the APPc-derived peptide is decreased throughout the titration series, but the overall amount of peptide remains the same, rather it is the volume of the whole reaction that is increasing. This eliminates the sizable error involved in measuring highly different amounts of peptide and neutravidin beads for the pulldown. This methodology does mean that the H4 neuroglioma WCL, and consequently the endogenous Hsp70, is diluted as the volume changes over the course of the titration. However the advantages to using this methodology are clear as binding is detected for $APPc_{657-687}$ concentrations as low as 1 μM (Figure 2.8A&B). This titration series was repeated and both $APPc_{657-687}$ and $pAPPc_{657-687}$ were used, which seemed prudent given the inconsistencies between the longer APPc-derived peptide (APPc657-687) (which seemed to bind equally well to phosphorylated and non-phosphorylated T668) and the shorter peptide (APPc658-676) and the NMR titration, which revealed a three-fold attenuation of binding upon phosphorylation. In these WBs, the phosphorylation event did not seem to attenuate binding

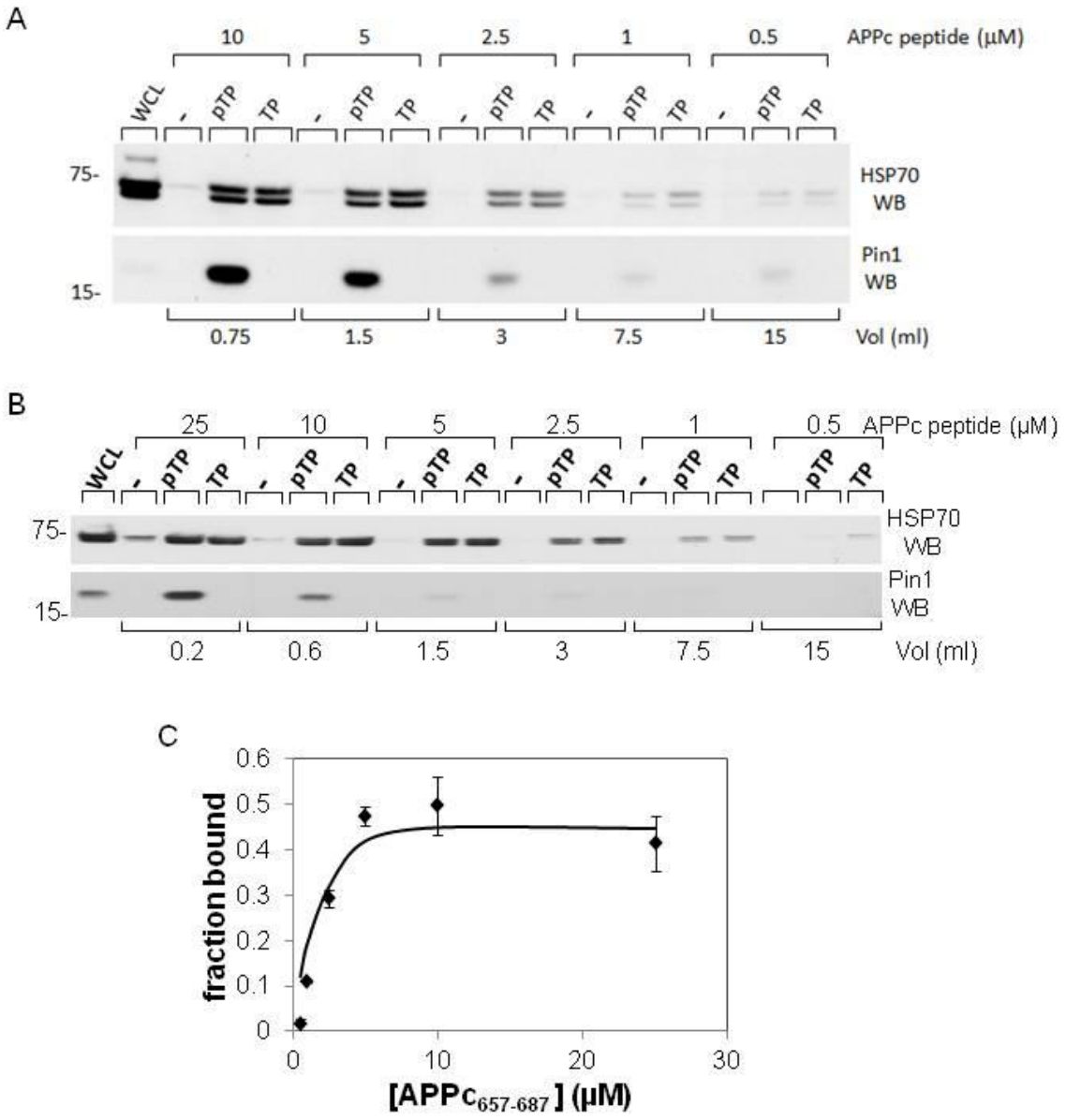

Figure 2.8 Interaction of Hsp70 and APPc via WB. A&B) WBs of Hsp70 from a titration of pulldowns with phosphorylated (pTP) and unphosphorylated (TP) $APPc_{657-687}$ in WCL from H4 Neuroglioma cells. Pin1 was used to test the assay as well as an example of a known phospho-specific interactor of APPc. B) Semi-quantitative binding curve of WB data collected by Ross Resnick and processed using ImageJ software and excel 2007 by Monique Rogals.

visibly, in agreement with our initial pulldowns using the longer peptide (Figure 2.2B), discussed above. In fact, the phospho-T668 and unphosphorylated T668 results were so close that they were treated as duplicates in the final fit so as to improve the statistics of the fit (Figure 2.8C). As mentioned above, this region of APPc includes motifs known to bind to other substrates, so the WCL pulldown system includes competition for other binding partners that are not accounted for in binding calculations. Therefore, since the presence of such competition would result in an apparent Hsp70 binding affinity weaker than the true binding affinity, the K_d obtained by fitting of this pulldown data represents an upper bound of the K_d for the interaction of $APPc_{657-687}$ and Hsp70 in N4 neuroglioma cells. The semi-quantitative fit of the WB binding data to a two-state binding reaction yields a K_d value of 6 μM with a fitted Hsp70 concentration of 12 μM in the fit corresponding to Figure 2.8A and 50 μM in the fit corresponding to Figure 2.8B. The number of pixels representing the total possible bound Hsp70 in each titration was also a fitted parameter. Changing any of these fitted parameters even two-fold resulted in a distortion to the fit, though the fit is least sensitive to changes in the total concentration of Hsp70 and most sensitive to the K_d. While this approach suggests that a much tighter interaction between APPc and full length Hsp70 indeed occurs, the comparable WB dilution experiments using known concentrations of purified recombinant Hsp70 and APPc peptide (where T668 is either phosphorylated or unphosphorylated) are required for accurate determination of the strength of this interaction and its dependence on T668 phosphorylation at physiological concentrations.

Notably, due to complexities of the *in vitro* system used, the role of *cis-trans* prolyl isomerization in the interaction of the phosphoT668-P669 motif in APPc with its binding partner Hsp70 could not be addressed. Specifically, because the interaction is in slow rather than fast-exchange, peaks corresponding to the *cis* and *trans* states of the free phosphoT668 APPc peptide

could not be tracked during titration (i.e., if binding were *trans*-specific, only the *trans* peaks would move during the course of titration). Moreover, identifying the isomer state of the bound peptide requires the acquisition of structural data for the bound state, which was precluded by the very low achievable concentration of the bound state. Ideally, with recombinant full-length deuterated Hsp70 and site-specifically ^{13}C-labeled APPc peptide (e.g., ^{13}C-P669), it might be feasible using TROSY-based experiments and cryoprobe technology to distinguish between bound *cis* and *trans* states by the ratio of the difference in ^{13}C chemical shift frequency between the beta and gamma carbon chemical shifts as we have done previously (Greenwood, Rogals et al. 2011).

Conclusions

In summary, APPc peptide binds to HSP70 family members. In particular, the region of APPc that sees a change in local chemical environment upon interaction with Hsp70 SBD, and likely other HSP70 family members, is from T654 to L674. There are several hydrophobic residues in this section that are likely binding site candidates including four valines in close proximity (660, 661,663, and 667). When Hsp70 SBD is titrated with $APPc_{659-682}$ peptide there is a three-fold stronger interaction when T668 is unphosphorylated according to NMR HSQC titrations and WCL pulldowns using the somewhat shorter peptide $APPc_{658-676}$. The Hsp70 SBD construct does not appear to be a stably folded monomer, and as such the binding-capable subpopulation of Hsp70 SBD in NMR experiments is substantially less than the total measured concentration, which results in weaker apparent binding affinities. Because the difficulties with the Hsp70 SBD are likely related to the length of the construct, titrations with $APPc_{657-687}$ peptide were run in whole cell lysates and stained for endogenous Hsp70, resulting in an upper bound for the interaction of 6 μM.

This study examined the interaction between varying constructs of Hsp70 and several different lengths of APPc via NMR and WBs for Hsp70. In the larger context this yields information on the interaction of APPc and any number of HSP70 family members. Not all HSP70 family members are cytosolic and therefore accessible to intact APP in an *in vivo* context, however Hsc70 is certainly also a viable potential binding partner and shares an 89% sequence identity with the construct of the Hsp70 SBD, for a similar length of its SBD. After the APP has been cleaved into its proteolytic pieces, AICD can end up in the nucleus thereby becoming accessible to nuclear localized HSP70 family members like Hsp70, which accumulates in the nucleus upon stress to protect DNA (Kotoglou, Kalaitzakis et al. 2009), which could impact AICD's mediation of transcription, which generally has a toxic outcome if allowed to continue unabated (Slomnicki and Lesniak 2008).

MATERIALS & METHODS

Preparation of recombinant Hsp70. Hsp70 substrate binding domain M381-A541 was sub-cloned from a full length human Hsp70 in a mammalian vector (a gift from Shu-Bing Qian's lab) into a pET28a(+) derived vector with kanamycin [IBI Scientific] resistance, a 6X-His tag and TEV cleavage site. Hsp70 was chosen based both on sequence similarity to Hsc70 in the substrate binding domain (Figure 2.2C) and the successful NMR structure (7HSC.pdb) of a highly similar construct by Morshauser et al (Morshauser, Hu et al. 1999). The length of our Hsp70 SBD construct was based on information gleaned from Morshauser's paper. They determined that their inability to perform binding studies on Hsp70 SBD was due to a binding event with the C-terminal tail of the construct centered on a leucine residue bound in the deep hydrophobic substrate binding pocket of the Hsp70 SBD. As the effective concentration of this

"binding partner" was so high, the most expedient way to prevent this undesirable binding event was to remove two residues (LE) from the end of the construct, leading to a shorter construct than was solved structurally (Morshauser, Hu et al. 1999). To purify Hsp70 SBD we transformed the construct into BL21 star *E. coli* [Invitrogen] and grew up in either LB media [BD] or M9 minimal media with $^{15}NH_4Cl$ [Isotec] at 37°C until the OD_{600} was between 0.6-0.8. The temperature of the culture was reduced to 18°C and it was induced using 1 mM IPTG [CalBioChem] overnight. The cells were harvested and frozen down. They were lysed the next day using lysis buffer (50 mM sodium phosphate [Fischer], 200 mM NaCl [Mallinckrodt Baker], 1.25 mM DTT [Gold Biotechnology], and pH 6.9) with 20 µg of Lysozyme [EMD]. The cells were sonicated, centrifuged and the supernatant was syringe filtered (0.8-µm [Corning]) to remove large precipitates. The soluble protein solution was passed over a Ni-NTA column [Qiagen] and the beads were washed using 25 mL (in five steps) of a low salt/imidazole buffer (50 mM sodium phosphate, 200 mM NaCl, 10 mM imidazole [Alfa Aesar], pH 6.9) followed by a quick wash with 15 mL of high salt/no imidazole buffer (50 mM sodium phosphate, 600 mM NaCl, pH 6.9), and elution with elution buffer (50 mM sodium phosphate, 250 mM NaCl, 10 mM imidazole, pH6.9). The imidazole was dialyzed away with 1.5 L of dialysis buffer (50 mM sodium phosphate, 10 mM NaCl, 0.1 mM TCEP [Thermo Scientific], pH 6.9) in three 0.5 L stages. His-tagged TEV [produced in-house] was added to the dialyzed protein and left to cut the Hsp70 SBD overnight at 4°C. A second Ni-NTA column was used to separate the cut Hsp70 SBD from the uncut his-tagged Hsp70 SBD, cut his-tags and the His-tagged TEV. NaN_3 [Fisher] and TCEP were added to the sample to finish the final storage buffer (50 mM sodium phosphate, 10 mM NaCl, 1 mM TCEP, 5 mM NaN_3). The concentrations of Hsp70 SBD were tracked in the following experiments via a NanoDrop 2000c [Thermo Scientific], where the extinction

coefficient of the Hsp70 SBD was 12,330 $M^{-1}cm^{-1}$.

Preparation of recombinant hAPPc. An APP-derived oligo encompassing 649 to 695 of APPc695, the form of APPc dominant in the human brain, was synthesized by DNA 2.0. We subcloned the APPc oligo to a pGEX-2T plasmid (gift of David Shalloway's lab) with ampicillin [Fisher] resistance, a GST solubility tag and a thrombin cut site and transformed this construct into BL21 star *E. coli*. We grew at 37°C in either LB media or M9 minimal media with 1 g of $^{15}NH_4C$ l until reaching an OD_{600} of 0.6-0.8, induced with 1 mM IPTG for two hours at 37°C and harvested the cells. They were frozen overnight and thawed with 200 mg of Lysozyme and 1.25mM of DTT. They were resuspended in a lysis buffer (50 mM sodium phosphate, 300 mM NaCl, pH 7.4) sonicated, centrifuged and then the supernatant with the soluble protein was syringe filtered (0.8-µm) to remove particulate before application to an Ni-NTA column for affinity purification. The column was washed with 40 mL of low salt wash buffer in step sizes of 10 mL apiece (50 mM sodium phosphate, 300 mM NaCl, 10% glycerol [Mallinckrodt-Baker], pH 7.0), followed by 10 mL of high salt wash buffer (600 mM NaCl instead of 300 mM) and another 10 mL of low salt wash buffer. The APPc was cut on the column using the biotinylated-thrombin cleavage kit [Novagen] for 16 hours overnight at 25°C. We collected the cut APPc the next day, using buffer (50 mM sodium phosphate, 300 mM NaCl, pH 7.0) to flush out the void volume. The thrombin was removed according to kit protocol. The APPc was then dialyzed into a storage buffer (50 mM sodium phosphate, 10 mM NaCl, 1 mM TCEP, pH 6.9) and concentrated to a manageable volume at which point 5 mM NaN_3 was added as a preservative. Concentrations of APPc for the following experiments were measured using a NanoDrop 2000c where the extinction coefficient of APPc was 3840 $M^{-1}cm^{-1}$.

APPc-derived peptides (WB & NMR). Synthetic peptides used for NMR studies were produced

via solid phase F-moc chemistry by Tufts University Core Facility and delivered as lyophilized powder. They were dissolved in appropriate buffer (either NMR or WB buffer) and their pH was adjusted to either 6.9 for NMR experiments or 8.0 for WB experiments. The peptide designed for NMR was APPc-659-682 either containing a phosphorylated T668 ($pAPPc_{659-682}$) or lacking it $APPc_{659-682}$). The peptides designed for pulldowns were APPc-658-676 and APPc-657-687 either with ($pAPPc_{658-676}$ or $pAPPc_{657-687}$) or without ($APPc_{658-676}$ or $APPc_{657-687}$) phosphorylated T668. They have an N-terminal Biotin linked to the peptide via a methyl linker. Sequences of peptides used in this study are in Figure 2.1. Concentrations of APPc-derived peptides for the following experiments were measured either by weight or via NanoDrop 2000c where the extinction coefficient of APPc-659-682 was 1420 $M^{-1}cm^{-1}$ and that of APPc-657-687 was 2840 $M^{-1}cm^{-1}$.

Cell culture. H4 neuroglioma cells [ATCC (Manassas, VA)] were maintained by Ross Resnick in monolayer culture in Dulbecco's Modified Eagle Medium [Corning Life Sciences] (4.5 g/L glucose, 3.7 g/L sodium bicarbonate) supplemented with 10% fetal bovine serum [Altanta Biologicals] and 100 IU /100 μg/ml penicillin/streptomycin [Corning Life Sciences] at 37°C in a humidified atmosphere (90%) containing 10% CO_2. Cells were isolated by trypsinization and routinely passaged to maintain stocks or plated for experiments as described.

Preparation of cell lysates. Cells were plated by Ross Resnick in 100 mm dishes [Corning Life Sciences] and after 48 hours confluent monolayers were scraped with a rubber policeman, centrifuged, washed twice with ice cold PBS cells and proteins were extracted in lysis buffer (LB; 50 mM HEPES, pH 7.2, 150 mM NaCl, 2 mM EDTA, 1% Triton X-100, 1mM sodium orthovanadate, 50 mM sodium fluoride, 10 mM β-glycerophosphate, 500 μM AEBSF, 10 μg /mL Aprotinin, 10 μg/mL Leupeptin, and 5 μg/mL Pepstatin) for 30 minutes at 4°C with rocking. Crude lysates were collected and centrifuged at 28,000 x g for 20 minutes at 4°C to remove

cellular debris and insoluble material. The clarified whole cell lysate (WCL) was removed, total protein was quantified using the DC Protein Assay with BSA as a standard and used as described.

Pulldown experiments. Pulldowns and western blots were carried out by Ross Resnick. WCL prepared from H4 neuroglioma cells (Figure 2.2A and Figure 2.2B) or recombinant Hsp70 SBD (Figure 2.3A) were incubated in the absence or presence of biotinylated AICD-derived peptides for 14-18 hours at 4^{o}C with rocking. Samples were then transferred to fresh tubes containing 50 µl or 25 µl respectively of neutravidin beads and incubated an additional 2-3 hours at 4^{o}C with rocking to immobilize AICD complexes. Beads were washed three times with 1 ml of LB, resuspended in 1.3X Laemmli SDS-sample buffer containing 25 mM DTT and analyzed either by immunoblotting (Figure 2.2A-B) or staining (Figure 2.3A) as described below.

For the titration experiment (Figure 2.7) WCL (3 mg) were incubated in the absence or presence of a constant amount of APPc-derived peptides (25 nmoles) in sequentially larger volumes of LB to achieve the indicated dilutions (25 µM, 1 ml; 10 µM, 2.5 ml; 5 µM, 5 ml; 2.5 µM, 10 ml; 1 µM, 25 ml; 0.5 µM, 50 ml) in order to maintain a constant ratio of peptide to HSP70. After all incubations, beads were transferred to microfuge tubes, washed and results were determined by immunoblotting.

SDS-PAGE and Immunoblotting. H4 neuroglioma WCL and AICD-immobilized cellular binding partners were analyzed by immunoblotting as indicated in the figure legends. Aliquots of WCL were combined with 4x sample buffer for use as an immunoblotting control. Samples were boiled for five minutes and proteins were separated in a 10-20% gradient gel using a Bis-Tris-Mes gel system, transferred to PVDF membrane without methanol [Towbin] with constant cooling. Membranes were blocked with TBST (25 mM Tris-HCl pH 7.2, 150 mM NaCl, and

0.1% Tween 20) containing 5% milk for 1-2 hours at RT and then incubated overnight at 4^{o}C with primary antibodies (diluted in TBST containing 0.5-1% BSA) according to the vendor's recommendations. Membranes were washed, incubated for two hours at RT with goat anti-rabbit HRP-conjugated secondary antibody (diluted 1:10,000 in TBST containing 1% milk), washed and results were visualized on X-ray film using the Pierce ECL Western Blotting substrate. Recombinant Hsp70 SBD samples were boiled and separated in a 12% SDS-PAGE (Laemmli) and results were visualized by Coomassie Brilliant Blue staining.

Antibodies. Rabbit monoclonal antibodies against Hsp70 (EP1007Y, ab45133), Hsc70 (EP1531Y, ab51052) and Pin1 (EP1479Y, ab76309) were purchased from Abcam (Cambridge, MA). Rabbit polyclonal antibody against Grp75 (sc-133137) was obtained from Santa Cruz Biotechnology (Dallas, TX) and the rabbit monoclonal antibody against Bip (C50B12, 3177) was from Cell Signaling Technology (Danvers MA). Goat anti-rabbit HRP-conjugated secondary antibody was from Jackson ImmunoResearch Laboratories (West Grove, PA).

NMR spectroscopy. NMR experiments were performed at a sample temperature of 25°C on a Varian Inova 600 MHz spectrometer equipped with a Z-axis gradient probe. ^{15}N-^{1}H HSQC data sets were acquired with a spectral width of 8000 ppm and 2048 points in the proton dimension and a spectral width of 2000 ppm and 512 points in the nitrogen dimension. The number of increments in each experiment is 256. The number of transients varies based on experiment. The ^{15}N-labeled APPc uses 96 transients, while the ^{15}N-labeled Hsp70 SBD titrations with APPc derived peptides used 64 transients. The serial dilution experiments performed using ^{15}N-labeled Hsp70 SBD were done with a varying number of transients to capture the best signal to noise for the spectra taken at low protein concentrations where 48 transients were taken for spectra with concentration ranging from 1 mM to 0.5 mM and 192 transients were taken for concentrations

under 0.5 mM. The processed data in this case was normalized by number of transients. All spectra were processed and analyzed using the software tools nmrPipe, nmrDraw (Delaglio, Grzesiek et al. 1995), and Sparky (T.D. Goddard and D.G. Kneller, University of California, San Fransisco). Data were apodized using a shifted sine bell function and zero-filled prior to Fourier transformation. Peak positions, volumes, and heights were measured using the peak detection modules of Sparky.

Analysis of NMR experiments.

^{15}N-APPc and unlabeled Hsp70 SBD: All titrations described in this study were performed by taking the sample with the most unlabeled ligand and diluting it with a stock of ^{15}N-labeled protein (the stock is also the apo sample), thereby avoiding the dilution of the labeled protein that would result if ligand had instead been added in increasing volumes. This technique was used for titrations throughout this study. 0.25 mM ^{15}N-labeled APPc was titrated with 2.1, 0.5, 0.25, 0.13, 0.06, 0.03, 0.02 mM Hsp70 SBD. The resonance assignments of phosphorylated and unphosphorylated APPc were mapped by Theresa Ramelot (Ramelot, Gentile et al. 2000), so each of the peak positions is already known. Even in the absence of enough volume or enough volume change to accurately assess peak identity of the bound peaks or quantify the binding affinity, the peaks that lose volume upon the addition of Hsp70 SBD contain information. The loss of peak volume of the known apo peaks indicates residues in the APPc that experience a change in chemical environment upon addition of Hsp70. The peak volumes of the apo sample were compared with those of the sample with the most Hsp70 and the difference was analyzed:

$$\Delta V = \frac{(V_{apo} - V_{bound})}{V_{apo}}$$

where V_{apo} is the volume of a peak n in the apo spectrum of ^{15}N-APPc and V_{bound} is the volume of n in the spectrum resulting from the titration sample with the most Hsp70 SBD.

^{15}N-Hsp70 SBD and unlabeled APPc$_{659-682}$: 0.5 mM recombinant Hsp70 SBD was titrated with 0, 0.33, 0.66, 1.32, 3.97, 7.93, 11.9 mM unphosphorylated APPc$_{659-682}$. In the next set of experiments 0.5 mM recombinant Hsp70 SBD was titrated with 0, 0.32, 0.64, 1.28, 3.83, 7.65, and 15.3 mM phospho-T668 APPc$_{659-682}$ (pAPPc$_{659-682}$). Ten residues (with matching chemical shifts) were selected from each titration as representative of Hsp70 and APPc binding. The peaks exhibited behavior consistent with the slow-exchange (i.e. on the order of 0-20s^{-1} (Cavanagh 2007)) regime and therefore the volume and fitted peak height were gathered using Sparky. The interaction between the APPc and the Hsp70 SBD can be described, simply, by

$$[Hsp70SBD] \; + \; [APPc] \underset{k_{-1}}{\overset{k_1}{\rightleftharpoons}} [Hsp70SBD{:}APPc] \text{ and } K_d = \frac{k_{-1}}{k_1}$$

Where [APPc] is the concentration of either phosphorylated or unphosphorylated APPc$_{659-682}$ peptide, k_1 is the rate constant of the forward reaction, k_{-1} is the rate constant of the reverse reaction, and [Hsp70SBD:APPc] is the concentration of the complex of APPc$_{659-676}$ and Hsp70 SBD. Ideally, when quantifying the interaction in slow-exchange (which can also be defined as $k_{ex} < |\Delta\delta|$, where $k_{ex} = k_1 + k_{-1}$ (Cavanagh 2007)) the percent saturation [i.e. $\left(\frac{[Hsp70SBD{:}APPc]}{[Hsp70SBD_{tot}]}\right)100$] can be charted through the changing peak intensities as slow-exchange is characterized by a the shrinking of one peak (free peptide) and corresponding rise of another peak (bound peptide) (Williamson 2013):

$$I^{free} = I_0^{free}\left(1 - \frac{[Hsp70SBD{:}APPc]}{[Hsp70SBD_{tot}]}\right)$$

$$I^{bound} = I_0^{bound}\left(\frac{[Hsp70SBD{:}APPc]}{[Hsp70SBD_{tot}]}\right)$$

Where I^{free} is the intensity of the peak representing the free peptide, I_0^{free} is intensity of

the peak representing the free peptide before the addition of the interacting protein, the fraction of saturation of the peptide is $\frac{[Hsp70SBD{:}APPc]}{[Hsp70SBD_{tot}]}$, I^{bound} is the intensity of the peak representing the bound peptide, and I_0^{bound} is the intensity of the peak representing the bound peptide population prior to the addition of the interacting protein. By fitting the intensity change to the standard equation defining a two-state interaction at equilibrium using Excel solver 2007 to minimize the difference between the data and fit, I was able to determine $K_{D,app}$ for each titration:

$$\frac{[Hsp70SBD{:}APPc]}{[Hsp70SBD_{tot}]}$$

$$= \frac{([Hsp70SBD_{tot}] + [APPc_{tot}] + K_d) - \sqrt{([Hsp70SBD_{tot}] + [APPc_{tot}] + K_d)^2 - 4[Hsp70SBD_{tot}][APPc_{tot}]}}{2[Hsp70SBD_{tot}]}$$

^{15}N-Hsp70 SBD serial dilution: ^{15}N-Hsp70SBD was serially diluted (1.16, 0.83, 0.58, 0.4, 0.28, 0.18 mM), taking a ^{15}N-HSQC at each dilution and increasing the number of transients at lower concentrations to increase signal resolution. The peak intensity was measured at both a high intensity peak present throughout the titration, suspected to belong to a mobile tail or loop, and at nine of the much smaller intensity peaks. The high intensity peak was linearly fit with increasing concentration. For the smaller intensity peaks, a linear scaling simulation was calculated predicting the peak intensity at lower concentrations assuming that the highest concentration point represented the intensity of a fully folded, monomeric protein.

Semi-quantitative WB titration analysis. Titrations (n=2) were performed by Ross Ressnick as described above. I analyzed the WBs using ImageJ software to isolate the pixels in each appropriate band for fitting the standard two-state binding equation above using Excel solver 2007. The fitted parameters were the total Hsp70 concentration in each WB, the K_d for the interaction of APPc-derived peptide and Hsp70, and the number of pixels representing Hsp70 in

the WCL of each WB. The fraction bound was measured by taking the pixels in each band and dividing by the total pixels associated with Hsp70 in the whole cell lysate. The concentration of APPc-derived peptide in each sample is known and the concentration of Hsp70 in each sample is based on the fitted parameter for the most concentrated Hsp70 sample. The concentration is adjusted for each sample based on the known volumes of the serial dilution.

ACKNOWLEDGEMENTS

I would foremost like to acknowledge Ross Resnick for this work on the pulldowns and WBs presented in this chapter. I would also like to acknowledge Shu-Bing Qian and David Shalloway for providing me with bacterial plasmids. The peak slice images in this chapter were generated using Evgenii Kovrigin's LineShapeKin extension in Sparky. I was supported during part of this work by an NIH-funded CMB training grant T32GM007273. This work was also supported in part by NIH grant R01-AG029385.

SUPPLEMENTARY INFORMATION AVAILABLE

One figure in Appendix 1, which contains overlaid ^{15}N-^{1}H HSQC spectra showing a pH titration of APPc from 4.98 to 7.24.

REFERENCES

Association., A. s. (2016). "Alzheimer's Disease Facts and Figures." Alzheimer's & Dementia **12**(4): 459-509.

Bai, Y., K. Markham, et al. (2008). "The in vivo brain interactome of the amyloid precursor protein." Mol Cell Proteomics **7**(1): 15-34.

Barbagallo, A. P., R. Weldon, et al. (2010). "Tyr(682) in the intracellular domain of APP regulates amyloidogenic APP processing in vivo." PLoS One **5**(11): e15503.

Bour, A., S. Little, et al. (2004). "A secreted form of the beta-amyloid precursor protein (sAPP695) improves spatial recognition memory in OF1 mice." Neurobiol Learn Mem **81**(1): 27-38.

Buxbaum, J. D., K. N. Liu, et al. (1998). "Evidence that tumor necrosis factor alpha converting enzyme is involved in regulated alpha-secretase cleavage of the Alzheimer amyloid protein precursor." J Biol Chem **273**(43): 27765-7.

Carbajo, R. J. and J. L. Neira (2013). NMR for Chemists and Biologists, Springer Netherlands.

Cavalli, V., P. Kujala, et al. (2005). "Sunday Driver links axonal transport to damage signaling." J Cell Biol **168**(5): 775-87.

Cavanagh, J. (2007). Protein NMR spectroscopy: principles and practice, Academic Pr.

Chafekar, S. M., S. Wisen, et al. (2012). "Pharmacological tuning of heat shock protein 70 modulates polyglutamine toxicity and aggregation." ACS Chem Biol **7**(9): 1556-64.

Chang, K. A., H. S. Kim, et al. (2006). "Phosphorylation of amyloid precursor protein (APP) at Thr668 regulates the nuclear translocation of the APP intracellular domain and induces neurodegeneration." Mol Cell Biol **26**(11): 4327-38.

Chartier-Harlin, M. C., F. Crawford, et al. (1991). "Early-onset Alzheimer's disease caused by mutations at codon 717 of the beta-amyloid precursor protein gene." Nature **353**(6347): 844-6.

Colangelo, V., J. Schurr, et al. (2002). "Gene expression profiling of 12633 genes in Alzheimer

hippocampal CA1: transcription and neurotrophic factor down-regulation and up-regulation of apoptotic and pro-inflammatory signaling." J Neurosci Res **70**(3): 462-73.

Colombo, A., A. Bastone, et al. (2009). "JNK regulates APP cleavage and degradation in a model of Alzheimer's disease." Neurobiol Dis **33**(3): 518-25.

Colombo, A., M. Repici, et al. (2007). "The TAT-JNK inhibitor peptide interferes with beta amyloid protein stability." Cell Death Differ **14**(10): 1845-8.

Delaglio, F., S. Grzesiek, et al. (1995). "NMRPipe: a multidimensional spectral processing system based on UNIX pipes." J Biomol NMR **6**(3): 277-93.

Di Domenico, F., R. Sultana, et al. (2011). "Quantitative proteomics analysis of phosphorylated proteins in the hippocampus of Alzheimer's disease subjects." J Proteomics **74**(7): 1091-103.

Elliott, E., O. Laufer, et al. (2009). "BAG-1M is up-regulated in hippocampus of Alzheimer's disease patients and associates with tau and APP proteins." J Neurochem **109**(4): 1168-78.

Esch, F. S., P. S. Keim, et al. (1990). "Cleavage of amyloid beta peptide during constitutive processing of its precursor." Science **248**(4959): 1122-4.

Fanghanel, J. (2003). "Enzymatic catalysis of the peptidyl-prolyl bond rotation: are transition state formation and enzyme dynamics directly linked?" Angew Chem Int Ed Engl **42**(5): 490-2.

Fu, M. M. and E. L. Holzbaur (2013). "JIP1 regulates the directionality of APP axonal transport by coordinating kinesin and dynein motors." J Cell Biol **202**(3): 495-508.

Furukawa, K., B. L. Sopher, et al. (1996). "Increased activity-regulating and neuroprotective efficacy of alpha-secretase-derived secreted amyloid precursor protein conferred by a C-terminal heparin-binding domain." J Neurochem **67**(5): 1882-96.

Glenner, G. G. and C. W. Wong (1984). "Alzheimer's disease: initial report of the purification and characterization of a novel cerebrovascular amyloid protein." Biochem Biophys Res Commun **120**(3): 885-90.

Goate, A., M. C. Chartier-Harlin, et al. (1991). "Segregation of a missense mutation in the amyloid precursor protein gene with familial Alzheimer's disease." Nature **349**(6311): 704-6.

Greenwood, A. I., M. J. Rogals, et al. (2011). "Complete determination of the Pin1 catalytic domain thermodynamic cycle by NMR lineshape analysis." J Biomol NMR **51**(1-2): 21-34.

Guenette, S. Y., J. Chen, et al. (1999). "hFE65L influences amyloid precursor protein maturation and secretion." J Neurochem **73**(3): 985-93.

Haass, C. and H. Steiner (2002). "Alzheimer disease gamma-secretase: a complex story of GxGD-type presenilin proteases." Trends Cell Biol **12**(12): 556-62.

Hardy, J. and R. Crook (2001). "Presenilin mutations line up along transmembrane alpha-helices." Neurosci Lett **306**(3): 203-5.

Hassan, A. Q., C. A. Kirby, et al. (2015). "The novolactone natural product disrupts the allosteric regulation of Hsp70." Chem Biol **22**(1): 87-97.

Hirsch, C., E. Jarosch, et al. (2004). "Endoplasmic reticulum-associated protein degradation--one model fits all?" Biochimica et Biophysica Acta (BBA)-Molecular Cell Research **1695**(1-3): 215-223.

Jorissen, E., J. Prox, et al. (2010). "The disintegrin/metalloproteinase ADAM10 is essential for the establishment of the brain cortex." J Neurosci **30**(14): 4833-44.

King, G. D., R. G. Perez, et al. (2003). "X11alpha modulates secretory and endocytic trafficking and metabolism of amyloid precursor protein: mutational analysis of the YENPTY sequence." Neuroscience **120**(1): 143-54.

Kotoglou, P., A. Kalaitzakis, et al. (2009). "Hsp70 translocates to the nuclei and nucleoli, binds to XRCC1 and PARP-1, and protects HeLa cells from single-strand DNA breaks." Cell Stress Chaperones **14**(4): 391-406.

Kouchi, Z., H. Sorimachi, et al. (1999). "Proteasome inhibitors induce the association of Alzheimer's amyloid precursor protein with Hsc73." Biochem Biophys Res Commun **254**(3): 804-10.

Kumar, P., R. K. Ambasta, et al. (2007). "CHIP and HSPs interact with -APP in a proteasome-dependent manner and influence A metabolism." Human molecular genetics **16**(7): 848.

Lee, M. S., S. C. Kao, et al. (2003). "APP processing is regulated by cytoplasmic

phosphorylation." J Cell Biol **163**(1): 83-95.

Lesne, S., M. T. Koh, et al. (2006). "A specific amyloid-beta protein assembly in the brain impairs memory." Nature **440**(7082): 352-7.

Li, H., S. Koshiba, et al. (2008). "Structure of the C-terminal phosphotyrosine interaction domain of Fe65L1 complexed with the cytoplasmic tail of amyloid precursor protein reveals a novel peptide binding mode." J Biol Chem **283**(40): 27165-78.

Mann, D. M. (1988). "Alzheimer's disease and Down's syndrome." Histopathology **13**(2): 125-37.

Massey, A. C., C. Zhang, et al. (2006). "Chaperone-mediated autophagy in aging and disease." Current topics in developmental biology **73**: 205-235.

Masters, C. L., G. Simms, et al. (1985). "Amyloid plaque core protein in Alzheimer disease and Down syndrome." Proc Natl Acad Sci U S A **82**(12): 4245-9.

Matsuda, S., T. Yasukawa, et al. (2001). "c-Jun N-terminal kinase (JNK)-interacting protein-1b/islet-brain-1 scaffolds Alzheimer's amyloid precursor protein with JNK." J Neurosci **21**(17): 6597-607.

Mattson, M. P. (1997). "Cellular actions of beta-amyloid precursor protein and its soluble and fibrillogenic derivatives." Physiol Rev **77**(4): 1081-132.

Morley, J. E., S. A. Farr, et al. (2010). "A physiological role for amyloid-beta protein:enhancement of learning and memory." J Alzheimers Dis **19**(2): 441-9.

Morshauser, R. C., W. Hu, et al. (1999). "High-resolution solution structure of the 18 kDa substrate-binding domain of the mammalian chaperone protein Hsc70." J Mol Biol **289**(5): 1387-403.

Mullan, M., F. Crawford, et al. (1992). "A pathogenic mutation for probable Alzheimer's disease in the APP gene at the N-terminus of beta-amyloid." Nat Genet **1**(5): 345-7.

Nikolaev, A., T. McLaughlin, et al. (2009). "APP binds DR6 to trigger axon pruning and neuron death via distinct caspases." Nature **457**(7232): 981-9.

Nishimoto, I., T. Okamoto, et al. (1993). "Alzheimer amyloid protein precursor complexes with brain GTP-binding protein G(o)." Nature **362**(6415): 75-9.

Oishi, M., A. C. Nairn, et al. (1997). "The cytoplasmic domain of Alzheimer's amyloid precursor protein is phosphorylated at Thr654, Ser655, and Thr668 in adult rat brain and cultured cells." Mol Med **3**(2): 111-23.

Okamoto, T., S. Takeda, et al. (1995). "Ligand-dependent G protein coupling function of amyloid transmembrane precursor." J Biol Chem **270**(9): 4205-8.

Perreau, V. M., S. Orchard, et al. (2010). "A domain level interaction network of amyloid precursor protein and Abeta of Alzheimer's disease." Proteomics **10**(12): 2377-95.

Pierpaoli, E. V. (2005). "The role of Hsp70 in age-related diseases and the prevention of cancer." Ann N Y Acad Sci **1057**: 206-19.

Podlisny, M. B., B. L. Ostaszewski, et al. (1995). "Aggregation of secreted amyloid beta-protein into sodium dodecyl sulfate-stable oligomers in cell culture." J Biol Chem **270**(16): 9564-70.

Prasher, V. P., M. J. Farrer, et al. (1998). "Molecular mapping of Alzheimer-type dementia in Down's syndrome." Ann Neurol **43**(3): 380-3.

Puzzo, D., L. Privitera, et al. (2008). "Picomolar amyloid-beta positively modulates synaptic plasticity and memory in hippocampus." J Neurosci **28**(53): 14537-45.

Radzimanowski, J., B. Simon, et al. (2008). "Structure of the intracellular domain of the amyloid precursor protein in complex with Fe65-PTB2." EMBO Rep **9**(11): 1134-40.

Ramelot, T. A., L. N. Gentile, et al. (2000). "Transient structure of the amyloid precursor protein cytoplasmic tail indicates preordering of structure for binding to cytosolic factors." Biochemistry **39**(10): 2714-25.

Ramelot, T. A. and L. K. Nicholson (2001). "Phosphorylation-induced structural changes in the amyloid precursor protein cytoplasmic tail detected by NMR." J Mol Biol **307**(3): 871-84.

Raychaudhuri, M. and D. Mukhopadhyay (2007). "AICD and its adaptors - in search of new players." J Alzheimers Dis **11**(3): 343-58.

Ring, S., S. W. Weyer, et al. (2007). "The secreted beta-amyloid precursor protein ectodomain APPs alpha is sufficient to rescue the anatomical, behavioral, and electrophysiological abnormalities of APP-deficient mice." J Neurosci **27**(29): 7817-26.

Scheinfeld, M. H., R. Roncarati, et al. (2002). "Jun NH2-terminal kinase (JNK) interacting protein 1 (JIP1) binds the cytoplasmic domain of the Alzheimer's beta-amyloid precursor protein (APP)." J Biol Chem **277**(5): 3767-75.

Scheuner, D., C. Eckman, et al. (1996). "Secreted amyloid beta-protein similar to that in the senile plaques of Alzheimer's disease is increased in vivo by the presenilin 1 and 2 and APP mutations linked to familial Alzheimer's disease." Nat Med **2**(8): 864-70.

Schmidt, V., A. Sporbert, et al. (2007). "SorLA/LR11 regulates processing of amyloid precursor protein via interaction with adaptors GGA and PACS-1." J Biol Chem **282**(45): 32956-64.

Selkoe, D. J. (1998). "The cell biology of beta-amyloid precursor protein and presenilin in Alzheimer's disease." Trends Cell Biol **8**(11): 447-53.

Seubert, P., C. Vigo-Pelfrey, et al. (1992). "Isolation and quantification of soluble Alzheimer's beta-peptide from biological fluids." Nature **359**(6393): 325-7.

Shankar, G. M. and D. M. Walsh (2009). "Alzheimer's disease: synaptic dysfunction and Abeta." Mol Neurodegener **4**: 48.

Shin, Y., J. Klucken, et al. (2005). "The co-chaperone carboxyl terminus of Hsp70-interacting protein (CHIP) mediates alpha-synuclein degradation decisions between proteasomal and lysosomal pathways." J Biol Chem **280**(25): 23727-34.

Shoji, M., T. E. Golde, et al. (1992). "Production of the Alzheimer amyloid beta protein by normal proteolytic processing." Science **258**(5079): 126-9.

Sinha, S., J. P. Anderson, et al. (1999). "Purification and cloning of amyloid precursor protein beta-secretase from human brain." Nature **402**(6761): 537-40.

Slomnicki, L. P. and W. Lesniak (2008). "A putative role of the Amyloid Precursor Protein Intracellular Domain (AICD) in transcription." Acta Neurobiol Exp (Wars) **68**(2): 219-28.

Sodhi, C. P., R. G. Perez, et al. (2008). "Phosphorylation of beta-amyloid precursor protein

(APP) cytoplasmic tail facilitates amyloidogenic processing during apoptosis." Brain Res **1198**: 204-12.

Sodhi, C. P., S. Rampalli, et al. (2004). "The endocytotic pathway is required for increased A beta 42 secretion during apoptosis." Brain Res Mol Brain Res **128**(2): 201-11.

Spoelgen, R., C. A. von Arnim, et al. (2006). "Interaction of the cytosolic domains of sorLA/LR11 with the amyloid precursor protein (APP) and beta-secretase beta-site APP-cleaving enzyme." J Neurosci **26**(2): 418-28.

Takahashi, K., T. Niidome, et al. (2008). "Phosphorylation of amyloid precursor protein (APP) at Tyr687 regulates APP processing by alpha- and gamma-secretase." Biochem Biophys Res Commun **377**(2): 544-9.

Tarr, P. E., R. Roncarati, et al. (2002). "Tyrosine phosphorylation of the beta-amyloid precursor protein cytoplasmic tail promotes interaction with Shc." J Biol Chem **277**(19): 16798-804.

Theuns, J., N. Brouwers, et al. (2006). "Promoter mutations that increase amyloid precursor-protein expression are associated with Alzheimer disease." Am J Hum Genet **78**(6): 936-46.

van der Kant, R. and L. S. Goldstein (2015). "Cellular functions of the amyloid precursor protein from development to dementia." Dev Cell **32**(4): 502-15.

Vassar, R., B. D. Bennett, et al. (1999). "Beta-secretase cleavage of Alzheimer's amyloid precursor protein by the transmembrane aspartic protease BACE." Science **286**(5440): 735-41.

Vieira, S. I., S. Rebelo, et al. (2010). "Retrieval of the Alzheimer's amyloid precursor protein from the endosome to the TGN is S655 phosphorylation state-dependent and retromer-mediated." Mol Neurodegener **5**: 40.

Vingtdeux, V., M. Hamdane, et al. (2007). "Alkalizing drugs induce accumulation of amyloid precursor protein by-products in luminal vesicles of multivesicular bodies." Journal of Biological Chemistry **282**(25): 18197.

Walsh, D. M., I. Klyubin, et al. (2002). "Naturally secreted oligomers of amyloid beta protein potently inhibit hippocampal long-term potentiation in vivo." Nature **416**(6880): 535-9.

Walsh, D. M., B. P. Tseng, et al. (2000). "The oligomerization of amyloid beta-protein begins intracellularly in cells derived from human brain." Biochemistry **39**(35): 10831-9.

Wang, A. M., Y. Miyata, et al. (2013). "Activation of Hsp70 reduces neurotoxicity by promoting polyglutamine protein degradation." Nat Chem Biol **9**(2): 112-8.

Wang, S., F. Cesca, et al. "Synapsin I is an oligomannose-carrying glycoprotein, acts as an oligomannose-binding lectin, and promotes neurite outgrowth and neuronal survival when released via glia-derived exosomes." J Neurosci **31**(20): 7275-90.

Williamson, M. P. (2013). "Using chemical shift perturbation to characterise ligand binding." Prog Nucl Magn Reson Spectrosc **73**: 1-16.

Yan, R., M. J. Bienkowski, et al. (1999). "Membrane-anchored aspartyl protease with Alzheimer's disease beta-secretase activity." Nature **402**(6761): 533-7.

Young-Pearse, T. L., A. C. Chen, et al. (2008). "Secreted APP regulates the function of full-length APP in neurite outgrowth through interaction with integrin beta1." Neural Dev **3**: 15.

Zhang, P., J. I. Leu, et al. (2014). "Crystal structure of the stress-inducible human heat shock protein 70 substrate-binding domain in complex with peptide substrate." PLoS One **9**(7): e103518.

Zhang, Y. W., R. Thompson, et al. (2011). "APP processing in Alzheimer's disease." Mol Brain **4**: 3.

Zhang, Z., C. H. Lee, et al. (1997). "Sequence-specific recognition of the internalization motif of the Alzheimer's amyloid precursor protein by the X11 PTB domain." EMBO J **16**(20): 6141-50.

Zhao, G., J. Tan, et al. (2007). "The same gamma-secretase accounts for the multiple intramembrane cleavages of APP." J Neurochem **100**(5): 1234-46.

Zhi, P., P. Z. Chia, et al. (2011). "Intracellular trafficking of the beta-secretase and processing of amyloid precursor protein." IUBMB Life **63**(9): 721-9.

CHAPTER 3

NEIGHBORING PHOSPHO-SER-PRO MOTIFS IN THE UNDEFINED DOMAIN OF IRAK1 IMPART BIVALENT ADVANTAGE FOR PIN1 BINDING[1]

ABSTRACT

Peptidyl prolyl isomerases (PPIases) are proteins that catalyze the exchange of Xxx-Pro peptide bonds between *trans* and *cis* isomer states (ω=180º and ω=0º). Pin1 is the only phosphorylation-directed PPIase known in humans, specifically targeting phosphoSer/Thr-Pro motifs. Pin1 has two domains, which are traditionally considered binding (WW) and catalytic (PPIase) domains, both of which interact with the same phosphoSer/Thr-Pro motif. The substrate overlap between the two domains may play an important role in substrate selection, since many known Pin1 substrates have multiple phosphoSer/Thr-Pro motifs in close proximity, including the protein IRAK1. Pin1 is necessary for the autophosphorylation and activation of IRAK1, a critical step in toll-like receptor/interleuken-1 receptor (TLR/IL-1R) signaling cascades. The IRAK1 undefined

[1] This chapter has been adapted from Rogals MJ, Greenwood AI, Kwon J, Lu KP, Nicholson LK (2016). Neighboring phospho-Ser-Pro in the undefined domain of IRAK1 impart bivalent advantage for Pin1 binding. Submitted to Federation of European Biochemists Society Journal.

domain (UD) contains multiple phosphoSer/Thr-Pro binding sites, including two sets of neighboring Ser-Pro motifs (Ser131/Ser144 and Ser163/Ser173), suggesting the potential for bivalent interactions. Using a series of NMR titrations with ^{15}N-labeled individual domains of Pin1 or full length Pin1, and unlabeled synthetic phosphopeptides derived from IRAK1-UD, the affinity enhancement of bivalent binding between Pin1 and peptides representing hyperphosphorylated IRAK1 is demonstrated. These results suggest that, given the many Pin1 substrates in the cell, hyperphosphorylation might provide a competitive advantage for engaging certain targets with Pin1.

INTRODUCTION

The peptidyl prolyl isomerase Pin1 is a key regulator of diverse cellular processes in humans (Zheng, You et al. 2002; Lu and Zhou 2007; Shaw 2007). Pin1 has a substantial effect on neuronal development and survival, and appears to regulate the processing of amyloid precursor protein (APP) in cell culture (Pastorino, Sun et al. 2006). It is also important for telomere maintenance (Lee, Tun-Kyi et al. 2009) and chromatin condensation (Xu and Manley 2007). The multitude of roles Pin1 plays is not surprising since it is unique in its ability to isomerize phosphorylated Ser-Pro or phosphorylated Thr-Pro (pS/T-P) motifs, which are highly prevalent in eukaryotes, constituting over a quarter of all protein phosphorylation sites (Lu, Hanes et al. 1996; Yaffe, Schutkowski et al. 1997; Ubersax and Ferrell 2007; Yeh and Means 2007; Innes, Bailey et al. 2013; Lu and Hunter 2014).

Pin1 has two domains, a catalytic PPIase domain that performs interconversion between *cis* and *trans* pS/T-P peptide bonds, and a type IV WW binding domain that binds to pS/T-P motifs (Ranganathan, Lu et al. 1997). The selection of targets by Pin1 will be driven by the

relative amounts and affinities of potential interaction partners, as well as their phosphorylation states. The balance of specific kinase and phosphatase activities at the multitude of pS/T-P motifs within the cell determines what substrates are available to Pin1 at any given moment.

A key factor in Pin1 substrate selection may be the number of pS/T-P motifs in close spatial proximity in a potential substrate protein. In principle, the WW domain could anchor the enzyme at one pS/T-P site, while the PPIase domain isomerizes a neighboring pS/T-P site. This simultaneous or bivalent binding can theoretically increase the effective binding affinity by orders of magnitude (Jencks 1981; Mammen, Choi et al. 1998; Daum, Lucke et al. 2007). Indeed, a PPIase inhibitor and a WW domain inhibitor, linked using various lengths of polyproline helices are more effective at inhibiting Pin1 activity than either inhibitor alone (Daum, Lucke et al. 2007). This suggests that cellular Pin1 partners with multiple motifs may use a similar mechanism to enhance their interaction with Pin1. Many known Pin1 substrates are phosphorylated at multiple nearby pS/T-Pro sites, including RNA polymerase II (Myers, Morris et al. 2001), tau (Smet, Wieruszeski et al. 2005), the transcription factor c-Jun (Wulf, Ryo et al. 2001), cdc25c (Innes, Bailey et al. 2013), Notch (Rustighi, Tiberi et al. 2009) and IRAK1 (Tun-Kyi, Finn et al. 2011).

IRAK1 is a kinase comprised of four domains: a death domain (DD), an undefined domain (UD), a kinase domain (KD) and a C-terminal domain (CTD) (Figure 3.1). IRAK1 plays a critical role in innate immunity in humans, specifically acting as part of the Toll-like receptor /Interlukein-1 receptor (TLR/IL-1R) signaling cascades. Upon receptor stimulation, a multi-protein signaling complex assembles on the cytoplasmic side of the receptor. This signaling complex is initiated by receptor dimerization, which creates a platform for recruitment of MyD88, which in turn recruits IRAK4 leading to formation of a scaffold thought to be comprised

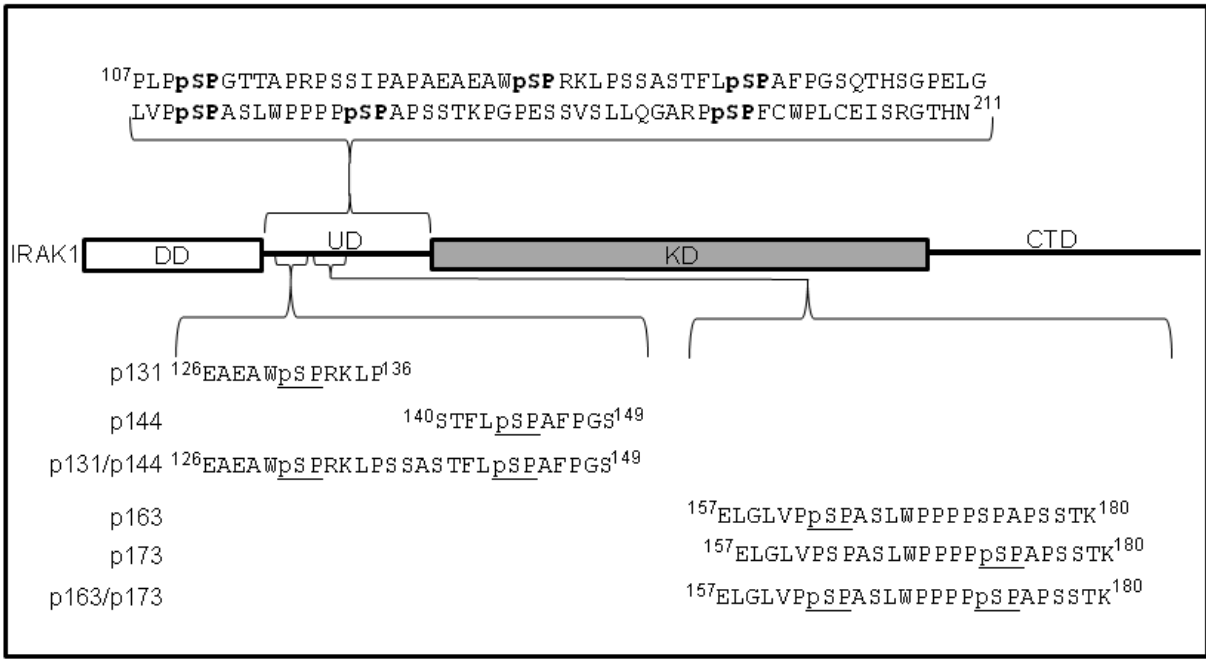

Figure 3.1 Diagram of the peptide sequences used, shown in context of full length IRAK1. The synthetic peptides used in these experiments are aligned by shared phosphorylation sites. The separation between the sets of proximal sites used in the bivalent binding-capable peptides is shown with regards to a diagram of IRAK1-FL where the DD is the death domain (residues 27-106), UD is the undefined domain (107-211), KD is the kinase domain (212-521), and CTD is the C-terminal domain (521-691). The rectangles represent areas of predicted stable 3D structure and the lines are predicted intrinsically disordered regions.

of four MyD88 and four IRAK4 subunits (Lin, Lo et al. 2010). This scaffold recruits and phosphorylates four IRAK1 molecules, leading to autophosphorylation of multiple Ser sites in the UD and activation of IRAK1, in a Pin1-dependent manner (Flannery and Bowie 2010; Tun-Kyi, Finn et al. 2011). Autophosphorylation of the IRAK1-UD results in six pS-P motifs, with two pairs of motifs (pS131/pS144 and pS163/pS173) separated by less than 12 residues (Figure 3.1). Intriguingly, these two IRAK1-UD regions are implicated in the mechanism of Pin1 activation of IRAK1 (Tun-Kyi, Finn et al. 2011).

Here, we have investigated potential bivalent interactions of Pin1 and the IRAK1-UD using NMR titration experiments with ^{15}N-labeled Pin1 (full-length (FL), PPIase, or WW domain) and phosphopeptides (either singly or dually phosphorylated) representing the pS133/pS144 and pS163/pS173 regions of IRAK1-UD. Binding of singly-phosphorylated peptides to isolated Pin1 domains was first measured, then binding of singly-phosphorylated peptides to Pin1-FL, and finally binding of dually phosphorylated peptides to Pin1-FL. The affinities determined using singly phosphorylated peptides provided parameters for analysis of the complex binding interaction between dually phosphorylated peptides and Pin1-FL, and allowed bivalent binding of these peptides to be modeled. These interactions were quantified using NMR titration analysis, a powerful technique to investigate multi-state equilibria of complex protein/ligand interactions. We have employed a novel combination of Virtual Cell modeling software (Dubitzky, Wolkenhauer et al.) in conjunction with in-house MATLAB code to perform simulations and to fit NMR titration data. These studies provide novel insights regarding the complexity of interactions between Pin1 and activated IRAK1, and more broadly suggest that phosphorylation of neighboring S/T-P motifs in proteins might provide competitive advantage for engaging with Pin1.

RESULTS & DISCUSSION

Isolated PPIase and WW domains display a range of binding affinities for singly phosphorylated IRAK1 UD-derived peptides. To provide a foundation for investigating bivalent interactions between Pin1 and IRAK1-UD, we first performed a series of NMR-detected titration experiments using isolated ^{15}N-labeled PPIase and WW domains and unlabeled, singly phosphorylated peptides representing the regions of interest in IRAK1-UD (Figure 3.1). The K_d values for WW binding to p131, p144 and p173 peptides were previously published (Tun-Kyi, Finn et al. 2011), and binding of p173 to the PPIase domain in full length Pin1 was extremely weak (*vide infra*) so was not investigated for the isolated PPIase domain. For the four remaining domain/peptide interactions (WW binding to p163, and PPIase binding to p131, p144, and p163), the ^{15}N-^{1}H HSQC spectrum for a constant concentration of each ^{15}N-labeled domain was used to monitor chemical shift perturbations of selected peaks as a function of peptide concentration to produce binding curves (Figure 3.2, Figure A1.8).

For the group of selected peaks in a given titration, the observed residue-specific chemical shift changes (relative to apo) in the^{15}N and ^{1}H dimensions ($\Delta\delta^{n,i}_{N,obs}$ and $\Delta\delta^{n,i}_{H,obs}$ for residue *n* and at titration point *i*, respectively) were globally fit to the standard bimolecular reaction scheme (Figure 3.3A). For this model, fitted parameters consist of the global K_d and residue-specific bound chemical shifts, $\Delta\delta^{n}_{N,bound}$ and $\Delta\delta^{n}_{H,bound}$. Errors in $\Delta\delta^{n,i}_{N,obs}$ and $\Delta\delta^{n,i}_{H,obs}$ were estimated by two methods as described in Materials and Methods, yielding $\sigma_{\Delta\delta N}$ = 0.028 ppm and $\sigma_{\Delta\delta H}$ = 0.0042 ppm (based on peaks insensitive to ligand addition) and $\sigma_{\Delta\delta N}$ = 0.0205 ppm and $\sigma_{\Delta\delta H}$ = 0.00407 ppm. The close agreement between these two sets of errors supports the use of the bimolecular model for each domain. The corresponding set of errors, $\sigma_{\Delta\delta N}$ = 0.0205 ppm and $\sigma_{\Delta\delta H}$ = 0.00407 ppm, were used here and for the more complex binding equilibria

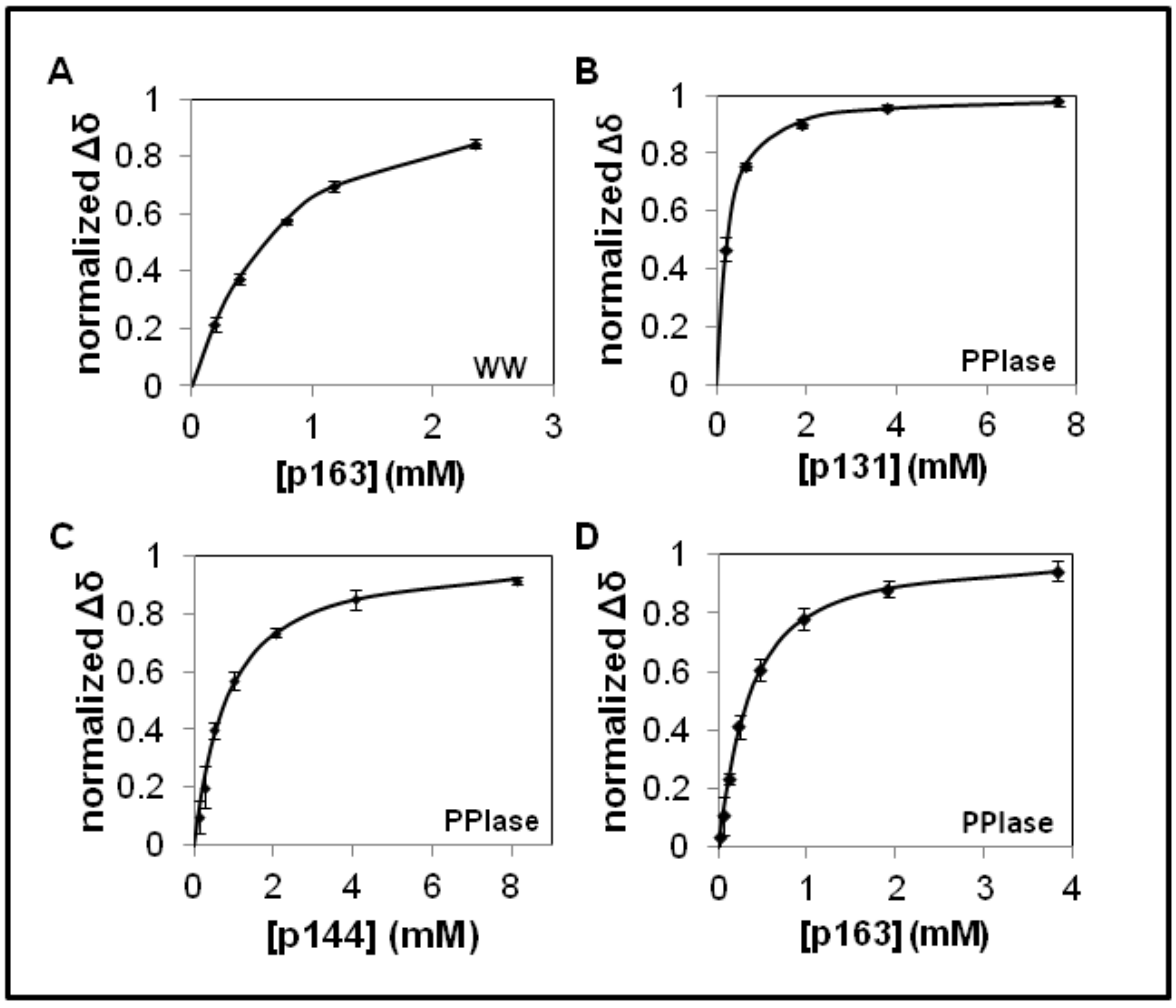

Figure 3.2 Goodness of fit of bimolecular model to data for titrations of isolated Pin1 domains with singly phosphorylated IRAK1-UD peptides. Binding curves are shown, where lines are calculated curves and diamonds are the normalized mean of the chemical shift perturbation of the binding of different IRAK1-UD-derived peptides to isolated domains of Pin1. Chemical shift perturbations were normalized by dividing the measured perturbation by the final chemical shift perturbation for each residue. The X-axis is the concentration of the individual peptide in mM and the y-axis is the mean of the normalized chemical shift perturbation of selected residues (see methods section). Error bars are the standard deviation of the individual residues from the mean. Plots are of A) WW domain binding to p163 (residues used were S18, R21, V22, W34e, W34, and E35 in the proton dimension and S18, R21, V22, Y23, Y24, W34, and E35 in the nitrogen dimension), B) PPIase domain binding to p131 (residues used were H59, R68, R69, S114, K117, L122, R127, G128, and M130 in the proton dimension, and H59, V62, R68, R69, S114, K117, L122, R127, G128, and M130 in the nitrogen dimension), C) PPIase domain binding to p144 (residues used were V62, R68, R69, S114, S115, A116, L122, G128, and Q129 in both dimensions), and D) PPIase domain binding to p163 (residues used were H59, L61, V62, R69, S115, A116, A118, R119, R127 and Q129 in both dimensions).

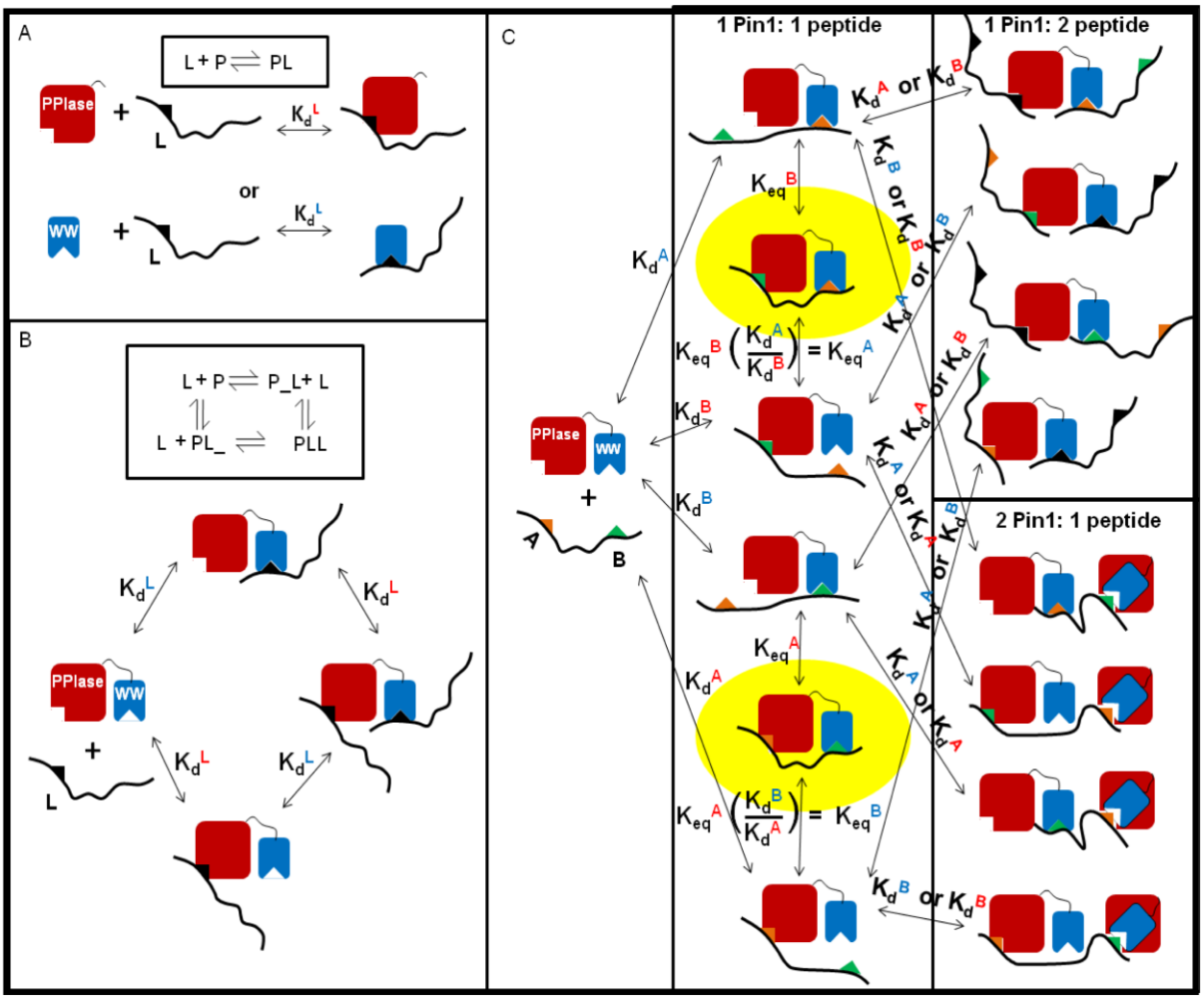

Figure 3.3 Models for interactions of monovalent and bivalent peptides with Pin1**.** A) Simple bimolecular binding equilibrium, [L] + [P] ↔ [PL], where P is either isolated WW or PPIase domain and L is a singly phosphorylated (monovalent) peptide. B) The four-state model for Pin1-FL (P in diagram) binding to a monovalent peptide (L) in a 1:1 fashion bound to either the WW domain (PL_) or the PPIase domain (P_L) or in a 2:1 fashion with two peptides bound to Pin1, one in each domain (PLL). C) Multi-state model for Pin1-FL binding to a bivalent peptide where A (orange triangle) is the N-terminal site (either p131 or p163) and B (green triangle) is the C-terminal site (either p144 or p173). For simplicity, black triangles represent either site and the overlayed binding sites on Pin1 represent binding to either domain

investigated (*vide infra*).

The resulting affinities for each singly phosphorylated peptide binding to the individual domains range between 120 to nearly 700 μM (Table 3.1), indicating that these *individual* pS-P motifs would not be expected to be significant Pin1 binding partners at low to submicromolar concentrations, as might be found in cells. These reported affinities are "apparent" binding constants (K_d^{app}) that do not distinguish the isomer state of the ligand. Although the intrinsic binding constants for each isomer can be determined (De, Greenwood et al. 2012), the focus of the present study is on bivalent binding, for which K_d^{app} provides the necessary measure of the total bound domain for given conditions. Notably, p131 and p163 both display tighter binding to the PPIase catalytic domain than to the WW binding domain. This is unusual, since for Pin1 the WW domain typically displays higher substrate affinity while the PPIase domain is a classical enzyme with weaker binding to substrates (Verdecia, Bowman et al. 2000). While the consensus Pin1 binding sequence Pintide (Yaffe, Schutkowski et al. 1997) displays appreciable binding to the PPIase domain (K_d = 86 μM), this peptide library-derived sequence does bind more strongly to the WW domain (K_d = 44 μM) (Verdecia, Bowman et al. 2000). In the context of the isolated Pin1 domains, the p131 and p163 peptides are to our knowledge the first natural Pin1 substrate sequences to display greater preference for the PPIase domain than to the WW domain.

The binding of singly phosphorylated peptides derived from natural Pin1 interactors to isolated domains of Pin1 has been studied previously (Verdecia, Bowman et al. 2000; De, Greenwood et al. 2012). The advantage of the current work lies in the use of NMR, which provides domain-specific information in Pin1-FL titrations. Fluorescence anisotropy, as used by Verdecia et al. (Verdecia, Bowman et al. 2000), is unable to distinguish between binding events

Table 3.1 Binding affinities for the interaction of isolated Pin1 domains and IRAK1-UD derived peptides.

	WW K_d	Proton reduced X^2	Nitrogen reduced X^2	PPIase K_d	Proton reduced X^2	Nitrogen reduced X^2
p131	220±15 μM*			161±31 μM	0.53	0.86
p144	120±12 μM*			689±149 μM	0.92	1.05
p163	385±96 μM	0.97	0.61	230±42 μM	0.90	0.61
p173	260 ± 75 μM*			n.d.		

*results published by Tun-Kyi, Greenwood et al., 2011.

to each domain and therefore their data was analyzed as bimolecular interactions. This lack of detail also affected analysis of the dually phosphorylated peptide included in their study; they were unable to study the possibility of bivalent interaction, which we explore in detail in this study.

PPIase and WW domains in full length Pin1 display distinct binding affinities to singly phosphorylated, IRAK1 UD-derived peptides when compared with isolated domains. NMR titration experiments were next performed using full-length ^{15}N-Pin1 (Pin1-FL) and the four singly-phosphorylated IRAK1 peptides (Figure 3.1). These measurements investigate whether linking the WW and PPIase domains alters binding affinity for these IRAK1 peptides, and provide necessary parameters for analyzing titrations with dually phosphorylated peptides (*vide infra*). Since each domain can in principle bind to the same singly phosphorylated peptide, titration data was analyzed using a four-state model (Figure 3.3B). This model includes two apparent binding constants, $K_d^{WW,app}$ and $K_d^{PPIase,app}$. As NMR allows direct observation of residues in each domain, it is uniquely suited for determining domain-specific affinities. Residues for each domain were selected based on their sensitivity to binding, as reflected by peak movement. Binding curves (Figure 3.4, Figure A1.9) for selected residues were simultaneously (i.e. globally) fit (proton and nitrogen dimensions were fit separately) to obtain $K_d^{WW,app}$ and $K_d^{PPIase,app}$ (Table 3.2), as well as the residue-specific bound chemical shifts, $\Delta\delta^n_{N,bound}$ and $\Delta\delta^n_{H,bound}$ for each domain.

Interestingly, several significant differences are observed in the resulting affinities of these singly phosphorylated peptides compared with their binding to the isolated PPIase and

Figure 3.4 Goodness of fit of four-state model to data for titrations of Pin1-FL with singly phosphorylated IRAK1-UD peptides. In these binding curves, datapoints represent the normalized mean of the observed chemical shift perturbations ($\Delta\delta^{n}_{obs}$) for the selected domain-specific residues, and lines are the corresponding normalized mean values from the resulting fits to the four-state model. Chemical shift perturbations were normalized by dividing the measured or calculated perturbation by the fitted $\Delta\delta^{n}_{bound}$ for each residue *n*. WW domain data are denoted by blue open diamonds (nitrogen dimension) and blue + (proton dimension), and PPIase domain data by red open squares (nitrogen dimension) and red X (proton dimension). Dashed lines represent the fits in the nitrogen dimension and solid lines represent the corresponding fits in the proton dimension, color coded by domain (WW=blue, PPIase=red). The error bars are the standard deviation of the individual residues from the mean. Plots of Pin1-FL binding to A) p131 (selected residues were F25, Q33, W34, W34e, E35, H59, R69, S114, S115, R127, G128, Q129, and M130 in the proton dimension, and Y23, Y24, Q33, W34, W34e, E35, V62, R69, S114, A116, R127, G128, Q129, and M130 in the nitrogen dimension), B) p144 (selected residues were Y24, F25, W34, W34e, E35, H59, V62, R69, S114, S115, A116, G128, and Q129 in the proton dimension, and Y23, Y24, F25, Q33 W34, W34e, V62, R69, S114, S115, A116, R127, G128, and Q129 in the nitrogen dimension), C) p163 (selected residues were Y23, Y24, W34, W34e, H59, V61, V62, R69, A116, K117, A118, G128, and Q129 in the proton dimension, and Y23, Y24, W34, E35, H59, V62, R69, S115, A116, A118, R127, Q129 and K132 in the nitrogen dimension), and D) p173 (selected residues were F25, W34, W34e, S114, and S115 in the proton dimension as well as Y23, Y24, F25, W34, E35, R68, Q129, and M130.).

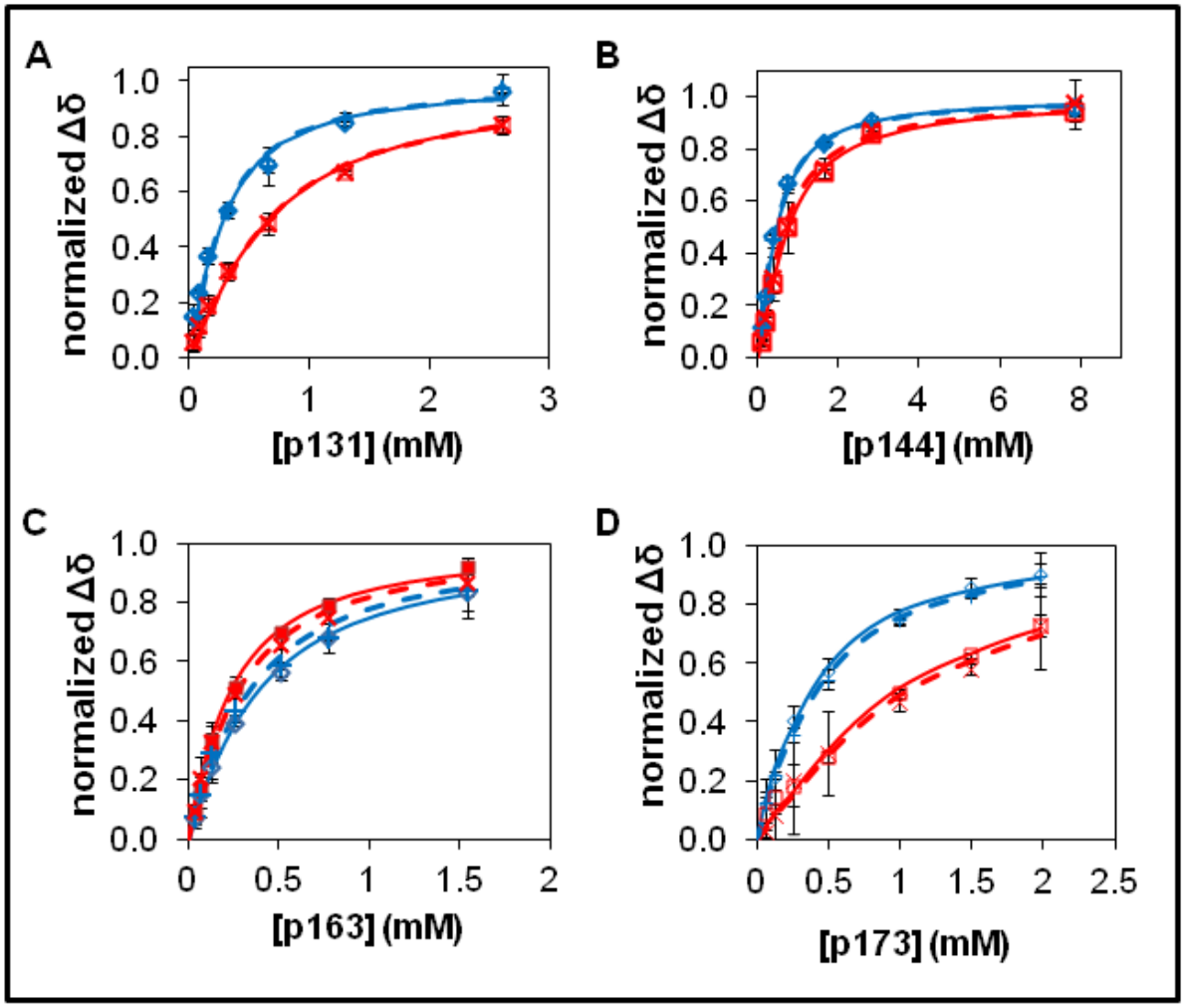
A
normalized Δδ
1.0
0.8
0.6
0.4
0.2
0.0
0
1
2
3
[p131] (mM)
B
normalized Δδ
1.0
0.8
0.6
0.4
0.2
0.0
0
2
4
6
8
[p144] (mM)
C
normalized Δδ
1.0
0.8
0.6
0.4
0.2
0.0
0
0.5
1
1.5
2
[p163] (mM)
D
normalized Δδ
1.0
0.8
0.6
0.4
0.2
0.0
0
0.5
1
1.5
2
2.5
[p173] (mM)

Table 3.2 Binding affinities for the interaction of Pin1-FL and IRAK1-UD derived peptides.

	WW K_d		PPIase K_d		Reduced X^2	
	Proton	Nitrogen	Proton	Nitrogen	Proton	Nitrogen
p131	145±11 μM	151±06 μM	424±24 μM	427±28 μM	1.17	2.25
p144	257 ±10 μM	255±17 μM	414±23 μM	470±33 μM	1.56	0.71
p163	233±27 μM	279±26 μM	185±15 μM	157±08 μM	1.17	0.5
p173	215±19 μM	186±25 μM	681±178 μM	611±236 μM	2.18	0.6

WW domains (Table 3.1 & 3.2). For the p131 site, linking the WW and PPIase domain in Pin1-FL significantly weakens binding to the PPIase domain, while slightly enhancing binding to the WW domain. Conversely, for the p144 site, linking the two domains strengthens affinity to the PPIase domain and weakens affinity to the WW domain. For the p163 site, Pin1-FL provides a binding enhancement for both domains relative to their isolated forms, and further accentuates the anomalous preference of this site for the PPIase domain. Finally, for the p173 site, the PPIase residues of Pin1-FL display very little chemical shift perturbation upon titration (reflecting very weak binding), while WW binding affinity is approximately the same as for the isolated WW domain. Due to the weak binding affinity observed for the p173 peptide with PPIase in Pin1-FL, the isolated PPIase domain titration with p173 peptide was not performed (*vide supra*). For three of the four pS-P sites examined, the intrinsic binding affinities display sensitivity to the presence of both Pin1 domains, suggesting allosteric interactions between domains.

Several prior studies support the presence of allosteric interactions between the PPIase and WW domains of Pin1. In terms of the PPIase domain catalytic function, its affinity and isomerization rate depend on the presence of the WW domain (Lu, Wulf et al. 1999; Namanja, Wang et al. 2011). Interestingly, numerous x-ray crystal structures of Pin1 reveal a clear interaction interface between the PPIase and WW domains (Ranganathan, Lu et al. 1997; Verdecia, Bowman et al. 2000; Potter, Oldfield et al. 2010; Potter, Ray et al. 2010; Urusova, Shim et al. 2011; Zhang, Wang et al. 2012; Chen, Li et al. 2015; Innes, Sowole et al. 2015). In solution, interdomain coupling, which was quantified in terms of global tumbling of each domain, is enhanced in a ligand-dependent manner (Jacobs, Saxena et al. 2003; VanWart, Eargle et al. 2012), and an allosteric conduit connecting the PPIase and WW domains in Pin1 has been elucidated through methyl group and backbone dynamics studies (Namanja, Wang et al. 2011;

Wilson, Bouchard et al. 2013).

Here, we also observe clear evidence for interdomain communication, not only in the altered affinities resulting from linking the PPIase and WW domains, but also in chemical shift changes induced by binding of singly phosphorylated ligands to isolated PPIase and WW domains. For example, titrations of isolated PPIase domain with each of the p131 and p144 peptides show chemical shift perturbations (Figure 3.5A) in the previously defined conduit residues (Namanja, Wang et al. 2011; Wilson, Bouchard et al. 2013). The p131 and p144 peptides (only 11 residues long) should avert non-specific encounters between extended segments of bound peptide and remote regions of the PPIase domain. For a given conduit residue, chemical shift changes induced by both ligands lie along a linear trajectory, with p131 imparting greater effect than p144 (Figure 3.5A, right column), suggesting a ligand-dependent shift in the conformational ensemble sampled by the dynamic conduit (Namanja, Wang et al. 2011; Wilson, Bouchard et al. 2013). In contrast, catalytic site residue peaks move in entirely different directions in response to addition of p131 versus p144 (Figure 3.5A, left column), reflecting the distinct chemical features of p131 and p144 peptides (Figure 3.1). Our observation that linkage of the PPIase and WW domains in Pin1-FL strengthens binding of p131 to the WW domain suggests that the dynamic conduit serves as a positive allosteric regulator of p131 binding to the WW domain. Since p144 binding to the WW domain in Pin1-FL is weaker than to the isolated WW domain, this suggests that the effect of the allosteric conduit is highly ligand-specific.

A similar analysis from the perspective of the isolated WW domain shows the same trend of linear chemical shift perturbations induced by p131 and p144 peptide binding for residues in the interdomain interface (Figure 3.5B). Remarkably, although p144 binds more tightly than

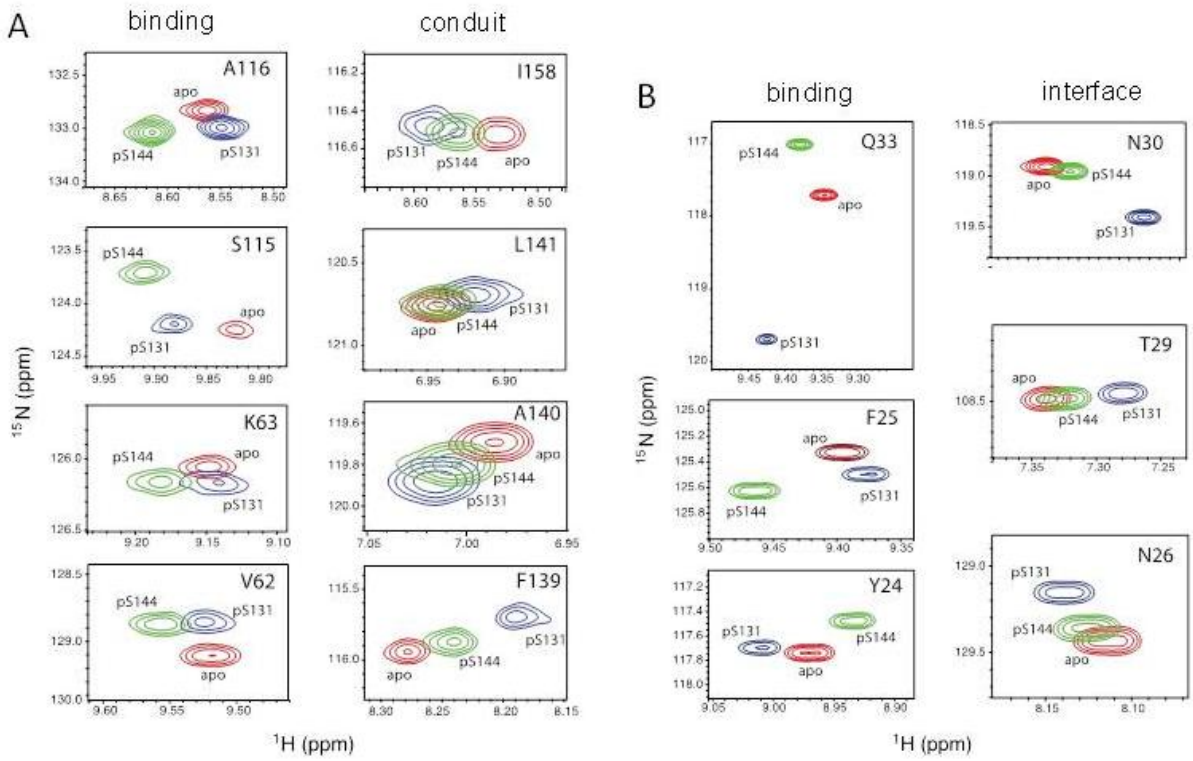

Figure 3.5 Difference between peak movements attributable to interdomain interactions versus protein-peptide binding induced by titration with p131 and p144. Regions extracted from ^{15}N-^{1}H HSQC spectra of Pin1-FL in apo (red), the most saturated spectrum from titration with p131 (blue), and the most saturated spectrum from titration with p144 (green). A) PPIase residues in either the binding site or implicated in conduit that informs on allostery (Namanja, Wang et al. 2011; Wilson, Bouchard et al. 2013). B) WW residues in either the binding site or at the interface between the two domains.

p131 to the isolated WW domain, p131 again imparts larger chemical shift changes in interface residues at the highest peptide concentrations examined. Specifically, T29 and N30 that directly hydrogen bond to the PPIase domain in Pin1-FL, and N26 that hydrogen bonds to T29 and I28, undergo ligand-induced peak movements along the same direction in the isolated WW domain, with larger perturbations induced by p131. Since binding of p131 to the PPIase domain in Pin1-FL is significantly weaker than to the isolated PPIase domain (Table 3.1 & 3.2), this suggests that the ligand-induced conformational shift at the WW domain interface region acts as a negative allosteric regulator of binding to the PPIase domain. The smaller p144-induced perturbation of interface residues correlates with the smaller weakening of PPIase affinity for this ligand in Pin1-FL (Table 3.1 & 3.2), and is consistent with a negative allosteric mechanism.

Evidence for Pin1-FL bivalent binding to dually phosphorylated IRAK1-derived peptides. To investigate possible simultaneous binding of Pin1 to neighboring pS-P motifs, the two IRAK1-UD derived peptides, p131/p144 and p163/p173 (Figure 3.1), were used in titration experiments with ^{15}N-Pin1-FL (Figure 3.6). For each dually phosphorylated peptide titration, either pS-P site can bind to either of the two Pin1 domains, generating a multi-state equilibrium (Figure 3.3C). This model accounts for all possible interaction states between Pin1-FL and a dually phosphorylated peptide, and includes two bivalent states that are each accessed via two monovalent states. While simpler models have been previously employed for Pin1 binding to ligands containing two binding motifs (Smet, Wieruszeski et al. 2005; Daum, Lucke et al. 2007), these models do not account for the full complexity of the binding reaction scheme for a two-domain protein interacting with a two-motif ligand, where both domains can interact with both motifs.

Figure 3.6 Modeling of data for titrations of Pin1 FL with dually phosphorylated peptides. The data points and corresponding globally fit or simulated binding curves (panels A – C and E – G) are color-coded by domain (blue = WW residues, red = PPIase residues), for titrations of Pin1-FL with p131/p144 (A – D) and with p163/173 (E – H), showing simulations without the bivalent states (A,E), fitting for the two global K_{eq} values (B,F) and fitting for the two global K_{eq} values and the the residue-specific bound chemical shift perturbations for the bivalent species (C,G). For p131/p144 plots (A-C), in the proton dimension Y24 is filled ◊, F25 filled Δ, H59 +, S115 x, R127 *, M130 open ◊; additionally in the nitrogen dimension, W34ε filled Δ, E35 filled ○, S114 *, A116 +, G128 -, and Q129 —). For p163/173 plots (E-G), in the proton dimension V22 is filled ◊, Y23 filled large □, Y24 filled Δ, W34ε filled small □, E35 filled ○, H59 +, L61 open Δ, V62 -, K117 x, L122 *, Q129 — ; additionally, in the nitrogen dimension V22 is filled ◊, Y23 filled □, W34 filled Δ, E35 filled ○, H59 +, V62 -, L122 *, and Q129 —. D) Equilibrium populations of the different types of species resulting from the fit in C, where species are grouped into: bivalent species (red), 2 pin1: 1 peptide species (blue), 1 Pin1:2 peptide species (green) and non-bivalent 1 Pin1:1 peptide species (purple). H) The equilibrium populations given different concentrations of peptide of the different types of species resulting from the fit where the species are grouped into: Bivalent species (red), 2 pin1: 1 peptide species (blue), 1 Pin1:2 peptide species (green) and non-bivalent 1 Pin1:1 peptide species (purple).

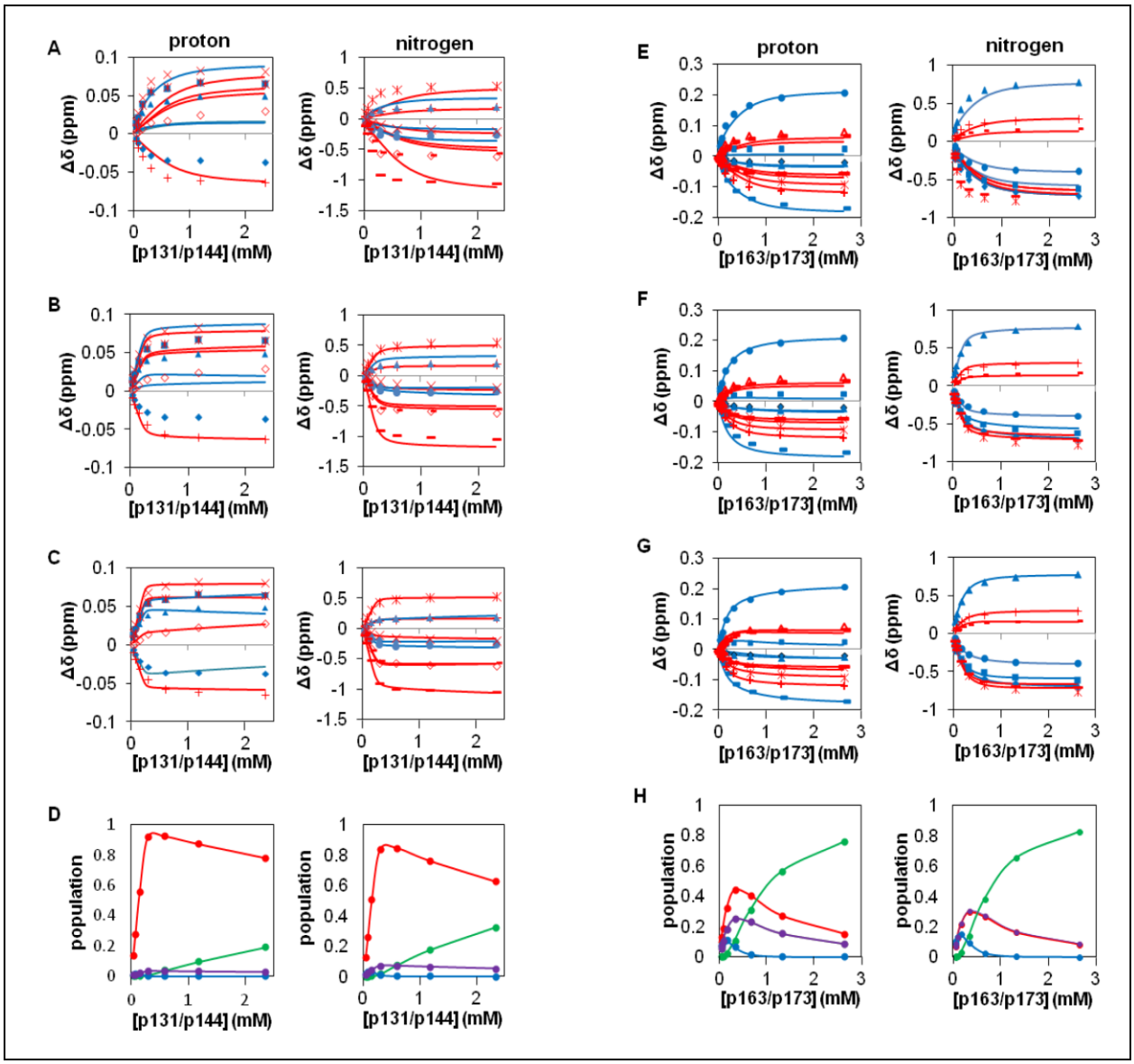
A
proton
nitrogen
Δδ (ppm)
[p131/p144] (mM)
B
C
D
population
E
[p163/p173] (mM)
F
G
H

To assess whether accounting for bivalency is necessary, we first asked whether the observed p131/p144 and p163/p173 titration data could be adequately simulated using the K_d and $\Delta\delta$ values obtained from the titrations of Pin1-FL with singly-phosphorylated peptides (above), without invoking the bivalent states (i.e., we set both K_{eq} values in the model to 10^7 and did not allow them to vary). These simulations (Figure 3.6A) indicate that the p131/p144 and p163/p173 titration data are not adequately explained by the predicted distribution over all possible non-bivalent states, if one assumes the same binding parameters as determined for the singly-phosphorylated peptides.

We next asked whether adding the two possible bivalent states to the model and fitting for their equilibrium constants could improve the fit. For simplicity, the bivalent state $\Delta\delta$ values were held fixed at their corresponding values determined from Pin1-FL titrations with singly phosphorylated peptides (e.g., WW domain bound to p131, etc.). For this model, only the two global K_{eq} values that are common to the system (one for each bivalent orientation) are fit. This approach yielded significant improvements (Figures 3.6B), but the reduced chi-square values, ranging from 1.9-24, did not indicate sufficiently good fits (reduced chi-square values for an appropriate model are expected to be close to one).

As a logical next step to improve the fits, the $\Delta\delta^n_{bound}$ values of the bivalent species were included as fitted parameters (Figure 3.6C). Values of $\Delta\delta^n_{bound}$ for the bivalent species might be expected to differ from the those determined from Pin1-FL titrations with singly phosphorylated peptides, since a bivalent interaction might require compromise in one or both interaction interfaces and/or might induce bivalent-specific allosteric changes. For this model, the fitted parameters include the two global K_{eq} values and, for each domain-specific residue *n*, two

$\Delta\delta^{n}_{bound}$ values corresponding to each of the two bivalent species. The resulting fits all yielded reduced chi-square values < 1.6, indicating adequate fits to this model. In general, the fitted $\Delta\delta^{n}_{bound}$ values for p131/p144 varied significantly from the corresponding values determined by titrations of Pin1-FL with monovalent ligands (Figure 3.7A-D), while p163/p173 values were in closer agreement to those values (Figure 3.7E-H), as expected based on better fits of p163/p173 with the simpler model (Figure 3.6B). For p131/p144, fitting of the proton and nitrogen dimensions yielded opposite orientation preferences, indicating an insensitivity of the fit to orientation. Regardless, the population of bivalently bound species is dominant in fits of data from both proton and nitrogen dimensions (Figure 3.6D). For p163/p173, fits in both proton and nitrogen dimensions show a preference for the orientation in which p173 is bound to WW and p163 is bound to PPIase (the "BA" orientation), and bivalent populations are dominant at lower concentrations (Figure 3.6H).

These results show that, for both bivalent ligands studied here, accounting for the bivalently bound species is required for obtaining adequate fits of the titration data, and that the influence of these states is dominant at low concentrations. Importantly, this model provides predictive power for exploring the competitive advantage achieved by bivalent interactions at micromolar concentrations as might be found in cells.

Model predicts that bivalent interactions for the p131/p144 and p163/p173 peptides impart competitive advantage in the cell. The overall goal of this study was to gain insight into the potential competitive advantage of a Pin1 substrate with two neighboring pS/T-P sites. To compare the effective affinity of dually versus singly phosphorylated peptides at approximate cellular concentrations, the binding models (Figure 3.3B&C) and the corresponding best-fit

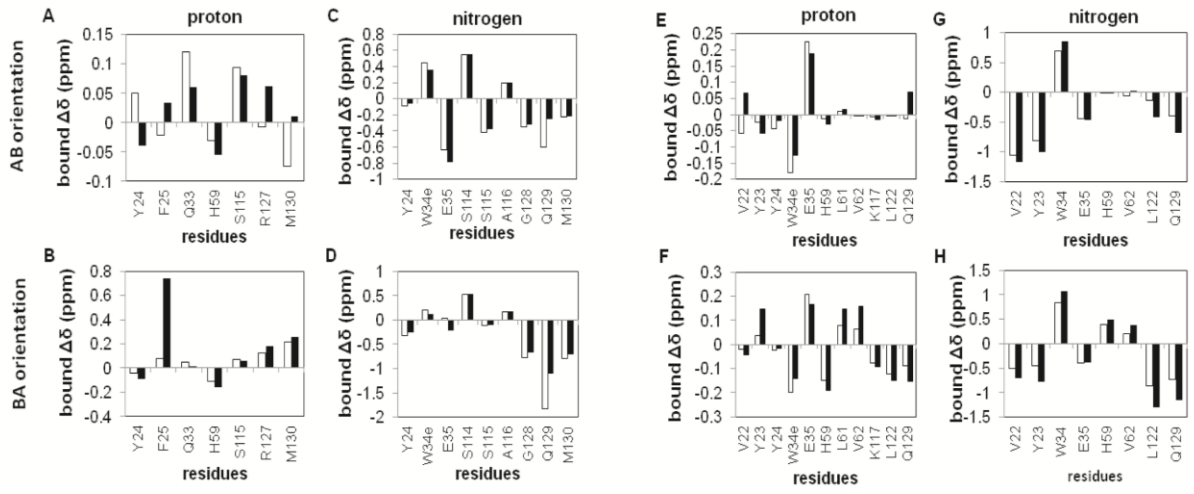

Figure 3.7 Comparison between fitted bound Δδ values for bivalent and corresponding non-bivalent species of Pin1-FL. Residue-specific bound Δδ values obtained by fitting of data from Pin1-FL titrated with dually phosphorylated peptides (black bars) and the corresponding fitted values from fitting of data from Pin1-FL titrated with singly phosphorylated peptides (white bars) are shown for the residues used in the bivalent fits shown in Figure 3.6C and 6G. The AB orientation is the species with WW bound to the first site (pS131-P132 or pS163-P164) and PPIase bound to the second site (pS144-P145 or pS173-P174). The BA orientation is the species with WW bound to the second site (pS144-P145 or pS173-P174) and PPIase bound to the first site (pS131-P132 or pS163-P164). A-D) Comparisons of fitted proton and nitrogen $\Delta\delta^{n}_{\text{bound}}$ values obtained for p131/p144, p131, and p144. E-H) Comparisons of fitted proton and nitrogen $\Delta\delta^{n}_{\text{bound}}$ values obtained for p163/p173, p163, and p173.

parameters (Tables 3.2 & 3.3) were used to simulate Pin1-FL binding to each pair of neighboring sites. In these simulations, the total fraction bound is the sum of all bound Pin1 species divided by total Pin1 (~0.5 μM (Shen, Stukenberg et al. 1998)), and the peptide concentration was varied between 0.01 μM and 100 μM. For the p131/p144 peptide, the capacity for bivalent binding imparts a marked advantage in Pin1 binding compared with the singly phosphorylated p131 or p144 peptides (Figure 3.8A). At 20 μM peptide, the total fraction of bound Pin1 is 0.85 for the p131/p144 peptide, which corresponds to an equivalent bimolecular interaction K_d value at these conditions of 3.5 μM (ΔG_{AB} = -7.49 kcal/mol). Similarly, for the p163/p173 peptide at the same conditions, the total fraction of bound Pin1 is 0.45 and the equivalent bimolecular interaction K_d value is 24 μM (ΔG_{AB} = -6.34 kcal/mol) (Figure 3.8B), representing a significant gain over the corresponding affinities of the p163 and p173 peptides. These simulations suggest that each of these bivalent IRAK1-UD sequences could effectively compete with other known biological Pin1 substrates in the cell (Verdecia, Bowman et al. 2000; Jacobs, Saxena et al. 2003; Smet, Wieruszeski et al. 2005) .

Avidity enhancement of Pin1 binding to linked targets has been studied previously using composite peptides comprised of inhibitors of each domain separated by a peptide-based linker that included four residues (or mimics) plus a variable number (three, five, or six) of sequential proline residues (Daum, Lucke et al. 2007). Avidity enhancement occurred in all cases, but was greatest when five prolines were utilized (Daum, Lucke et al. 2007). This suggests a preferred linker length of ten residues between the corresponding pS/T residues of neighboring motifs. Relative to this inferred optimal linker, our p163/p173 peptide has one fewer linker residue and contains four sequential prolines, while p131/p144 peptide has two additional linker residues and lacks any proline.

Table 3.3 Fitted K_{eq} values for the bivalent binding steps that generate the AB or BA orientation.

		Fitted bivalent K_{eq}s* (residue-specific $\Delta\delta^{n}_{bound}$ values not fit)			Fitted bivalent K_{eq}s* (residue-specific $\Delta\delta^{n}_{bound}$ for bivalent states also fit)		
		K_{eq}_AB	K_{eq}_BA	Reduced X^2	K_{eq}_AB	K_{eq}_BA	Reduced X^2
p131/p144	Proton	0.12	0.08	24	0.02	0.43	1.25
	Nitrogen	0.25	0.10	12	0.35	0.02	1.55
p163/p173	Proton	100	0.32	3.67	0.35	0.29	1.30
	Nitrogen	0.44	0.13	1.93	0.98	0.41	1.29

*A is the most N-terminal phosphorylated site on the peptide, B is the C-terminal site.

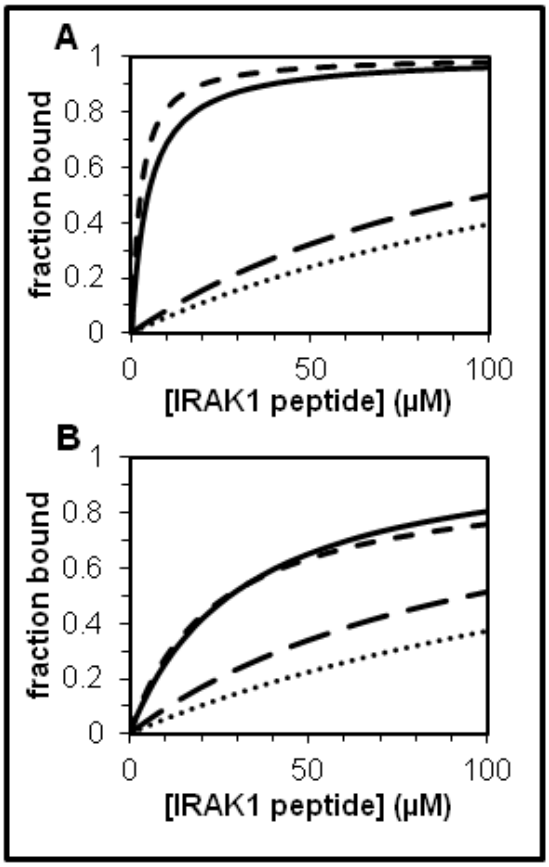

Figure 3.8 Prediction of significance of bivalent binding at low (micromolar) concentrations. Simulation of fraction of Pin1-FL bound (sum of all species including bound Pin1 in the system) when 0.5 μM Pin1-FL is titrated with various IRAK1-UD derived, phosphorylated peptides using the models from Figure 3.3. A) Comparison of predicted fraction bound for Pin1-FL with IRAK1 where S131-P132 is phosphorylated (long dashes), S144-P145 is phosphorylated (dotted), or both S131-P132 and S144-P145 are phosphorylated (unbroken and short dashes). The K_d and K_{eq} values were taken from the fits of titrations with p131, p144 (where in both cases the simulation in the proton dimension is recapitulated with the nitrogen dimension), and the nitrogen (unbroken) and proton (short dashes) dimension based fits of the p131/p144 titration. B) Comparison of calculated fraction bound for Pin1-FL and phosphorylated S163-P164 (long dashes), pS173-P174 (dotted), or pS163-P164 and pS173-P174, where the parameters used are based on fits of the p163, p173 (where in both cases the simulation in the proton dimension is recapitulated with the nitrogen dimension), and p163/p173 titrations (nitrogen dimension based parameters yielded the solid line simulation and the proton dimension yielded the short dashed line.

To compare the relative linkage contributions for our two bivalent IRAK1-UD peptides with the composite peptides comprised of linked inhibitors, we employed the effective concentration, C_{eff}, that reflects the concentration of one pS-P site once the other pS-P site is bound (Daum, Lucke et al. 2007). This value is obtained from $C_{eff} = \exp(-\Delta G^S/RT)$ (Daum, Lucke et al. 2007), where ΔG^S is the entropy barrier for bivalent binding and is the difference between the sum of free energies for the monovalent binding events ($\Delta G_A + \Delta G_B$) and the bivalent free energy (ΔG_{AB}), or $\Delta G^S = (\Delta G_A + \Delta G_B) - \Delta G_{AB}$ (Jencks 1981). For the two IRAK1-UD bivalent peptides studied here, ΔG_{AB} was determined at the same Pin1 concentration as was used for the composite peptide measurements (20 μM, (Daum, Lucke et al. 2007)), and ΔG_A and ΔG_B were obtained from the domain-specific monovalent ligand affinities for Pin1-FL, yielding C_{eff} values of 21 mM and 35 mM for the two orientations of p131/p144, and 1.4 mM and 6.8 mM for the two orientations of p163/p173. For comparison, the reported C_{eff} values for the composite peptides ranged from 0.58 mM to 2.07 mM (Daum, Lucke et al. 2007). Hence, although the affinities of the monovalent and bivalent IRAK1-UD peptides are weaker, the bivalent IRAK1-UD peptides achieve more of the additive free energies of binding than the composite inhibitor-based peptides (Daum, Lucke et al. 2007), resulting in greater effective concentrations of one pS-P site once the other pS-P site is bound.

The relatively high C_{eff} values obtained for these IRAK1-UD substrates raises the question of how such bivalent interactions might impact the catalytic efficiency of Pin1 acting on a bivalent substrate. Based on our model, the differences in population between bivalent and monovalent IRAK1-UD peptides would be negligible at the high peptide and protein concentrations used here in our NMR studies. Indeed, ROESY measurements at 3 mM peptide

and 10 μM Pin1 showed no significant enhancement of catalysis for bivalent as compared to monovalent versions of pSP sites in these IRAK1-UD peptides (unpublished data), as anticipated due to the saturation of Pin1 in both cases. Investigation of the impact on catalysis of these IRAK1-UD bivalent substrates relative to their monovalent counterparts will require measurement of bond-specific isomerization rates at peptide and Pin1 concentrations at or below ~50 – 100 μM, highly challenging for NMR exchange spectroscopy and beyond the scope of the present work.

Conclusions

Here we have shown that connecting the two binding modules in Pin1-FL alters the intrinsic binding affinities of the individual domains for IRAK1-UD peptides. We have also explored the modeling of complex, multi-state equilibria using NMR ^{15}N-^{1}H HSQC titration data, finding that the inclusion of bivalent states is necessary to fit the data produced when titrating dually phosphorylated peptides derived from the IRAK1-UD with Pin1-FL. We also simulated the effects of that fitting in the context of comparing binding of Pin1-FL to either singly or dually phosphorylated peptide, determining that the inclusion of the bivalent species leads to the anticipated avidity enhancement of effective K_d values.

MATERIALS & METHODS

Pin1 expression and purification. Pin1 was expressed using either an ampicillin-resistant pGEX vector with a GST tag and thrombin cut site as used previously (Zhou, Kops et al. 2000) (Yaffe, Schutkowski et al. 1997) or a newly constructed kanamycin resistant pET28a vector with a 6X-His tag and a TEV protease cut site. Both vectors express full length Pin1 (residues 1-163) that after cleavage from the affinity tag has either 20 (pGEX) or two (pET28a) additional N-

terminal residues. Importantly, both constructs give rise to essentially identical NMR spectra for peaks arising from Pin1 residues, allowing them to be used interchangeably. GST-Pin1 was expressed in BL21 star *E. Coli* [Invitrogen] cells grown in 1 L of either LB [BD] or M9 minimal media (using 19 mM $^{15}NH_4Cl$ [Isotec] with 100 μg/mL ampicillin [Fisher]) at 37ºC. Expression was induced at an OD_{600} ~0.6, with 1 mM IPTG [CalBioChem] and growth was continued at 15ºC for ~20 hours. Cells were pelleted and resuspended in lysis buffer (25 mM HEPES [Fisher, sodium salt], 150 mM NaCl [Mallinckrodt Baker], 10 mM Imidazole [Alfa Aesar], pH 7.5, 100 μL protease inhibitor [Sigma], 1 mM DTT [Gold Biotechnology], and 2 mM EDTA [Fisher]). Cells were then lysed by freezing and thawing on ice, adding 1 mg/ml lysozyme [EMD], and sonicating (10 cycles). Lysed cells were centrifuged at 23,000 x g and the supernatant was filtered with a 0.8-μm syringe filter (Corning). Filtrate was then applied to a glutathione sepharose column [GE Health Sciences] and washed with 20 bed volumes wash buffer (25 mM HEPES, 150 mM NaCl, 10 mM Imidazole, pH 7.5). The column was then equilibrated with cleavage buffer (20 mM Tris-HCl [Mallinckrodt Baker], 150 mM NaCl, 2.5 mM $CaCl_2$ [Fisher], pH 8.4), and 5 units of biotinylated thrombin [Novagen] were added. Cleavage of the Pin1 protein from the GST tag was performed while tumbling overnight at room temperature. The biotinylated thrombin was removed from the eluted Pin1 protein solution with streptavidin agarose beads [Novagen] and Pin1 was dialyzed into NMR buffer (10 mM HEPES, 10mM NaCl, 1 mM TCEP [Thermo Scientific], pH 6.8). NMR samples also included 5 mM NaN_3 [Fisher]. Protein was concentrated with VivaSpin-20 5000 MWC centrifugal concentrators [GE Health Sciences]. The concentration of Pin1 was measured by the UV absorbance spectrum, using the theoretical extinction coefficient at 280 nm of 21,220 $cm^{-1}M^{-1}$. Protein purity was verified by SDS-PAGE. The pH of buffers and samples was adjusted using HCl [Mallinckrodt Baker] and

NaOH [Sigma].

The 6xHis-Pin1 construct was expressed and affinity purified as previously described for 6xHis-PPIase (Greenwood, Rogals et al. 2011). The protein was dialyzed into NMR buffer, and 5mMNaN_3 was added. The construct for the PPIase domain of Pin1, comprised of residues 46-163, (also in a pET28a vector with kanamycin resistance, a 6X-His tag and a TEV cleavage site) was purified using the same procedure. This protocol was also utilized in the preparation of WW domain (residues 1-50) as previously described (De, Greenwood et al. 2012).

IRAK1 Peptides. All peptides (Figure 3.1) were purchased from the Tufts University Core Facility and had unblocked ends, except p131/p144 which was purchased in the acetyl-peptide-amide form. Peptides were dissolved in NMR buffer, and their pH was adjusted with NaOH to 6.9.

NMR spectroscopy. NMR experiments were performed at a sample temperature of 25°C on a Varian Inova 600 MHz spectrometer equipped with a (H,C,N) Z-axis gradient probe. For each titration point, a ^{15}N-^{1}H fast HSQC spectrum (Ref Mori, S., et al. (1995) J. Magn. Reson. Ser. B 108, 94-98) was recorded with a spectral width of 8 kHz in the proton dimension (total of 2048 complex data points) and either 1.77 kHz or 2.0 kHz in the nitrogen dimension (total of 256 complex data points). Spectra were processed and analyzed using the software tools nmrPipe, nmrDraw (Delaglio, Grzesiek et al. 1995), and Sparky (T.D. Goddard and D.G. Kneller, University of California, San Fransisco). Data were apodized using a shifted sine bell function and zero filled prior to Fourier transformation. Peak positions were measured using the peak detection modules of Sparky.

Titration of isolated Pin1 domains. All NMR titration experiments were performed using the reverse titration method, where titration begins with the sample containing the highest ligand concentration and subsequent samples are prepared by mixing a portion of the previous sample with a stock solution of equal protein concentration. In this manner, the protein concentration remains constant and the ligand is sequentially diluted. Isolated WW and PPIase domains were individually titrated with one of three peptides derived from IRAK1-UD (p131, p144, and p163). For titration of WW with p163, WW concentration was 0.4 mM and p163 concentrations were 2.3, 1.1, 0.71, 0.37, 0.20, and 0 mM (the physical titration was performed by Alex Greenwood). For titration of PPIase with p131, PPIase concentration was 0.16mM and p131 concentrations were 7.6, 3.8, 1.9, 0.63, 0.21 or 0 mM. For titration of PPIase with p144, PPIase concentration was 0.22mM and p144 concentrations were 8.1, 4.05, 2.02, 1.01, 0.51, 0.25, 0.13 and 0 mM. For titration of PPIase with p163, PPIase concentration was 0.20mM and p163 concentrations were 3.8, 1.9, 0.96, 0.48, 0.24, 0.12, 0.06, 0.03 and 0 mM.

Each titration was analyzed using a representative selection of residues. Criteria for residue choice were: the largest observed chemical shift change (relative to apo) must reach a threshold value ($\Delta\delta^{i}_{N,obs} \geq 0.1$ ppm for nitrogen, $\Delta\delta^{i}_{H,obs} \geq 0.0154$ ppm for proton); the titration data must produce a reasonable binding curve; and the residue must be within the vicinity of the established binding site of its resident domain. Commonly accepted binding site residues lie within WW domain residues 22-25 and 34-35, and within PPIase domain residues 57-63, 68-9, 113-118, and 128-130 (Wilson, Bouchard et al. 2013). Since the observed residue-specific chemical shift changes in the ^{15}N and ^{1}H dimensions ($\Delta\delta^{n,i}_{N,obs}$ and $\Delta\delta^{n,i}_{H,obs}$) were treated separately, residue choice can differ for the two dimensions.

The experimental data for each domain was fit to a simple bimolecular binding model (Figure 3.3A) using the solver function in Excel 2007. Both dimensions were simultaneously fit to produce one global K_d for each peptide, where $(\Delta\delta^{n,i}_{N,obs} - \Delta\delta^{n,i}_{N,calc})^2$ values (in the nitrogen dimension) were multiplied by 0.154 to appropriately scale their contribution to the fit. The uncertainty in the global K_d value obtained for each titration was approximated by individually fitting the corresponding selected residues, and determining the standard deviation of the resulting distribution of K_d values.

Errors in $\Delta\delta^{n,i}{}_{N,obs}$ and $\Delta\delta^{n,i}{}_{H,obs}$, required for evaluating the goodness of fit of a given model to the data, were estimated in two ways. First, the positions of peaks insensitive to ligand addition were monitored in spectra across the titration series to estimate the average uncertainty in peak location. The average standard deviation of these changes in each dimension were taken as the chemical shift uncertainty, $\sigma_{\delta N}$ and $\sigma_{\delta H}$, for all peaks. Standard error propagation was applied to obtain the corresponding errors for the differences relative to apo, $\Delta\delta^{n,i}{}_{N,obs}$ and $\Delta\delta^{n,i}{}_{H,obs}$. Additionally, assuming the bimolecular model is valid for each individual domain, the average error values that produced reduced chi-square values of 1.0 for the best fits of the individual domain titration data in each dimension were determined. Since smaller errors produce more conservative assessments of model complexity, the smallest resulting set of values was used for all model assessments.

Goodness of fit was assessed using the reduced chi-square, given by:

$$\chi^2_{red} = \sum_{1}^{N} \frac{\left[\left(\Delta\delta^{n,i}_{obs} - \Delta\delta^{n,i}_{calc} \right) \Big/ \sigma_{\Delta\delta} \right]^2}{\rho}$$

where $\Delta\delta^{n,i}{}_{obs}$ and $\Delta\delta^{in,i}{}_{calc}$ are the experimental and calculated chemical shift perturbations for

residue *n* and titration point *i*, the sum is over N residues used in the fit, $\sigma_{\Delta\delta}$ is the error in $\Delta\delta^{i}_{obs}$ (i.e. $\sigma_{\Delta\delta N}$ and $\sigma_{\Delta\delta H}$), and ρ is the number of degrees of freedom: $\rho = (\#\ titration\ pts * \#of\ residues) - \#fitted\ parameters - 1$.

Titration of full-length Pin1. All NMR titration experiments were performed using the reverse titration method as described above. Pin1-FL was titrated with each of six peptides derived from IRAK1-UD (p131, p144, p163, p173, p131/p144 or p163/p173). For titration with p131, Pin1-FL concentration was 0.2 mM and p131 concentrations were 2.6, 1.3, 0.65, 0.33, 0.16, 0.08, 0.04, and 0 mM. For titration with p144, Pin1-FL concentration was 0.25 mM, and p144 concentrations were 7.85, 2.82, 1.66, 0.76, 0.37, 0.21, 0.103 and 0 mM. For titration with p163, 0.1 mM Pin1-FL was titrated with 1.54, 0.77, 0.51, 0.26, 0.13, 0.064, 0.032 and 0 mM p163 (Alex Greenwood performed the physical titration). For titration with p173, Pin1-FL concentration was 0.25 mM and p173 concentrations were 2.0, 1.5, 1.0, 0.5, 0.25, 0.12, 0.06 and 0 mM of p173 (Alex Greenwood performed the physical titration). For titration with p131/p144, Pin1-FL concentration was 0.25 mM and p131/p144 concentrations were 2.36, 1.18, 0.59, 0.30, 0.15, 0.07, 0.04, and 0 mM. For titration with p163/p173, Pin1-FL concentration was 0.2 mM and p163/p173 concentrations were 2.64, 1.32, 0.66, 0.33, 0.17, 0.08, 0.06, 0.04, and 0 mM (Alex Greenwood performed the physical titration).

Residues were selected for use in model analysis and fitting based on the following criteria. For all Pin1-FL titrations, the largest values of ($\Delta\delta^{n,i}_{N,obs}$ and $\Delta\delta^{n,i}_{H,obs}$ must reach a threshold value ($\Delta\delta^{n,i}_{N,obs} \geq$ 0.1 ppm for nitrogen, $\Delta\delta^{n,i}_{H,obs} \geq 0.0154$ ppm for proton), peaks must move in the same direction in the isolated domain and Pin1-FL titrations (see Appendix 1 for details related to p131 and p144 titrations), residues with peaks that overlap with other peaks

during titration were excluded, and residues previously implicated in either the PPIase conduit or the interface between the PPIase and WW domains were excluded (to the extent possible given the small size of the WW domain). An emphasis was placed on selecting residues known to be important for binding and residues in close spatial proximity to the Ala-Pro dipeptide or the sulfate ion in the 1PIN.pdb crystal structure (Ranganathan, Lu et al. 1997). Additionally, for the dually-phosphorylated peptide titrations, in order to allow for possible differentiation between different binding orientations, selected residues were required to display disparate bound chemical shifts for each binding motif. In some cases, residues selected for bivalent analysis were not previously selected in the monovalent analysis. For such residues, the residue-specific bound $\Delta\delta^{n}_{bound}$ values were obtained by using the previously determined global K_d values (Table 3.2) and fitting for $\Delta\delta^{n}_{bound}$.

Chemical shift perturbation data were analyzed separately for the nitrogen and proton dimensions, which enhanced sensitivity of peak trajectories to shifting populations among the multiple states during the titration and yielded independent measures of each K_d. Titrations of Pin1-FL binding to a singly phosphorylated peptide were fit to an analytical model in which the peptide can either bind the PPIase domain or the WW domain with distinct affinities (Figure 3.3B). The error in a given K_d value is the standard deviation of a series of K_d values calculated using Monte Carlo analysis, in which artificial noise is added to the data to generate 100 synthetic data sets, each of which are fit. The artificial noise was generated for each data point using the output of a normally distributed, random number generator scaled by $\sigma_{\Delta\delta H} = 0.00407$ ppm in the proton dimension and $\sigma_{\Delta\delta N} = 0.0205$ ppm in the nitrogen dimension). The initial guesses for parameters being fit were also allowed to vary randomly in a normal distribution about the determined values (Table 3.2), where the boundaries are set at half and twice the

reported value.

Pin1-FL binding to a dually phosphorylated peptide is more complex (Figure 3.3C), requiring numerical solution. Our method employed Virtual Cell modelling software (Dubitzky, Wolkenhauer et al.) to generate the MATLAB code for numerical solution of the set of coupled ordinary differential equations that describe the model, yielding equilibrium populations for each state in the model. These populations were employed in fits of chemical shift perturbations, carried out in MATLAB using the nonlinear multivariable function fmincon. For these analyses, K_d and $\Delta\delta^{n,i}_{bound}$ values for all non-bivalent states were set to their corresponding values obtained from Pin1-FL titrations with singly-phosphorylated peptides. For inclusion of bivalent states (Figure 3.3C, highlighted by yellow background), two independent equilibrium constants (K_{eq}) are required to describe the closure of each monovalent precursor state into the corresponding bivalent state (Figure 3.3C), given by:

$$K_{eq}^{A:WW} = K_{eq}^{B:PPIase}\left(\frac{K_d^{A:WW}}{K_d^{B:PPIase}}\right)$$

and

$$K_{eq}^{B:WW} = K_{eq}^{A:PPIase}\left(\frac{K_d^{B:WW}}{K_d^{A:PPIase}}\right)$$

where the superscripts denote the relevant binding event (e.g. A:WW refers to the WW domain interacting with motif A, the N-terminal most motif). A set of simulations was carried out with K_{eq}s for the two routes set at 10^7, so as to remove the pathway to either bivalent species, in order to determine if the bivalent species is necessary to fit the data. Reduced chi-square values were employed to assess the quality of all simulations and fits (using a $\sigma_{\Delta\delta H}$ of 0.00407 ppm in the proton dimension and a $\sigma_{\Delta\delta N}$ of 0.0205 ppm in the nitrogen dimension, as determined in the isolated domain titrations).

Simulation of Pin1-FL interactions with IRAK1-UD motifs at low micromolar concentrations. Using Virtual Cell in conjunction with MATLAB and the fitted K_d and K_{eq} values, two models based on Figures 3.3B and 3.3C were constructed to simulate the bound population of Pin1 that would occur under biologically-relevant conditions where Pin1 is 0.5 μM (Shen, Stukenberg et al. 1998), for varying concentrations and phosphorylation states of IRAK1.

ACKNOWLEDGEMENTS

This work would not have been possible without the titrations that were physically performed by Alex Greenwood, who also worked on the early MATLAB coding involved in this project. I would also like to acknowledge Jeahoo Kwon, who found a flaw in an early model that allowed us to reevaluate our modeling protocol. Andrea Acevedo also contributed feedback on the recent modeling. This work was done in collaboration with the Kun Ping Lu's lab at Beth Israel Deaconess Medical Center at Harvard University. This work was supported by NIH-CMB training grants T32GM007273 (MJR) and T32GM0008267(AIG), NSF MCB-1157806 (LKN), and NIH R01 HL111430 (K.P.L).

SUPPLEMENTARY INFORMATION AVAILABLE

There are eight figures in Appendix 1 that pertain to this chapter. Six are overlaid ^{15}N-^{1}H HSQC titrations of intact or isolated domains of Pin1 titrated with either p131, p144, p163 or p131/p144. Two are collections of residue-specific binding curves from all of the singly phosphorylated peptide titrations explored here. Appendix 2 is also focused on the mathematical modeling that was featured here.

REFERENCES

Chen, C. H., W. Li, et al. (2015). "Pin1 cysteine-113 oxidation inhibits its catalytic activity and cellular function in Alzheimer's disease." Neurobiol Dis **76**: 13-23.

Daum, S., C. Lucke, et al. (2007). "On the benefit of bivalency in peptide ligand/pin1 interactions." J Mol Biol **374**(1): 147-61.

De, S., A. I. Greenwood, et al. (2012). "Complete thermodynamic and kinetic characterization of the isomer-specific interaction between Pin1-WW domain and the amyloid precursor protein cytoplasmic tail phosphorylated at Thr668." Biochemistry **51**(43): 8583-96.

Delaglio, F., S. Grzesiek, et al. (1995). "NMRPipe: a multidimensional spectral processing system based on UNIX pipes." J Biomol NMR **6**(3): 277-93.

Dubitzky, W., O. Wolkenhauer, et al. Virtual Cell (VCell) Modeling and Analysis Platform. Encyclopedia of Systems Biology, Springer New York**:** 2342-2347.

Flannery, S. and A. G. Bowie (2010). "The interleukin-1 receptor-associated kinases: critical regulators of innate immune signalling." Biochem Pharmacol **80**(12): 1981-91.

Greenwood, A. I., M. J. Rogals, et al. (2011). "Complete determination of the Pin1 catalytic domain thermodynamic cycle by NMR lineshape analysis." J Biomol NMR **51**(1-2): 21-34.

Innes, B. T., M. L. Bailey, et al. (2013). "Non-catalytic participation of the Pin1 peptidyl-prolyl isomerase domain in target binding." Front Physiol **4**: 18.

Innes, B. T., M. A. Sowole, et al. (2015). "Peroxide-mediated oxidation and inhibition of the peptidyl-prolyl isomerase Pin1." Biochim Biophys Acta **1852**(5): 905-12.

Jacobs, D. M., K. Saxena, et al. (2003). "Peptide binding induces large scale changes in inter-domain mobility in human Pin1." J Biol Chem **278**(28): 26174-82.

Jacobs, D. M., K. Saxena, et al. (2003). "Peptide binding induces large scale changes in inter-domain mobility in human Pin1." Journal of Biological Chemistry **278**(28): 26174-26182.

Jencks, W. P. (1981). "On the attribution and additivity of binding energies." Proc Natl Acad Sci U S A **78**(7): 4046-50.

Lee, T. H., A. Tun-Kyi, et al. (2009). "Essential role of Pin1 in the regulation of TRF1 stability and telomere maintenance." Nat Cell Biol **11**(1): 97-105.

Lin, S. C., Y. C. Lo, et al. (2010). "Helical assembly in the MyD88-IRAK4-IRAK2 complex in TLR/IL-1R signalling." Nature **465**(7300): 885-90.

Lu, K. P., S. D. Hanes, et al. (1996). "A human peptidyl-prolyl isomerase essential for regulation of mitosis." Nature **380**(6574): 544-7.

Lu, K. P. and X. Z. Zhou (2007). "The prolyl isomerase PIN1: a pivotal new twist in phosphorylation signalling and disease." Nat Rev Mol Cell Biol **8**(11): 904-16.

Lu, P. J., G. Wulf, et al. (1999). "The prolyl isomerase Pin1 restores the function of Alzheimer-associated phosphorylated tau protein." Nature **399**(6738): 784-788.

Lu, Z. and T. Hunter (2014). "Prolyl isomerase Pin1 in cancer." Cell Res **24**(9): 1033-49.

Mammen, M., S.-K. Choi, et al. (1998). "Polyvalent interactions in biological systems: implications for design and use of multivalent ligands and inhibitors." Angewandte Chemie International Edition **37**(20): 2754-2794.

Myers, J. K., D. P. Morris, et al. (2001). "Phosphorylation of RNA polymerase II CTD fragments results in tight binding to the WW domain from the yeast prolyl isomerase Ess1." Biochemistry **40**(29): 8479-86.

Namanja, A. T., X. D. J. Wang, et al. (2011). "Stereospecific gating of functional motions in Pin1." Proceedings of the National Academy of Sciences of the United States of America **108**(30): 12289-12294.

Namanja, A. T., X. J. Wang, et al. (2011). "Stereospecific gating of functional motions in Pin1." Proc Natl Acad Sci U S A **108**(30): 12289-94.

Pastorino, L., A. Sun, et al. (2006). "The prolyl isomerase Pin1 regulates amyloid precursor protein processing and amyloid-beta production." Nature **440**(7083): 528-34.

Potter, A., V. Oldfield, et al. (2010). "Discovery of cell-active phenyl-imidazole Pin1 inhibitors by structure-guided fragment evolution." Bioorg Med Chem Lett **20**(22): 6483-8.

Potter, A. J., S. Ray, et al. (2010). "Structure-guided design of alpha-amino acid-derived Pin1 inhibitors." Bioorg Med Chem Lett **20**(2): 586-90.

Ranganathan, R., K. P. Lu, et al. (1997). "Structural and functional analysis of the mitotic rotamase Pin1 suggests substrate recognition is phosphorylation dependent." Cell **89**(6): 875-86.

Rustighi, A., L. Tiberi, et al. (2009). "The prolyl-isomerase Pin1 is a Notch1 target that enhances Notch1 activation in cancer." Nat Cell Biol **11**(2): 133-42.

Shaw, P. E. (2007). "Peptidyl-prolyl cis/trans isomerases and transcription: is there a twist in the tail?" EMBO Rep **8**(1): 40-5.

Shen, M., P. T. Stukenberg, et al. (1998). "The essential mitotic peptidyl-prolyl isomerase Pin1 binds and regulates mitosis-specific phosphoproteins." Genes Dev **12**(5): 706-20.

Smet, C., J. M. Wieruszeski, et al. (2005). "Regulation of Pin1 peptidyl-prolyl cis/trans isomerase activity by its WW binding module on a multi-phosphorylated peptide of Tau protein." FEBS Lett **579**(19): 4159-64.

Tun-Kyi, A., G. Finn, et al. (2011). "Essential role for the prolyl isomerase Pin1 in Toll-like receptor signaling and type I interferon-mediated immunity." Nat Immunol **12**(8): 733-41.

Ubersax, J. A. and J. E. Ferrell, Jr. (2007). "Mechanisms of specificity in protein phosphorylation." Nat Rev Mol Cell Biol **8**(7): 530-41.

Urusova, D. V., J. H. Shim, et al. (2011). "Epigallocatechin-gallate suppresses tumorigenesis by directly targeting Pin1." Cancer Prev Res (Phila) **4**(9): 1366-77.

VanWart, A. T., J. Eargle, et al. (2012). "Exploring Residue Component Contributions to Dynamical Network Models of Allostery." Journal of Chemical Theory and Computation **8**(8): 2949-2961.

Verdecia, M. A., M. E. Bowman, et al. (2000). "Structural basis for phosphoserine-proline recognition by group IV WW domains." Nat Struct Biol **7**(8): 639-43.

Wilson, K. A., J. J. Bouchard, et al. (2013). "Interdomain interactions support interdomain communication in human Pin1." Biochemistry **52**(40): 6968-81.

Wulf, G. M., A. Ryo, et al. (2001). "Pin1 is overexpressed in breast cancer and cooperates with Ras signaling in increasing the transcriptional activity of c-Jun towards cyclin D1." EMBO J **20**(13): 3459-72.

Xu, Y. X. and J. L. Manley (2007). "The prolyl isomerase Pin1 functions in mitotic chromosome condensation." Mol Cell **26**(2): 287-300.

Yaffe, M. B., M. Schutkowski, et al. (1997). "Sequence-specific and phosphorylation-dependent proline isomerization: a potential mitotic regulatory mechanism." Science **278**(5345): 1957-60.

Yeh, E. S. and A. R. Means (2007). "PIN1, the cell cycle and cancer." Nat Rev Cancer **7**(5): 381-8.

Zhang, M., X. J. Wang, et al. (2012). "Structural and kinetic analysis of prolyl-isomerization/phosphorylation cross-talk in the CTD code." ACS Chem Biol **7**(8): 1462-70.

Zheng, H., H. You, et al. (2002). "The prolyl isomerase Pin1 is a regulator of p53 in genotoxic response." Nature **419**(6909): 849-53.

Zhou, X. Z., O. Kops, et al. (2000). "Pin1-dependent prolyl isomerization regulates dephosphorylation of Cdc25C and tau proteins." Mol Cell **6**(4): 873-83.

CHAPTER 4

PERSPECTIVES & REFLECTIONS

The unifying theme of this dissertation was the application of biophysical methods and computational modeling to quantitatively characterize protein-protein interactions. Chapter two explored the sensitivity of the interaction of Hsp70 and APPc to phosphorylation of T668 on APPc and the possible implications for APP processing. Chapter three focused on how multiple proximal phosphorylated binding sites can lead to avidity enhancement for the interaction of IRAK1-UD and Pin1. In addition to this work, I was involved in two other projects that were focused on the interaction of APPc and Pin1 (Greenwood, Rogals et al. 2011; De, Greenwood et al. 2012). The first involved the complete thermodynamic and kinetic characterization of the isomer-specific interaction between the WW domain of Pin1 and the APPc (De, Greenwood et al. 2012), where APPc has one possible phosphorylation site, T668, that would make it a target for Pin1 interaction. The second was the complete determination of the PPIase domain's thermodynamic cycle when binding with APPc as monitored via NMR lineshape analysis

(Greenwood, Rogals et al. 2011). Both Pin1 and APP were integral components of either chapter two or three, but not with regards to binding to each other. In fact, it is easy to see how the studies in chapters two and three arose from our lab's earlier work on the binding of Pin1 and APP. Ultimately, both chapters attempt to elucidate binding between one partner with a pS/T-P motif, which in both cases acts as a binding site for Pin1, and a protein interacting at or near that motif.

In retrospect, the focus of my work at Cornell can be summed up as an expansive and highly detailed study on binding affinity and binding schemes for protein-protein interactions. NMR is a powerful tool to examine these types of interactions (Gao, Williams et al. 2004). Through ^{15}N-labeling of a protein, I am able to look at precisely which residues in that protein are sensitive to the interaction when titrating in a binding partner, whether their environment changes as a direct result of the binding partner or as an indirect result of (binding-induced) rearrangement of the labeled protein. I am also able to titrate in different binding partners and some of the residues that are sensitive to binding are also sensitive to the identity of the binding partner. Given that the chemical shift perturbation ($\Delta\delta$), in the fast-exchange regime, is the population weighted average of the various free and bound residue-specific $\Delta\delta$s associated with different species in the binding scheme (Williamson 2013), an NMR titration is a rich source of information. This information can be teased out through thoughtful use of less complex preliminary experiments. The level of detail collected allows calculation of populations and therefore of binding affinities (K_ds) associated with specific parts of the binding scheme rather than one effective observed K_d that describes the whole system. Such a K_d is what standard biochemical methods (i.e. fluorescence anisotropy, ITC, FRET, etc) (Martin, Tatham et al. 2008; Duff, Grubbs et al. 2011; Rossi and Taylor 2011) are commonly able to collect.

While NMR titrations can reveal multi-state equilibria, elucidating complex binding schemes also requires considerable computing power. In the simplest case, a titration involving two components that experience two-state binding (at equilibrium conditions) can be understood with a simply derived equation (Appendix 2), and the titration data can be fit using a standard minimization software (Excel 2007 with Solver Add-in). However, there are still a number of simultaneous calculations that must occur to fit several residues globally for residue-specific $\Delta\delta$s as well as the K_d of the interaction. This approach was employed in my studies of the interaction of APP and Hsp70 as well as the interaction of isolated WW and PPIase domains with monovalent peptides.

My studies of intact Pin1 required more complex models and analysis. The next stage of complexity is the four-state interaction ($Pin1_{free}$, WW_{bound}, $PPIase_{bound}$, and $Pin1_{both\ domains\ bound}$) with two domains that bind the same ligand. The analytical expression is more complex (Appendix 2) and must account for two domains with unique K_ds as well as residue-specific $\Delta\delta$s, requiring additional computing power. The analytical derivation for this four-state model was carried out with MuPAD software (MuPAD 2010, The MathWorks Inc., Natick, MA, 2010). Solving this analytical expression for given conditions necessitated the use of in-house MATLAB codes (MATLAB 2010, The MathWorks Inc., Natick, MA, 2010), in which, the fitting utilizes the built-in function fmincon to minimize the difference between the observed and calculated $\Delta\delta$s. The MATLAB code is again designed to allow for simultaneous peak fitting.

When dealing with larger reaction schemes, such as the binding of two domains with the same target motif to a ligand with two such motifs, analytically deriving the expression for this interaction scheme via MuPAD proved exceptionally cumbersome. Given the readily available computing power on Cornell campus and the existence of pre-made programs to model

biological interactions (e.g. Virtual Cell, ANIMO, SimBiology app in MATLAB), the preferable approach was to use MATLAB (MATLAB 2014b, The MathWorks Inc., Natick, MA, 2014) in conjunction with an online server Virtual Cell (instead of MuPAD) (Dubitzky, Wolkenhauer et al.). Rather than generating an analytic expression for a reaction scheme, Virtual Cell creates a series of ordinary differential equations to describe the reaction. Not only is this less cumbersome, generation of the mathematical equations is simplified via a GUI interface where one builds the reaction scheme graphically and then the simple system of equations describing parts of the interaction scheme is generated. This can greatly benefit the biologically, rather than computationally, minded individual. The equations can be exported into a MATLAB code which can then be integrated into existing in-house MATLAB codes for fitting NMR titration data. I took this approach, which allowed simultaneous peak fits for the more complex system to be carried out using the familiar minimization functions and built-in minimization software. While the trade-off is the substantial time required for each run through of the Virtual Cell/MATLAB code, this approach produced a highly versatile computational tool that can serve as a starting point for lab members tackling similar problems in the future.

While analysis of K_ds was my primary objective throughout my graduate studies, I would like to reflect briefly on the biological theme linking my projects, namely the regulation of interactions through phosphorylation. Phosphorylation is a major regulatory mechanism in the cell (Humphrey, James et al. 2015). One very common set of phosphorylation events is carried out by proline-directed kinases, which target Serine or Threonine followed by Proline (Lu, Liou et al. 2002). Phosphorylation of that serine or threonine can create a recognition motif for binding to Pin1. This means that every potential binding site for Pin1 is inherently regulated. Therefore hyper-phosphorylation, hypo-phosphorylation, or temporally inaccurate

phosphorylation of binding partners could easily disrupt Pin1 binding, potentially leading to undesirable interactions (i.e. phosphorylation of a site that happens to be S/T-P, but would not normally be phosphorylated), lack of necessary interactions, or incorrect timing of interactions. It is easy to see how this could lead to problems with the cell cycle, simply given that Pin1 stands for protein interacting with never in mitosis-1 (Shen, Stukenberg et al. 1998). My dissertation has also been a detailed-oriented look at how phosphorylation could influence cellular processes and impact disease states through regulations of protein-protein interactions. During my graduate studies, I have examined multiple phosphorylation-dependent interactions implicated in AD and asthma. It is my hope that the detailed characterizations that I have contributed will help to advance our understanding of the progression of these diseases and lead to the development of strategies to prevent or combat them.

Finally, I would like to offer my thoughts on a potential future direction. I have studied the binding of Pin1 and asthma-related IRAK1 which, with its multiple proximal S-P sites, is an excellent model for examining bivalent interactions. It is also an example of Pin1 in a tunable system, which you can imagine could display far more complex phosphorylation patterns than I was able to elucidate in this work. In fact, a future direction that could be explored would be to look at the full IRAK1-UD and, through competitive binding studies with other strong, monovalent Pin1 substrates, explore the advantage that a hyper-phosphorylated IRAK1-UD would actually have in binding to Pin1. Such a study, while even more complex than investigated in this dissertation, could reveal a higher level of regulation, possibly encoded in the relative spacing of the S-P motifs. The tools I have developed in my graduate work provide a foundation for pursuing these and other studies involving complex multi-state equilibria.

REFERENCES

De, S., A. I. Greenwood, et al. (2012). "Complete thermodynamic and kinetic characterization of the isomer-specific interaction between Pin1-WW domain and the amyloid precursor protein cytoplasmic tail phosphorylated at Thr668." Biochemistry **51**(43): 8583-96.

Dubitzky, W., O. Wolkenhauer, et al. Virtual Cell (VCell) Modeling and Analysis Platform. Encyclopedia of Systems Biology, Springer New York**:** 2342-2347.

Duff, M. R., Jr., J. Grubbs, et al. (2011). "Isothermal titration calorimetry for measuring macromolecule-ligand affinity." J Vis Exp(55).

Gao, G., J. G. Williams, et al. (2004). "Protein-protein interaction analysis by nuclear magnetic resonance spectroscopy." Methods Mol Biol **261**: 79-92.

Greenwood, A. I., M. J. Rogals, et al. (2011). "Complete determination of the Pin1 catalytic domain thermodynamic cycle by NMR lineshape analysis." J Biomol NMR **51**(1-2): 21-34.

Humphrey, S. J., D. E. James, et al. (2015). "Protein Phosphorylation: A Major Switch Mechanism for Metabolic Regulation." Trends Endocrinol Metab **26**(12): 676-87.

Lu, K. P., Y. C. Liou, et al. (2002). "Pinning down proline-directed phosphorylation signaling." Trends Cell Biol **12**(4): 164-72.

Martin, S. F., M. H. Tatham, et al. (2008). "Quantitative analysis of multi-protein interactions using FRET: application to the SUMO pathway." Protein Sci **17**(4): 777-84.

Rossi, A. M. and C. W. Taylor (2011). "Analysis of protein-ligand interactions by fluorescence polarization." Nat Protoc **6**(3): 365-87.

Shen, M., P. T. Stukenberg, et al. (1998). "The essential mitotic peptidyl-prolyl isomerase Pin1 binds and regulates mitosis-specific phosphoproteins." Genes Dev **12**(5): 706-20.

Williamson, M. P. (2013). "Using chemical shift perturbation to characterise ligand binding." Prog Nucl Magn Reson Spectrosc **73**: 1-16.

APPENDIX 1

SUPPLEMENTARY FIGURES PERTAINING TO CHAPTER TWO & THREE

The following figures were not necessary for inclusion in the main text as they were not critical for comprehension of the material presented. However, they may prove to be useful reference figures with regards to the material presented in this dissertation. This includes a pH titration of APPc, the full spectra overlays of the titrations that I performed with Pin1 and IRAK1-UD derived peptides, and the goodness of fit for all of the individual residues used in the analysis from the titrations with singly phosphorylated peptide.

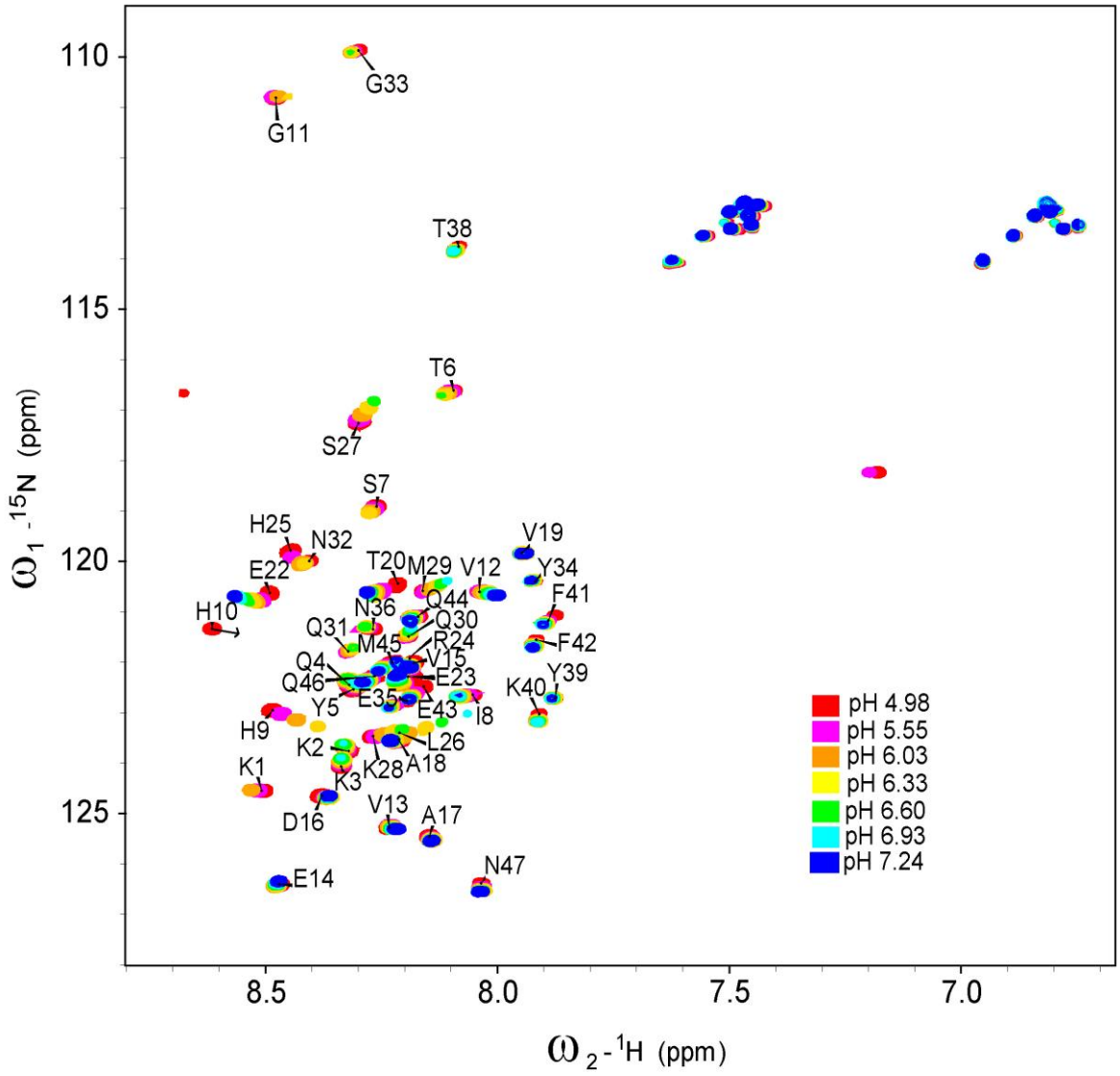

Figure A1.1 pH titration of ^{15}N-APPc via NMR. A Sparky generated image of a series of overlayed ^{15}N-^{1}H HSQC spectra taken at various pHs. All spectra are displayed at the same minimum contour level of 6e06. The pH levels are as labeled. The arrow by H10 denotes the trajectory of said peak as it broadens at low pH and no longer meets the minimum contour cutoff by the second sample.

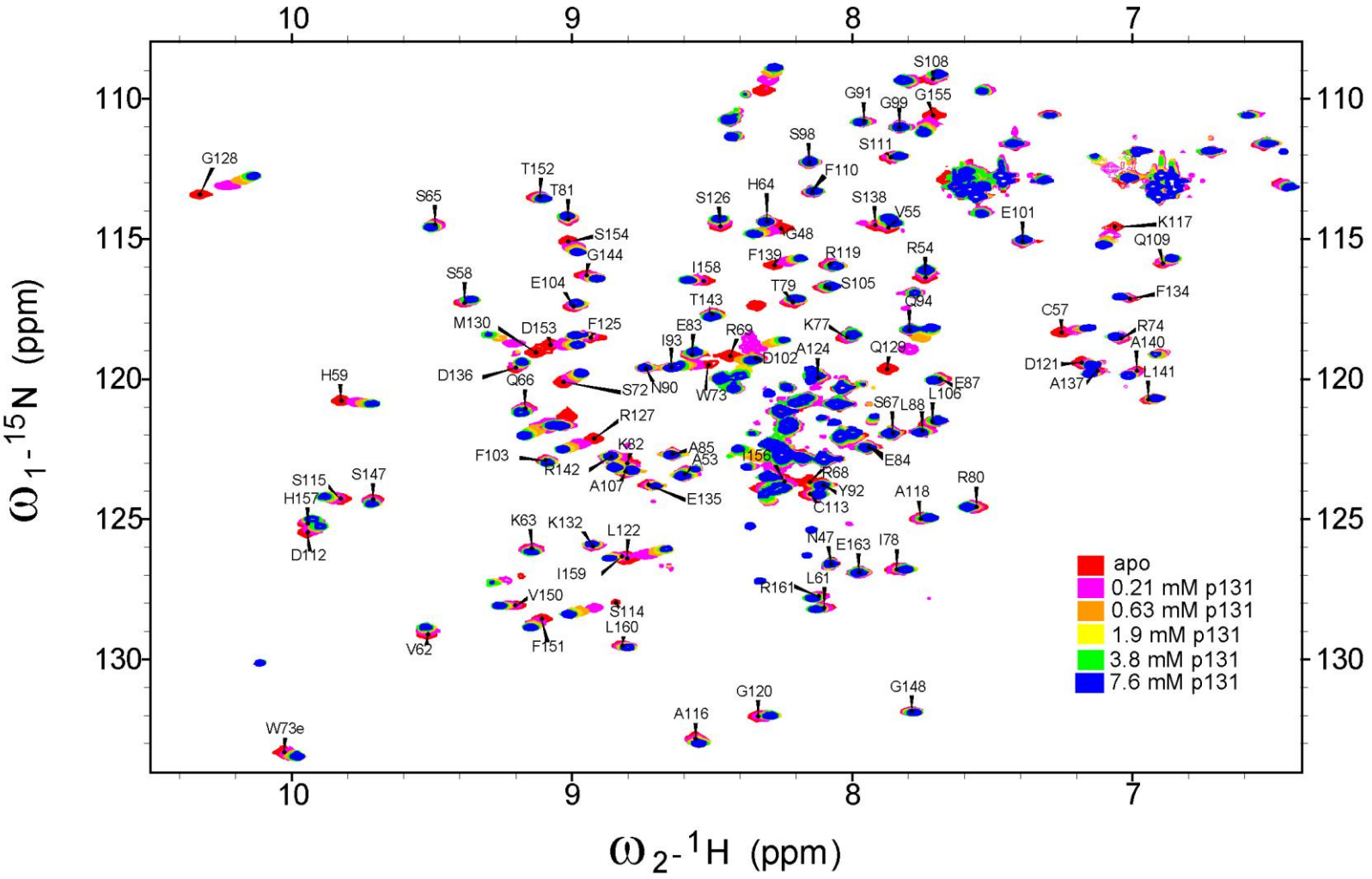

Figure A1.2 Titration of ^{15}N-PPIase, isolated domain of Pin1, with p131. Overlay of ^{15}N-^{1}H HSQC spectra where PPIase is at 0.16 mM and the concentrations of p131 vary as shown. This image was generated via Sparky and annotated via Adobe Illustrator.

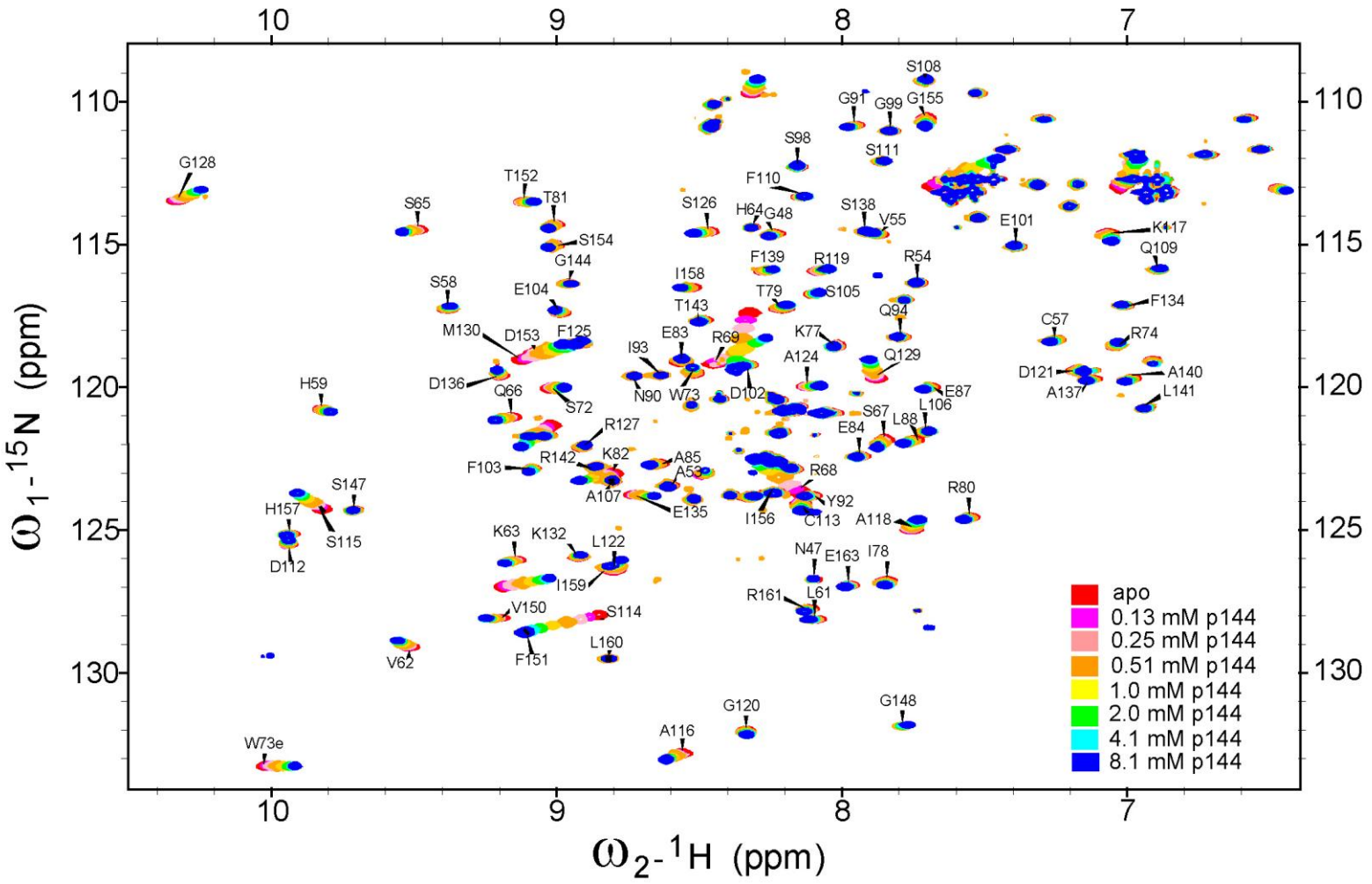

Figure A1.3 Titration of ^{15}N-PPIase domain of Pin1 with p144. Overlay of ^{15}N-^{1}H HSQC spectra where PPIase is at 0.22 mM and the concentrations of p144 vary as shown. This image was generated via Sparky and annotated via Adobe Illustrator.

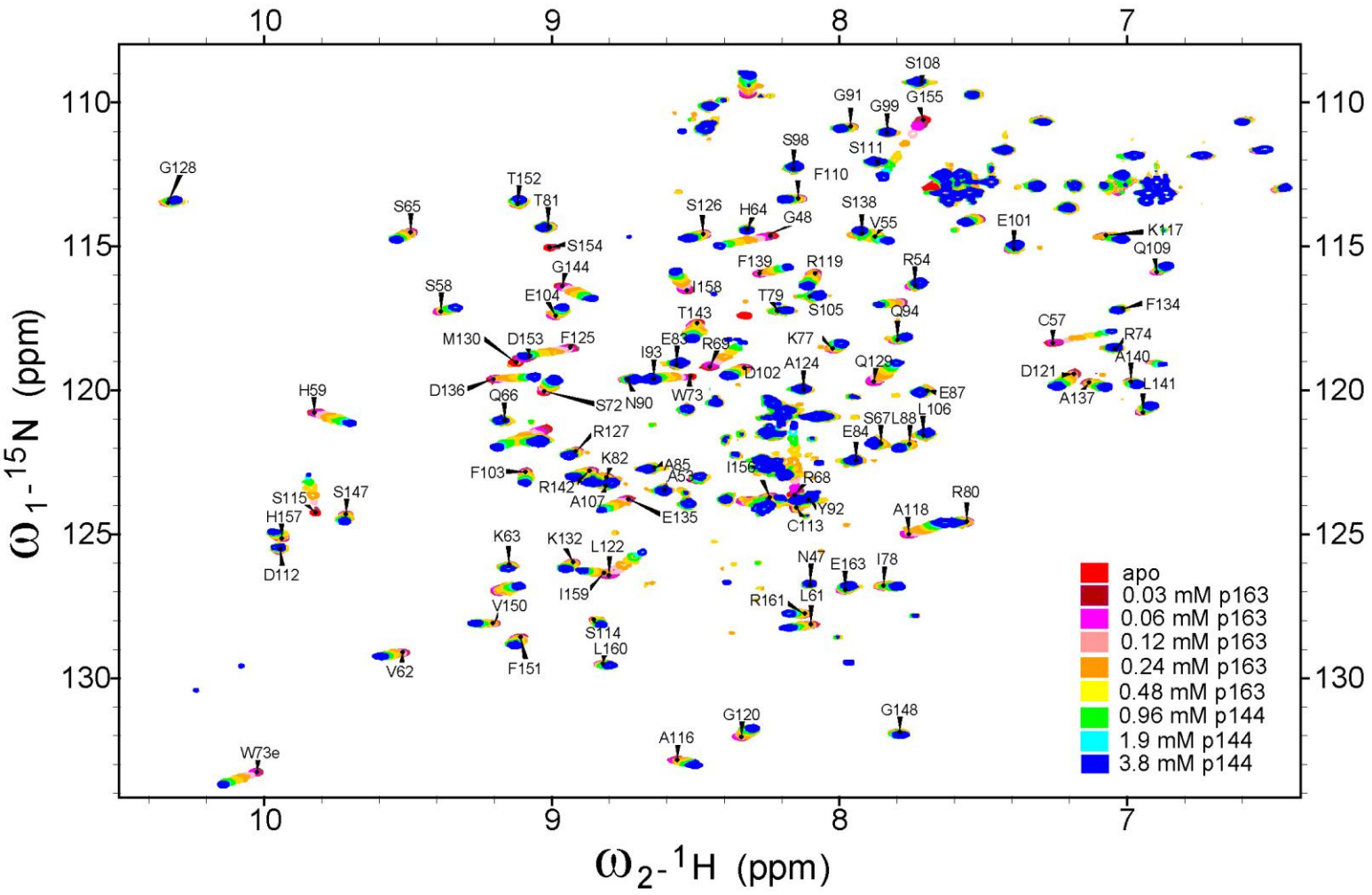

Figure A1.4 Titration of ^{15}N-PPIase domain of Pin1 with p163. Overlay of ^{15}N-^{1}H HSQC spectra where PPIase is at 0.20 mM and the concentrations of p163 vary as shown. This image was generated via Sparky and annotated via Adobe Illustrator.

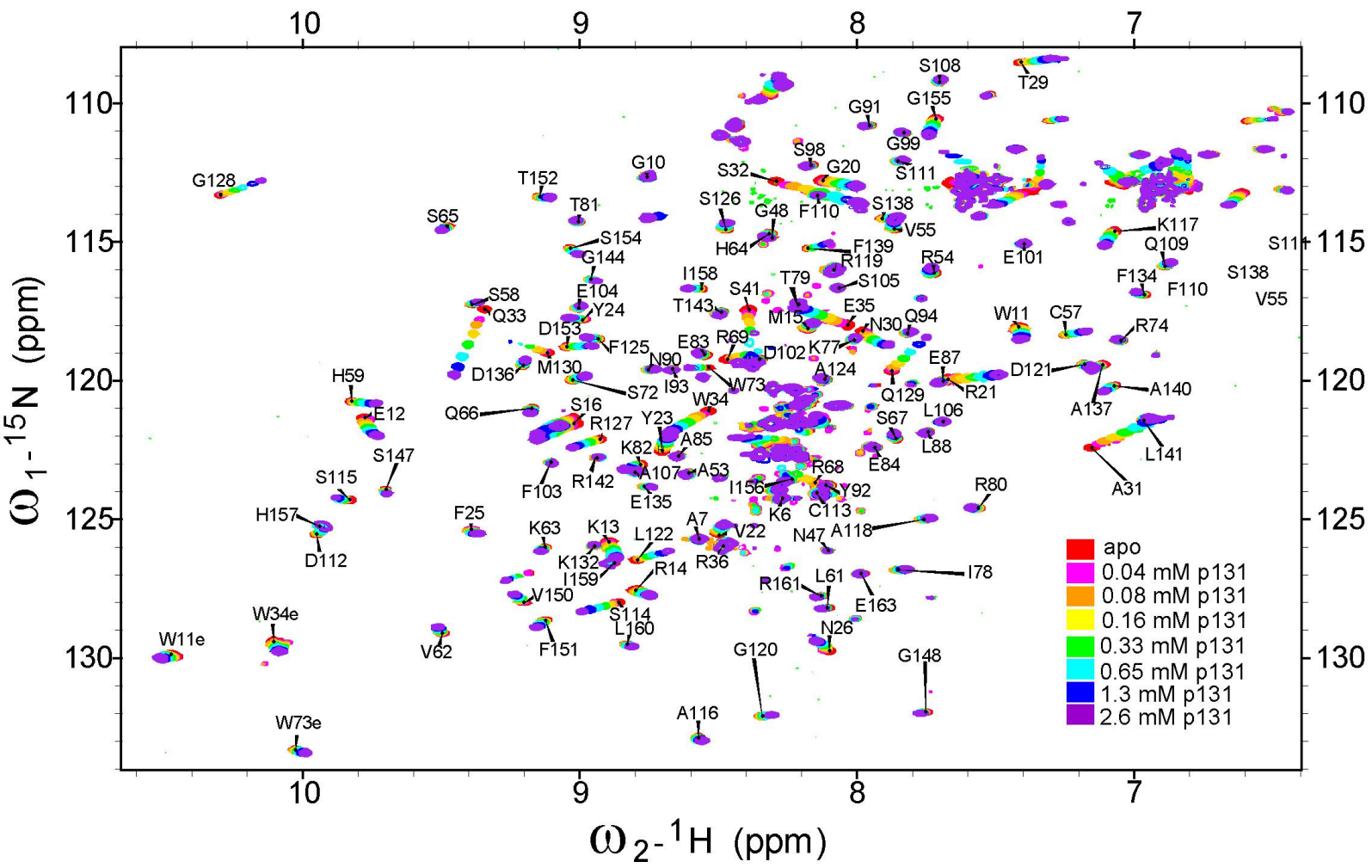

Figure A1.5 Titration of ^{15}N-Pin1-FL with p131. Overlay of ^{15}N-^{1}H HSQC spectra where Pin1 is at 0.20 mM and the concentrations of p131 vary as shown. This image was generated via Sparky and annotated via Adobe Illustrator.

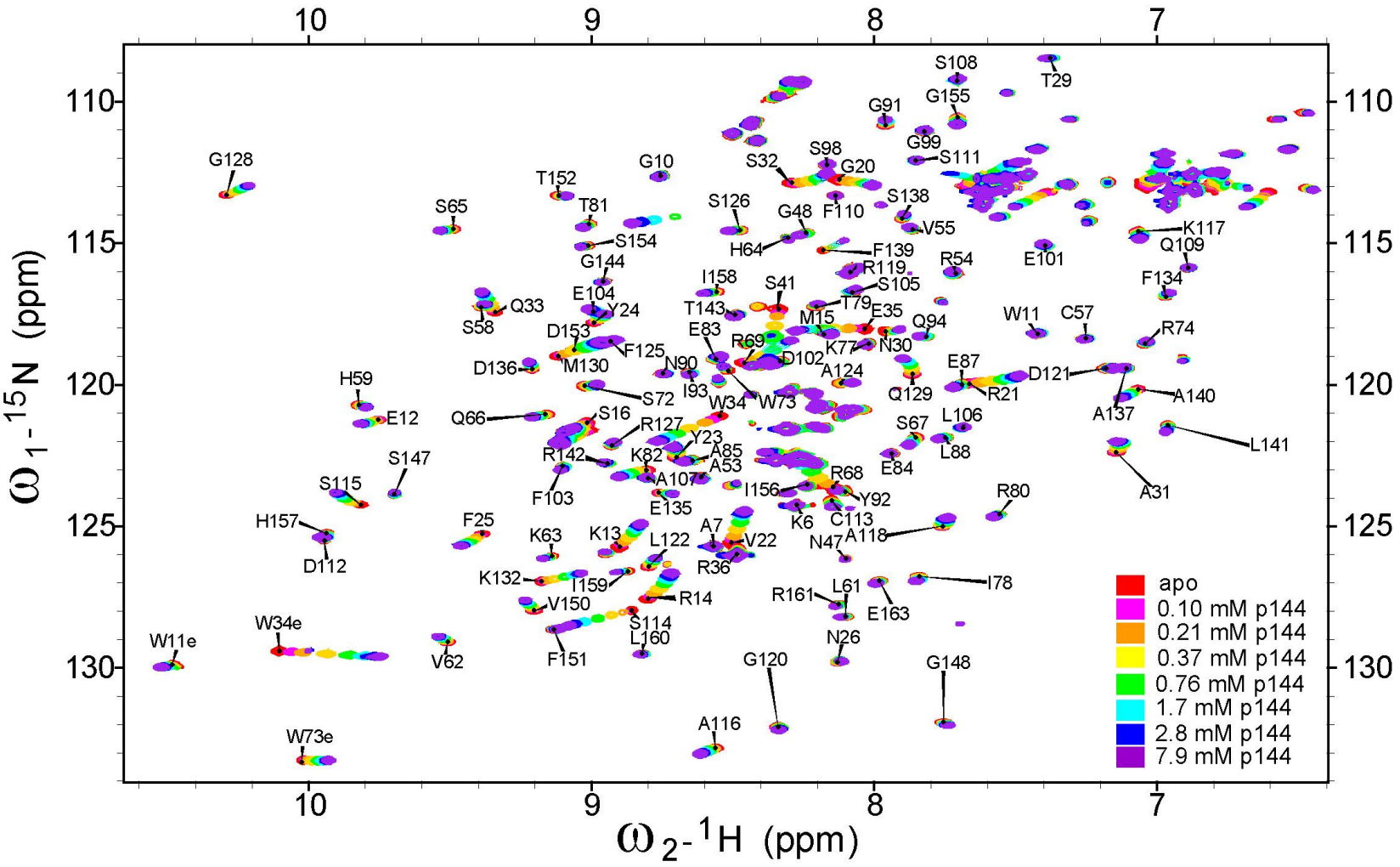

Figure A1.6 Titration of ^{15}N-Pin1-FL with p144. Overlay of ^{15}N-^{1}H HSQC spectra where Pin1 is at 0.25 mM and the concentrations of p144 vary as shown. This image was generated via Sparky and annotated via Adobe Illustrator.

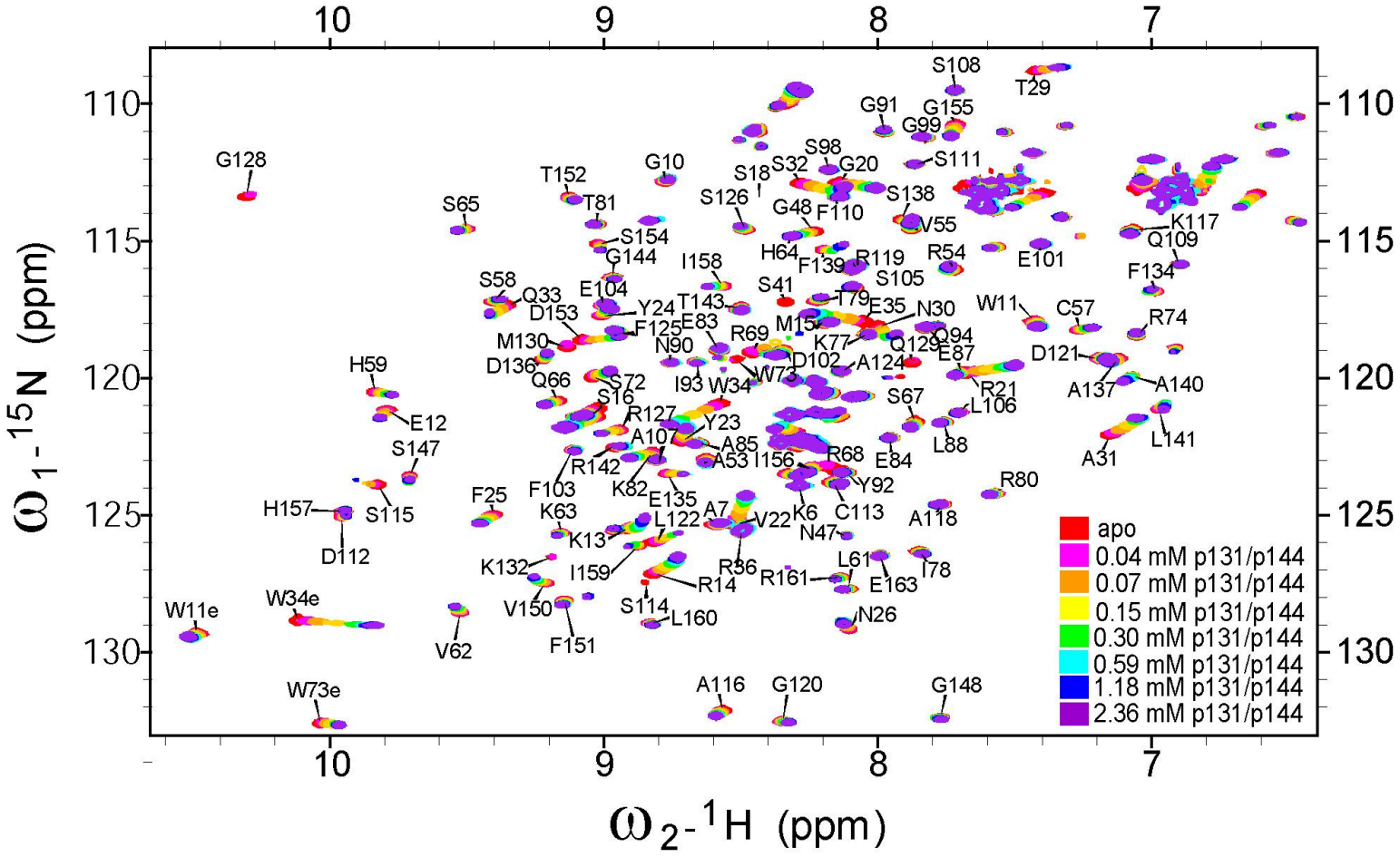

Figure A1.7 Titration of ^{15}N-Pin1-FL with p131/p144. Overlay of ^{15}N-^{1}H HSQC spectra where Pin1 is at 0.25 mM and the concentrations of p131/p144 vary as shown. This image was generated via Sparky and annotated via Adobe Illustrator.

Figure A1.8 The simultaneous fits of isolated domains of Pin1 titrated with singly phosphorylated IRAK1-UD derived peptides shown in terms of chemical shift perturbation of selected residues in individual dimensions. The x-axis represents the amount of peptide titrated in and the y-axis is the chemical shift perturbations. The points represent the data and the lines represent the two-state fit of said data. A) selected residues in the proton dimension (S18 filled◊, R21 unfilled□, V22 filledΔ, W34 *, W34e X, E35 filled ○) for WW domain titrated with p163. B) selected residues in the nitrogen dimension (S18 filled◊, R21 filled□, V22 filledΔ, Y23 X, Y24 *, W34 filled ○, E35 +) for WW domain titrated with p163 C) selected residues in the proton dimension (H59 filled◊, R68 filled□, R69 filledΔ, S114 X, K117 *, L122 filled ○, R127 +, G128 -, M130 —) for PPIase domain titrated with p131 D) selected residues in the nitrogen dimension (H59 filled◊, V62 filled□, R68 filledΔ, R69 X, S114 *, K117 filled ○, L122 +, R127 -, G128 —, M130 filled ◊) for PPIase domain titrated with p131 E) selected residues in the proton dimension (V62 filled◊, R68 filled□, R69 filledΔ, S114 X, S115 *, A116 filled ○, L122 +, G128 -, Q129 —) for PPIase domain titrated with p144 F) selected residues in the nitrogen dimension (V62 filled◊, R68 filled□, R69 filledΔ, S114 X, S115 *, A116 filled ○, L122 +, G128 -, Q129 —) for PPIase domain titrated with p144 G) selected residues in the proton dimension (H59 filled◊, L61 unfilled□, V62 filledΔ, R69 X, S115 *, A116 filled ○, A118 +, R119 small unfilled□, R127 —, Q129 unfilled ◊) for PPIase domain titrated with p163 H) selected residues in the nitrogen dimension (H59 filled◊, L61 filled□, V62 filledΔ, R69 X, S115 *, A116 filled ○, A118 +, R119 -, R127 —, Q129 unfilled ◊) for PPIase domain titrated with p163.

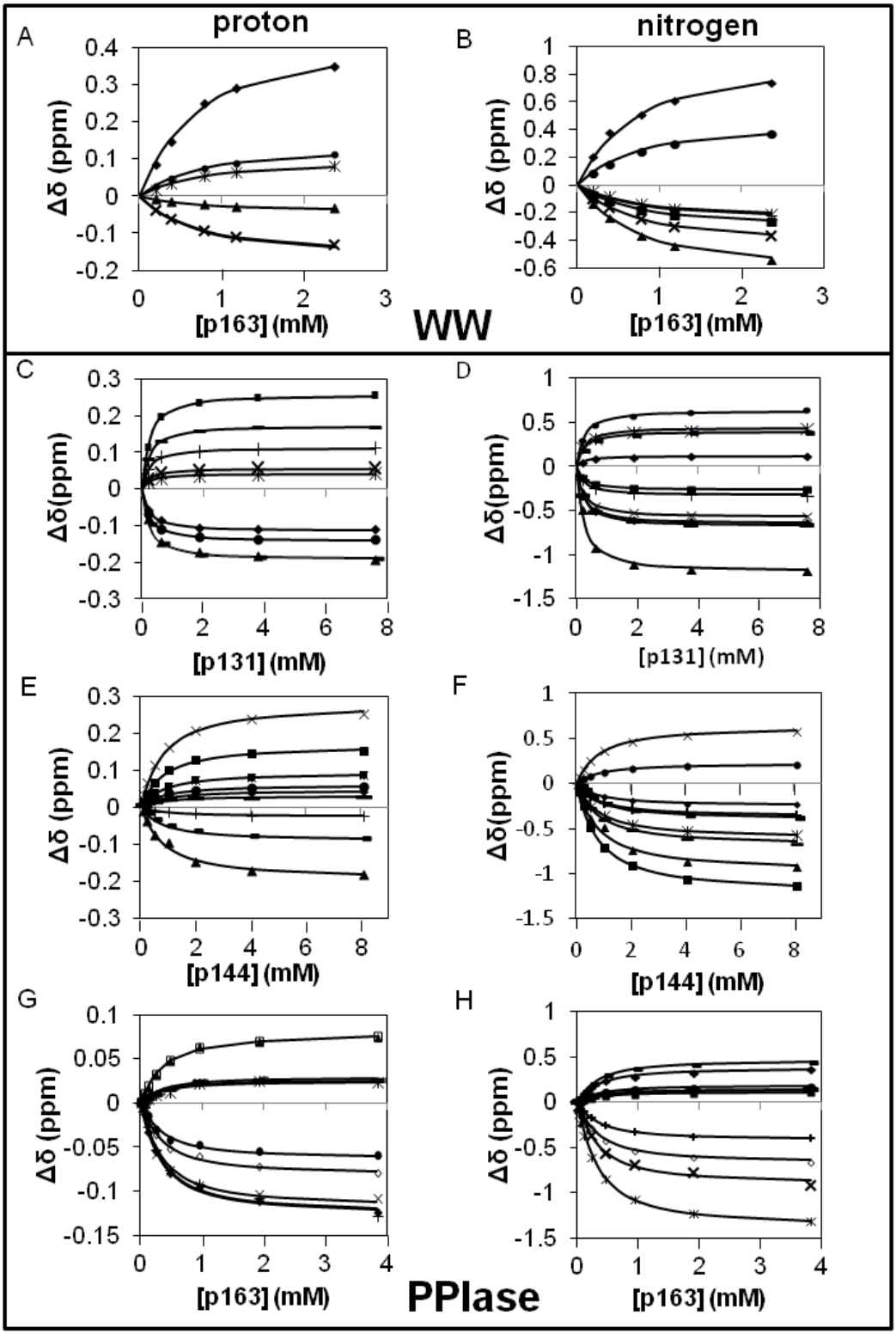
A
proton
Δδ (ppm)
[p163] (mM)
B
nitrogen
Δδ (ppm)
[p163] (mM)
WW
C
Δδ(ppm)
[p131] (mM)
D
Δδ(ppm)
[p131] (mM)
E
Δδ (ppm)
[p144] (mM)
F
Δδ(ppm)
[p144] (mM)
G
Δδ (ppm)
[p163] (mM)
H
Δδ (ppm)
[p163] (mM)
PPIase

Figure A1.9 The simultaneous fits of intact Pin1 with singly phosphorylated IRAK1-UD derived peptides shown in terms of chemical shift perturbation of selected residues in individual dimensions. The x-axis is the concentration of peptide titrated in and the y-axis is the chemical shift perturbation. Blue represents WW domain residues while red represents PPIase residues. The symbols are the experimental data and the lines are the simultaneous fits. A) selected residues in the proton dimension (F25 unfilled□, Q33 filled◊, W34 filled ○, W34e X, E35 filledΔ, H59 filled○, R69 X, S114 -, S115 *, R127 X, G128 filledΔ, Q129 filled□, and M130 —) for Pin1 titrated with p131. B) selected residues in the nitrogen dimension (Y23 filledΔ, Y24 X, Q33 *, W34 filled ○, W34e +, E35 -, V62 —, R69 filled◊, S114 unfilled□, A116 filledΔ, R127 X, G128 unfilled ○, Q129 filled ○, M130 +) for Pin1 titrated with p131. C) selected residues in the proton dimension (Y24 *, F25 filled ○ , W34 +, W34e -, E35 — , H59 filled◊, V62 -, R69 filled□, S114 filledΔ, S115 *, A116 X, G128 +, Q129 filled ○) for Pin1 titrated with p144. D) selected residues in the nitrogen dimension (Y23 filled ○, Y24 +, F25 -, Q33 —, W34 filled◊, W34e filled□, V62 *, R69 unfilled◊, S114 filled□, S115 X, A116 filled◊, R127 -, G128 filledΔ, Q129 filled ○) for Pin1 titrated with p144. E) selected residues in the proton dimension (Y23 filled□, Y24 filled ○, W34 filledΔ, W34e filled◊, H59 unfilledΔ, L61 X, V62 *, R69 unfilled□, A116 unfilled ○, K117 —, A118 unfilled◊, G128 -, Q129 +) for Pin1 titrated with p163. F) selected residues in the nitrogen dimension (Y23 *, Y24 filled ○, W34 filled◊, E35 -, H59 —, V62 -, R69 filled◊, S115 filled□, A116 unfilledΔ, A118 X, R127 filled ○, Q129 filled◊, K132 *) for Pin1 titrated with p163. G) selected residues in the proton dimension (F25 +, W34 -, W34e —, E35 filled◊, S114 filled□, S115 filled ○) for Pin1 titrated with p173 H) selected residues in the nitrogen dimension (Y23 —, Y24 filled◊, F25 filled□, W34 filledΔ, E35 X, R68 unfilledΔ, Q129 unfilled ○, M130 +) for Pin1 titrated with p173.

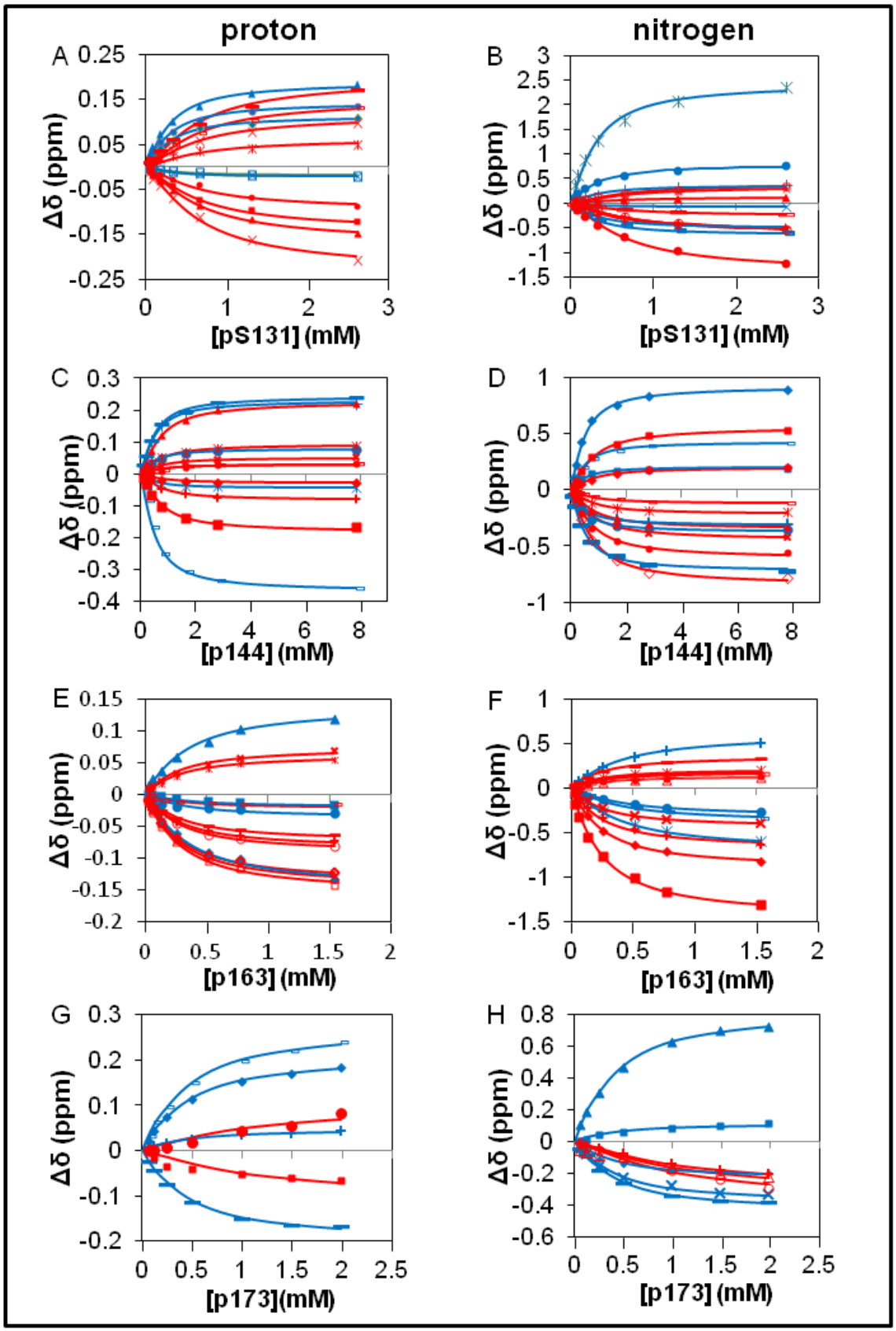
proton
nitrogen
A
B
C
D
E
F
G
H
Δδ (ppm)
[pS131] (mM)
[p144] (mM)
[p163] (mM)
[p173](mM)

APPENDIX 2

MATHEMATICAL MODELING OF VARIOUS BINDING SCHEMES DESCRIBED IN CHAPTER THREE.

Model 1. Simple two-state interaction.

A simple biomolecular interaction between a protein with one binding site and a ligand with one binding site.

$$[\mathbf{L}] + [\mathbf{P}] \leftrightarrow [\mathbf{LP}]$$

Where:

$$K_d = \frac{[L][P]}{[LP]}$$

$$[\mathrm{LP}] = \frac{([L_{tot}] + [P_{tot}] + K_d) - \sqrt{([L_{tot}] + [P_{tot}] + K_d)^2 - 4[L_{tot}][P_{tot}]}}{2}$$

where L_{tot} is the total concentration of ligand, P_{tot} is the total concentration of protein, LP is the protein:ligand complex and K_d is the binding affinity of the interaction.

In the context of this NMR-based binding study, a two-state interaction has one fitted K_d as well as a fitted scaling factor for each peak ($\Delta\delta^{n}_{bound}$, the chemical shift perturbation of the bound protein where *n* is any residue), which is necessary in order to calculate the chemical shift perturbation ($\Delta\delta^{n,i}$) at each titration point (*i*) and therefore a binding curve. The squared difference between the calculated $\Delta\delta^{n,i}$ and the observed $\Delta\delta^{n,i}$ is minimized using Excel solver 2007, which also allows simultaneous peak fitting.

Model 2. Four-state interaction.

In this interaction the protein has two domains that bind the same ligand and each binding site can have a distinct binding affinity. The protein will be presented in terms of Pin1, where the first site is in the WW domain and the second site is in the PPIase domain.

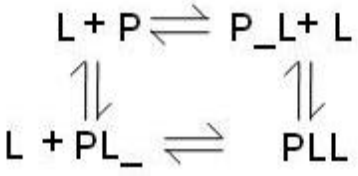

Figure A2.1 Reaction scheme for a four-state interaction. P_ _ represents a protein with two binding sites, where the first underbar represents binding to the WW domain and the second underbar represents binding to the PPIase domain (i.e. PL_ is a species where ligand is bound to the WW domain of Pin1).

Where:

$$L_{tot} = [L] + [LP^{WW}] + [LP^{PPIase}] + 2[2LP]$$

$$P_{tot} = [P] + [LP^{WW}] + [LP^{PPIase}] + [2LP]$$

$$K_a^{WW} = \frac{[LP^{WW}]}{[L][P^{WW}]}$$

$$K_a^{PPIase} = \frac{[LP^{PPIase}]}{[L][P^{PPIase}]}$$

$$K_a^{WW\&PPIase} = \frac{[2LP]}{[L][LP^{WW}]}$$

$$K_a^{PPIase\&WW} = \frac{[2LP]}{[L][LP^{PPIase}]} = \frac{K_a^{WW} K_a^{WW\&PPIase}}{K_a^{PPIase}}$$

$$[P_{tot}]$$

$$= \frac{-([L]-[L_{tot}])}{\frac{(K_a^{WW}[L]+K_a^{PPIase}[L]+2K_a^{WW}K_a^{WW\&PPIase}[L]^2-K_a^{WW}[L]([L]-[L_{tot}]))}{\frac{\left(K_a^{WW}[L]+K_a^{PPIase}[L]+2K_a^{WW}K_a^{WW\&PPIase}[L]^2-K_a^{PPIase}[L]([L]-[L_{tot}])\right)}{\frac{\left(K_a^{WW}[L]+K_a^{PPIase}[L]+2K_a^{WW}K_a^{WW\&PPIase}[L]^2-K_a^{WW}K_a^{WW\&PPIase}[L]^2([L]-[L_{tot}])\right)}{\left(K_a^{WW}[L]+K_a^{PPIase}[L]+2K_a^{WW}K_a^{WW\&PPIase}[L]^2-K_a^{WW}[L]([L]-[L_{tot}])\right)}}}}$$

$$[P] = \frac{-([L]-[L_{tot}])}{K_a^{WW}[L]+K_a^{PPIase}[L]+2K_a^{WW}K_a^{WW\&PPIase}[L]^2}$$

where L_{tot} is the total concentration of ligand, P_{tot} is the total concentration of protein, L is the free ligand, P is free protein, LP^{WW} is the WW domain of Pin1 bound to ligand, LP^{PPIase} is the PPIase domain of Pin1 bound to ligand, LLP is when both domains are bound to ligand at once, and the K_as are the association constants (the superscript denotes which domain is being bound to L, when two domains are present the first denotes the domain that was previously bound and the second the domain that is being bound).

In the modeling done in chapter three, allostery was unnecessary to fit the data and so in that case additional relationships include:

$$K_a^{PPIase} = K_a^{WW\&PPIase}$$

and

$$K_a^{WW} = K_a^{PPIase\&WW}$$

Therefore, in the four-state model utilized in chapter three, the fitted parameters include two K_ds and two bound Δδs per residue (one for binding to WW domain and one for PPIase). The bound $\Delta\delta^n_{bound}$s are used to scale the calculated concentrations to the individual peak movement of each residue (so binding information recorded by NMR is equivalent to fraction bound). For the purposes of this appendix, I will provide the equation for fraction bound only, however for

utilization of the actual minimization function in MATLAB (which is minimized by fmincon) (MATLAB 2010&2014b, The MathWorks Inc., Natick, MA, 2014) it is necessary to convert fraction bound into $\Delta\delta^{n,i}$ (which will change over the course of a titration).

$$FractionBoundP_{calc}^{WW} = \frac{[LP^{WW}]+[LLP]}{P_{tot}}$$

$$FractionBoundP_{calc}^{PPIase} = \frac{[LP^{PPIase}] + [LLP]}{P_{tot}}$$

Where the function actually minimized is

$$\frac{\sqrt{(frobeniusnormdiff^{WW})^2 + (frobeniusnormdiff^{PPIase})^2}}{\frac{\#\ of\ residues}{\#\ of\ titration\ points}}$$

Where

$$frobeniusnormdiff^{domain} = \sqrt{\sum diag\left((X^{domain})' \times X^{domain}\right)}$$

$$X^{domain} = \begin{matrix} diff_{1,1}^{domain} & diff_{1,2}^{domain} & diff_{1,3}^{domain} \\ diff_{2,1}^{domain} & diff_{2,2}^{domain} & diff_{2,3}^{domain} \\ diff_{3,1}^{domain} & diff_{3,2}^{domain} & diff_{3,3}^{domain} \end{matrix}$$

$$diff_{n,i}^{domain} = FractionBoundP_{calc_{n,i}}^{domain} - FractionBoundP_{obs_{n,i}}^{domain}$$

where *n* is the residue number, *i* is the titration sample number, domain is either WW or PPIase, *obs* refers to the collected NMR data and *calc* to the value calculated via MATLAB.

Model 3. Multi-state equilibria (16 species).

In this interaction the protein has two domains, both of which are capable of binding to either of two sites on the ligand. The following is adapted from an output summary file generated by VCELL(Dubitzky, Wolkenhauer et al.):

1.1. General Info

BioModel Name: bivalent_physical_model_revised_Pin1&IRAK1-UD
Owner: mjr323

1.2. Reaction(s) in c0

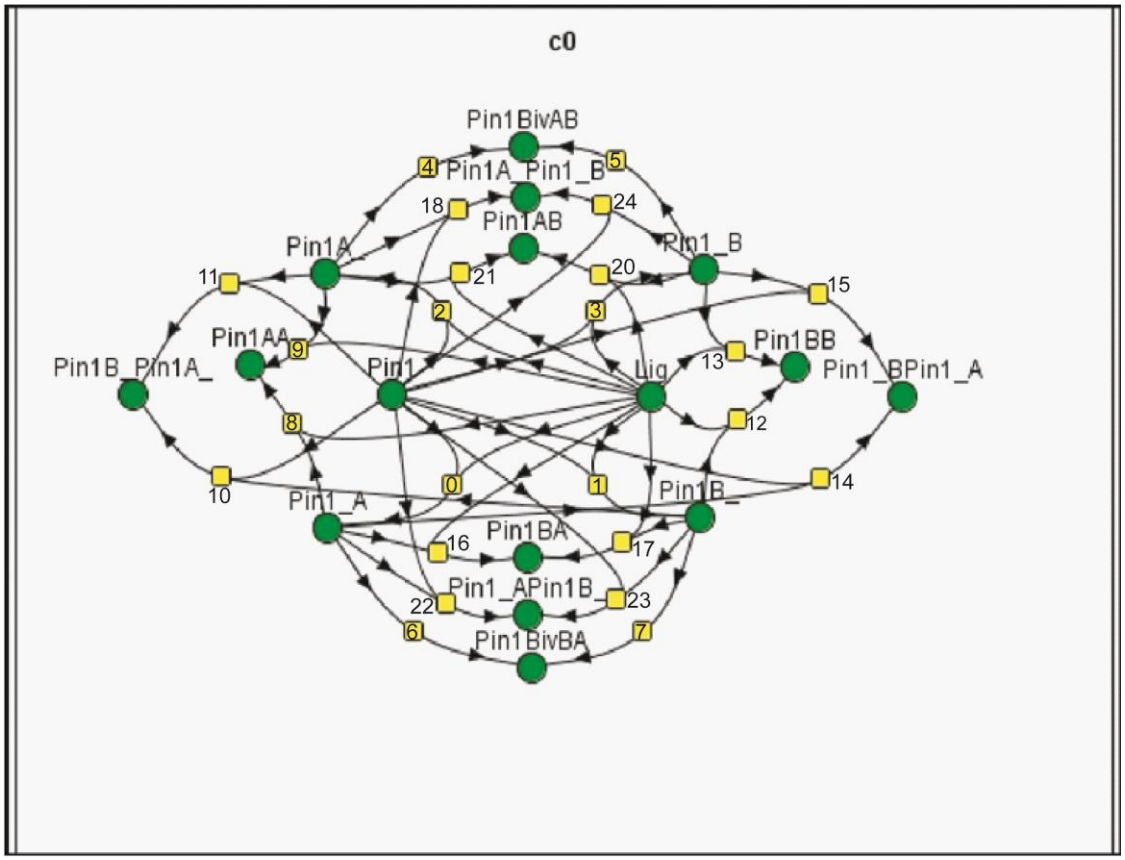

Figure A2.2 Reaction scheme of a protein with two binding domains and a ligand with two binding sites, show in terms of Pin1 binding, where Pin1_ _ has two binding domains: the WW domain (first underbar) and the PPIase domain (second underbar). For example, Pin1AB is bound to the A site of one peptide at the WW domain and the PPIase domain is bound to a second peptide at site B. At low ligand concentrations, multiple Pin1 molecules could bind to one ligand, which is represented by species names with two Pin1s. The bivalent species, where one ligand is connected to both domains, are distinguished by the "biv" in their names.

Reaction r4

$$\text{Pin1A\_} \longleftrightarrow \text{Pin1BivAB}$$

Kinetics Parameters			
Name	**Expression**	**Role**	**Unit**
J	((Kf * Pin1A_) - (Kr * Pin1BivAB))	reaction rate	$M.s^{-1}$
Kf	100.0	forward rate constant	s^{-1}
Kr	$K_{eq}^{B:PPIase} * 100$	reverse rate constant	s^{-1}

Reaction r0

$$\text{Pin1} + \text{Lig} \longleftrightarrow \text{Pin1\_A}$$

Kinetics Parameters			
Name	**Expression**	**Role**	**Unit**
J	(((Kf * Pin1) * Lig) - (Kr * Pin1_A))	reaction rate	$M.s^{-1}$
Kf	100.0	forward rate constant	$s^{-1}.M^{-1}$
Kr	$K_d^{A:PPIase} * 100$	reverse rate constant	s^{-1}

Reaction r1

$$\text{Pin1} + \text{Lig} \longleftrightarrow \text{Pin1B\_}$$

Kinetics Parameters			
Name	**Expression**	**Role**	**Unit**
J	(((Kf * Pin1) * Lig) - (Kr * Pin1B_))	reaction rate	$M.s^{-1}$
Kf	100.0	forward rate constant	$s^{-1}.M^{-1}$
Kr	$K_d^{B:WW} * 100$	reverse rate constant	s^{-1}

Reaction r6

Pin1_A ⟷ Pin1BivBA

Kinetics Parameters			
Name	**Expression**	**Role**	**Unit**
J	((Kf * Pin1_A) - (Kr * Pin1BivBA))	reaction rate	M.s ^{1}
Kf	100.0	forward rate constant	s ^{1}
Kr	$K_{eq}^{B:WW} * 100$	reverse rate constant	s ^{1}

Reaction r7

Pin1B_ ⟷ Pin1BivBA

Kinetics Parameters			
Name	**Expression**	**Role**	**Unit**
J	((Kf * Pin1B_) - (Kr * Pin1BivBA))	reaction rate	M.s ^{1}
Kf	100.0	forward rate constant	s ^{1}
Kr	$K_{eq}^{A:PPIase} * 100$	reverse rate constant	s ^{1}

Reaction r8

Pin1_A + Lig ⟷ Pin1AA

Kinetics Parameters			
Name	**Expression**	**Role**	**Unit**
J	(((Kf * Pin1_A) * Lig) - (Kr *	reaction rate	M.s ^{1}
Kf	100.0	forward rate constant	s ^{1}. M ^{1}
Kr	$K_{d}^{A:PPIase\&A:WW} * 100$	reverse rate constant	s ^{1}

Reaction r9

Lig + Pin1A_ ⟷ Pin1AA

Kinetics Parameters			
Name	**Expression**	**Role**	**Unit**
J	(((Kf * Lig) * Pin1A_) - (Kr *	reaction rate	M.s ^{1}
Kf	100.0	forward rate constant	s ^{1}. M ^{1}
Kr	$K_d^{A:WW\&A:PPIase} * 100$	reverse rate constant	s ^{1}

Reaction r12

Pin1B_ + Lig ⟷ Pin1BB

Kinetics Parameters			
Name	**Expression**	**Role**	**Unit**
J	(((Kf * Pin1B_) * Lig) - (Kr *	reaction rate	M.s ^{1}
Kf	100.0	forward rate constant	s ^{1}. M ^{1}
Kr	$K_d^{B:WW\&B:PPIase} * 100$	reverse rate constant	s ^{1}

Reaction r13

Pin1_B + Lig ⟷ Pin1BB

Kinetics Parameters			
Name	**Expression**	**Role**	**Unit**
J	(((Kf * Pin1_B) * Lig) - (Kr *	reaction rate	M.s ^{1}
Kf	100.0	forward rate constant	s ^{1}. M ^{1}
Kr	$K_d^{B:PPIase\&B:WW} * 100$	reverse rate constant	s ^{1}

Reaction r16

Pin1_A + Lig ⟷ Pin1BA

Kinetics Parameters			
Name	**Expression**	**Role**	**Unit**
J	(((Kf * Pin1_A) * Lig) - (Kr *	reaction rate	M.s ^{1}
Kf	100.0	forward rate constant	s ^{1}. M ^{1}
Kr	$K_d^{A:PPIase\&B:WW} * 100$	reverse rate constant	s ^{1}

Reaction r17

Pin1B_ + Lig ⟷ Pin1BA

Kinetics Parameters			
Name	**Expression**	**Role**	**Unit**
J	(((Kf * Pin1B_) * Lig) - (Kr *	reaction rate	M.s ^{1}
Kf	100.0	forward rate constant	s ^{1}. M ^{1}
Kr	$K_d^{B:WW\&A:PPIase} * 100$	reverse rate constant	s ^{1}

Reaction r5

Pin1_B ⟷ Pin1BivAB

Kinetics Parameters			
Name	**Expression**	**Role**	**Unit**
J	((Kf * Pin1_B) - (Kr * Pin1BivAB))	reaction rate	M.s ^{1}
Kf	100.0	forward rate constant	s ^{1}
Kr	$K_{eq}^{A:WW} * 100$	reverse rate constant	s ^{1}

Reaction r20

Pin1_B + Lig ⟷ Pin1AB

Kinetics Parameters			
Name	**Expression**	**Role**	**Unit**
J	(((Kf * Pin1_B) * Lig) - (Kr *	reaction rate	M.s ^{1}
Kf	100.0	forward rate constant	s ^{1}. M ^{1}
Kr	$K_d^{B:PPIase\&A:WW} * 100$	reverse rate constant	s ^{1}

Reaction r21

Pin1A_ + Lig ⟷ Pin1AB

Kinetics Parameters			
Name	**Expression**	**Role**	**Unit**
J	(((Kf * Pin1A_) * Lig) - (Kr *	reaction rate	M.s ^{1}
Kf	100.0	forward rate constant	s ^{1}. M ^{1}
Kr	$K_d^{A:WW\&B:PPIase} * 100$	reverse rate constant	s ^{1}

Reaction r2

Pin1 + Lig ⟷ Pin1A_

Kinetics Parameters			
Name	**Expression**	**Role**	**Unit**
J	(((Kf * Pin1) * Lig) - (Kr * Pin1A_))	reaction rate	M.s ^{1}
Kf	100.0	forward rate constant	s ^{1}. M ^{1}
Kr	$K_d^{A:WW} * 100$	reverse rate constant	s ^{1}

Reaction r3

$$\text{Pin1} + \text{Lig} \longleftrightarrow \text{Pin1\_B}$$

Kinetics Parameters			
Name	**Expression**	**Role**	**Unit**
J	(((Kf * Pin1) * Lig) - (Kr * Pin1_B))	reaction rate	M.s ^{1}
Kf	100.0	forward rate constant	s ^{1}. M ^{1}
Kr	$K_d^{B:PPIase} * 100$	reverse rate constant	s ^{1}

Reaction r10

$$\text{Pin1} + \text{Pin1B\_} \longleftrightarrow \text{Pin1B\_Pin1A\_}$$

Kinetics Parameters			
Name	**Expression**	**Role**	**Unit**
J	(((Kf * Pin1) * Pin1B_) - (Kr *	reaction rate	M.s ^{1}
Kf	100.0	forward rate constant	s ^{1}. M ^{1}
Kr	$K_d^{B:WW\&2ndWW:A} * 100$	reverse rate constant	s ^{1}

Reaction r15

$$\text{Pin1} + \text{Pin1\_B} \longleftrightarrow \text{Pin1\_BPin1\_A}$$

Kinetics Parameters			
Name	**Expression**	**Role**	**Unit**
J	(((Kf * Pin1) * Pin1_B) - (Kr *	reaction rate	M.s ^{1}
Kf	100.0	forward rate constant	s ^{1}. M ^{1}
Kr	$K_d^{B:PPIase\&2ndPPIase:A} * 100$	reverse rate constant	s ^{1}

Reaction r18

Pin1 + Pin1A_ ⟷ Pin1A_Pin1_B

Kinetics Parameters			
Name	**Expression**	**Role**	**Unit**
J	(((Kf * Pin1) * Pin1A_) - (Kr *	reaction rate	M.s ^{1}
Kf	100.0	forward rate constant	s ^{1}. M ^{1}
Kr	$K_d^{A:WW\&2ndPPIase:B} * 100$	reverse rate constant	s ^{1}

Reaction r22

Pin1 + Pin1_A ⟷ Pin1_APin1B_

Kinetics Parameters			
Name	**Expression**	**Role**	**Unit**
J	(((Kf * Pin1) * Pin1_A) - (Kr *	reaction rate	M.s ^{1}
Kf	100.0	forward rate constant	s ^{1}. M ^{1}
Kr	$K_d^{A:PPIase\&2ndWW:B} * 100$	reverse rate constant	s ^{1}

Reaction r24

Pin1_B + Pin1 ⟷ Pin1A_Pin1_B

Kinetics Parameters			
Name	**Expression**	**Role**	**Unit**
J	(((Kf * Pin1_B) * Pin1) - (Kr *	reaction rate	M.s ^{1}
Kf	100.0	forward rate constant	s ^{1}. M ^{1}
Kr	$K_d^{B:PPIase\&2ndWW:A} * 100$	reverse rate constant	s ^{1}

Reaction r14

Pin1_A + Pin1 ⟷ Pin1_BPin1_A

Kinetics Parameters			
Name	**Expression**	**Role**	**Unit**
J	(((Kf * Pin1_A) * Pin1) - (Kr *	reaction rate	M.s ^{1}
Kf	100.0	forward rate constant	s ^{1}. M ^{1}
Kr	$K_d^{A:PPIase\&2ndPPIase:B} * 100$	reverse rate constant	s ^{1}

Reaction r23

Pin1B_ + Pin1 ⟷ Pin1_APin1B_

Kinetics Parameters			
Name	**Expression**	**Role**	**Unit**
J	(((Kf * Pin1B_) * Pin1) - (Kr *	reaction rate	M.s ^{1}
Kf	100.0	forward rate constant	s ^{1}. M ^{1}
Kr	$K_d^{B:WW\&2ndPPIase:A} * 100$	reverse rate constant	s ^{1}

Reaction r11

Pin1A_ + Pin1 ⟷ Pin1B_Pin1A_

Kinetics Parameters			
Name	**Expression**	**Role**	**Unit**
J	(((Kf * Pin1A_) * Pin1) - (Kr *	reaction rate	M.s ^{1}
Kf	100.0	forward rate constant	s ^{1}. M ^{1}
Kr	$K_d^{A:WW\&2ndWW:B} * 100$	reverse rate constant	s ^{1}

1.1.1. Structure Mapping For Application0

Structure Mapping				
Structure	**Subdomain**	**Resolved (T/F)**	**Surf/Vol**	**VolFract**
c0	Compartment	F		

1.1.2. Reaction Mapping For Application0

Initial Conditions				
Species	**Structure**	**Initial Conc.**	**Diffusion Const.**	**Fixed**
s8	c0	0.0 M	0.0 $m^2.s^{-1}$	F
s9	c0	0.0 M	0.0 $m^2.s^{-1}$	F
s10	c0	0.0 M	0.0 $m^2.s^{-1}$	F
s11	c0	0.0 M	0.0 $m^2.s^{-1}$	F
s0	c0	[Ligand] M, varies by titration pt	0.0 $m^2.s^{-1}$	F
s1	c0	[Protein] M, varies by titration pt	0.0 $m^2.s^{-1}$	F
s5	c0	0.0 M	0.0 $m^2.s^{-1}$	F
s6	c0	0.0 M	0.0 $m^2.s^{-1}$	F
s2	c0	0.0 M	0.0 $m^2.s^{-1}$	F
s3	c0	0.0 M	0.0 $m^2.s^{-1}$	F
s4	c0	0.0 M	0.0 $m^2.s^{-1}$	F
s7	c0	0.0 M	0.0 $m^2.s^{-1}$	F
s12	c0	0.0 M	0.0 $m^2.s^{-1}$	F
s14	c0	0.0 M	0.0 $m^2.s^{-1}$	F
s16	c0	0.0 M	0.0 $m^2.s^{-1}$	F
s19	c0	0.0 M	0.0 $m^2.s^{-1}$	F

1.1.1. Geometry: non-spatial120107596

1.1.1.1. Constants

Constant Name	Expression
_F_	96480.0
_F_nmol_	9.648E-5
_K_GHK_	1.0E-9
_N_pmol_	6.02E11
_PI_	3.141592653589793
_R_	8314.0
_T_	300.0
K_millivolts_per_volt	1000.0
Kf_r0	100.0
Kf_r1	100.0
Kf_r10	100.0
Kf_r11	100.0
Kf_r12	100.0
Kf_r13	100.0
Kf_r14	100.0
Kf_r15	100.0
Kf_r16	100.0
Kf_r17	100.0
Kf_r18	100.0
Kf_r2	100.0
Kf_r20	100.0
Kf_r21	100.0
Kf_r22	100.0
Kf_r23	100.0
Kf_r24	100.0
Kf_r3	100.0
Kf_r4	100.0

Constant Name	Expression
Kf_r5	100.0
Kf_r6	100.0
Kf_r7	100.0
Kf_r8	100.0
Kf_r9	100.0
KMOLE	(1.0 / 602.0)
Kr_r0	$K_d^{A:PPIase} * 100$
Kr_r1	$K_d^{B:WW} * 100$
Kr_r10	$K_d^{B:WW\&2ndWW:A} * 100$
Kr_r11	$K_d^{A:WW\&2ndWW:B} * 100$
Kr_r12	$K_d^{B:WW\&B:PPIase} * 100$
Kr_r13	$K_d^{B:PPIase\&B:WW} * 100$
Kr_r14	$K_d^{A:PPIase\&2ndPPIase:B} * 100$
Kr_r15	$K_d^{B:PPIase\&2ndPPIase:A} * 100$
Kr_r16	$K_d^{A:PPIase\&B:WW} * 100$
Kr_r17	$K_d^{B:WW\&A:PPIase} * 100$
Kr_r18	$K_d^{A:WW\&2ndPPIase:B} * 100$
Kr_r2	$K_d^{A:WW} * 100$
Kr_r20	$K_d^{B:PPIase\&A:WW} * 100$
Kr_r21	$K_d^{A:WW\&B:PPIase} * 100$
Kr_r22	$K_d^{A:PPIase\&2ndWW:B} * 100$
Kr_r23	$K_d^{B:WW\&2ndPPIase:A} * 100$
Kr_r24	$K_d^{B:PPIase\&2ndWW:A} * 100$
Kr_r3	$K_d^{B:PPIase} * 100$
Kr_r4	$K_{eq}^{B:PPIase} * 100$
Kr_r5	$K_{eq}^{A:WW} * 100$
Kr_r6	$K_{eq}^{B:WW} * 100$
Kr_r7	$K_{eq}^{A:PPIase} * 100$
Kr_r8	$K_d^{A:PPIase\&A:WW} * 100$

Constant Name	**Expression**
Kr_r9	$K_d^{A:WW\&A:PPIase} * 100$
Lig_init_uM	[L] uM dependent on titration sample
Pin1_A_init_uM	0.0
Pin1_APin1B init_u_M	0.0
Pin1_B_init_uM	0.0
Pin1_BPin1_A_init_u M	0.0
Pin1_init_uM	[P] uM dependant on titration sample
Pin1A_init_uM	0.0
Pin1A_Pin1_B_init_u M	0.0
Pin1AA_init_uM	0.0
Pin1AB_init_uM	0.0
Pin1B_init_uM	0.0
Pin1B_Pin1A init_u_M	0.0
Pin1BA_init_uM	0.0
Pin1BB_init_uM	0.0
Pin1BivAB_init_uM	0.0
Pin1BivBA_init_uM	0.0
Size_c0	50000.0

where K_ds are dissociation constants, K_{eq}s are equilibrium constants and the superscript for each K_{eq} or K_d describes the binding events. For instance, a superscript A:PPIase describes a reaction in which ligand site A is interacting with the PPIase domain. If there is an ampersand, the binding event to the left has already happened and the event to the right of the ampersand is the event described by that affinity constant. The use of "2^{nd}" to the right of the ampersand denotes the presence of a second Pin1 molecule binding by the named domain to the ligand that is already bound to a Pin1 at the other binding site.

In terms of the data fitting done in chapter three, this Virtual Cell software generated model was integrated into an in-house NMR fitting code based on that used for fitting the four-state model (Model 2). The equations applicable to fitting the fraction bound in that case are also used here. It is also important to note that in chapter three additional assumptions are made, whereby:

$$K_d^{A:PPIase} = K_d^{B:PPIase\&2ndPPIase:A} = K_d^{B:WW\&A:PPIase} = K_d^{B:WW\&2ndPPIase:A} = K_d^{A:WW\&A:PPIase}$$

$$K_d^{B:WW\&2ndWW:A} = K_d^{A:WW} = K_d^{B:PPIase\&A:WW} = K_d^{B:PPIase\&2ndWW:A} = K_d^{A:PPIase\&A:WW}$$

$$K_d^{B:WW} = K_d^{A:WW\&2ndWW:B} = K_d^{B:PPIase\&B:WW} = K_d^{A:PPIase\&B:WW} = K_d^{A:PPIase\&2ndWW:B}$$

$$K_d^{B:WW\&B:PPIase} = K_d^{A:PPIase\&2ndPPIase:B} = K_d^{A:WW\&2ndPPIase:B} = K_d^{A:WW\&B:PPIase} = K_d^{B:PPIase}$$

These assumptions dramatically reduce the number of fitted parameters in the model.

Cited Literature

Dubitzky, W., O. Wolkenhauer, et al. Virtual Cell (VCell) Modeling and Analysis Platform. Encyclopedia of Systems Biology, Springer New York: 2342-2347.